UNIVERSITY OF MINNESOTA
ST. ANTHONY FALLS LABORATORY
Engineering, Environmental and Geophysical Fluid Dynamics

Project Report No. 406

Measurements and Models of Snow and Ice Albedo on a Lake:

Reports from the 1996 to 1997 Ryan Lake Winter Field Studies

by

Heather E. Henneman and Heinz G. Stefan

Prepared for

U.S. ENVIRONMENTAL PROTECTION AGENCY

Office of Research and Development
Washington, D.C.
and
Mid-Continent-Ecology Division
Duluth, Minnesota

August 1997
Minneapolis, Minnesota

UNIVERSITY OF MINNESOTA
ST. ANTHONY FALLS LABORATORY
Engineering, Environmental and Geophysical Fluid Dynamics

Project Report No. 406

Measurements and Models of Snow and Ice Albedo on a Lake:
Reports from the 1996 to 1997 Ryan Lake Winter Field Studies

by

Heather E. Henneman and Heinz G. Stefan

Prepared for

U.S. ENVIRONMENTAL PROTECTION AGENCY

Office of Research and Development
Washington, D.C.
and
Mid-Continent-Ecology Division
Duluth, Minnesota

August 1997
Minneapolis, Minnesota

Prepared for: For Record/USEPA
Last Revised: August 25, 1997
Disk Locators: (Zip Disk #2/Stefan/Heather)
Intmemo\text.doc;fig3_1&2.pm6;photos.pm6

Overview

The albedos of snow and ice over a freshwater lake were measured in two separate field studies: (1) February 21 to March 16, 1996 and (2) December 17, 1996, to March 21, 1997. Both field studies were conducted on Ryan Lake, Minneapolis, Minnesota.

Included herein (Section 1) is the report from the first winter field study. Two papers concerning the results of the second field study were submitted for publication and are included in Appendix A and B of this report. The titles of the manuscripts are (1) Snow and Ice Cover Albedos of a Winter Lake and (2) Pyranometer Comparison in Measuring Snow and Ice Albedo.

In addition to the albedo winter field study report, a number of short reports are included herein. The albedos measured during February and March of 1996 were for a limited waveband (0.4 to 1.1 μm). Therefore, a set of adjustment equations were developed during the 1996-1997 field study which allowed the 1996 albedo data to be adjusted to the waveband of 0.4 to 2.8 μm. The results of the adjustments are reported in Section 2. Section 3 gives the results of a literary search conducted to find the albedos of snow and ice at different wavelengths, specifically in the photosynthetically active radiation waveband of 0.4 to 0.7 μm. During the 1996-1997 winter study, snow depths were measured over Ryan Lake. In Section 4 these data are reported and compared to snow depths measured over land. Lastly, in Section 5, the field observations from both winter field studies are reported along with selected photographs taken during each field study on Ryan Lake.

Acknowledgments

The investigation described herein was conducted for the U.S. Environmental Protection Agency as part of a project to anticipate the possible effects of projected climate change on water resources and ecosystems. Barbara M. Levinson (Office of Research and Development, Washington, D.C.) and John G. Eaton and Virginia M. Snarski (Mid-Continent-Ecology Division, Duluth, MN) were project officers.

David Ruschy of the Department of Soil, Water and Climate, University of Minnesota, St. Paul, provided albedo data collected at the University of Minnesota, St. Paul, and informational support for the field studies. Greg Spoden, Minnesota State Climatology Office provided climate data. Their cooperation is gratefully acknowledged.

Table of Contents

List of Figures

List of Photos

List of Tables

1. Snow And Ice Cover Albedos Of A Winter Lake

Abstract: The albedos of snow and ice covers of a lake in Minnesota were measured in February and March of 1996. A quasi steady-state relationship between albedo and air temperature showed an average snow albedo of 0.84 when air temperatures were below freezing and an average ice albedo of 0.38 when air temperatures were above freezing. The albedo quickly dropped from near 0.84 for snow to near 0.38 for a slushy ice surface when air temperatures climbed above freezing. Both the snow and the ice albedo exhibited some daily and long term decay. Decay equations for two types of snow albedo transitions were developed: (1) albedo decay due to the metamorphism of snow when air temperatures are below freezing (0^{o}C), (2) albedo decay during snow melt when air temperatures are above freezing.

1.1 Introduction

Albedo refers to the ratio of reflected solar radiation to incoming solar radiation at a surface. It is a critical parameter for the surface heat balance in any part of the world. Radiative fluxes dominate the surface energy balance of many snow and ice covered regions, and the albedo has a controlling influence on the absorption of radiative energy in those regions (Conway et al. 1996).

Radiation transmitted through the ice and snow cover of a lake is an energy source for both lake water temperature and photosynthesis of plants in the lake (Ellis and Stefan 1989). The amount of radiation transmitted through the ice and snow cover depends in part on the depth of these covers and on the albedos of the snow and/or ice. Deterministic year-round lake water quality simulation models such as MINLAKE95 (Fang and Stefan 1996a), use albedo in the winter energy balance to predict ice cover growth over fresh water lakes (Gu and Stefan 1990). Because the ice is at times snow-covered during the winter months, albedo values for both ice and snow are needed in the models.

Snow albedo values can be found in the literature for snow on land or snow on sea ice. These values may also be appropriate for snow on lake ice if the snow cover is deep, but not necessarily if the snow cover is shallow (Male and Gray 1981). Albedos for ice are typically smaller than for snow and are variable with ice conditions (Bolsenga 1969, 1977). For MINLAKE95 it was not clear whether the literature values for snow and ice albedos used in modeling were appropriate. Hence, a field study was conducted to measure the albedo of the snow and/or ice cover of a freshwater lake.

1.2 Albedo

The albedo of snow has been more widely studied than that of ice; however, many of the determinants of snow albedo may also be applicable to ice albedo. Snow albedo depends on the grain size, density, impurity content, and surface roughness of the snow (Male and Gray 1981). Sun angle (Dirmhirn and Eaton 1975; Warren 1982), cloud cover (Male and Granger 1981), and wind (Bergen et al. 1983) have also been shown to effect the albedo of snow.

Albedos for freshly fallen, dry snow on land typically range from 0.80 to 0.87 (Perovich et al. 1986; Baker et al. 1990; Conway et al. 1996). Depending on the ice type, ice albedos are reported to vary from 0.10 to 0.58 (Bolsenga 1969, 1977; Perovich et al. 1986).

The reflectance of ice or snow is made up of diffuse and specular components (Dirmhirn and Eaton 1975). When the reflecting surface of a material is rough, with irregularities on a scale comparable to or larger than the wavelength of light, reflection occurs not in a single direction but in all directions; such reflection is called diffuse reflection. Conversely, reflections in a single direction from smooth surfaces are called specular reflections. Usually, the specular component of the reflection of snow and ice is much smaller than the diffuse component; however, the effect of specular reflection may increase after melting and refreezing of a snow or ice surface.

Snow and ice albedos have been observed to undergo both daily variations and long term changes. Albedo decay has previously been studied on snow-covered land (U. S. Army Corps of Engineers 1956; Dirmhirn and Eaton 1975; Baker et al. 1990), on sea ice (Curry et al. 1995) and on freshwater ice (Bolsenga 1977).

According to Dirmhirn and Eaton (1975) daily variations in albedo measurements may be attributed to three factors: the varying contribution of specular reflection from the snow surface with solar angle, the metamorphism of snow (recrystallization on the surface and within the snowpack), the instrumental error due to the deviation of the pyranometer from the cosine law.

The effects of specular reflection and instrumental error on albedo may both depend on the angle of the sun. Low solar angles increase the instrumental error and the effect of specular reflection (Warren 1982).

The effect of the metamorphism of snow on albedo depends on the amount of radiation received by the snow cover (Dirmhirn and Eaton 1975). During the day as heat is applied to a snow cover by radiative and convective processes the many facets of the snow crystals are decreased. As the amount of light scattering is decreased in the uppermost layer of snow, more radiation is absorbed and the albedo is reduced. This metamorphism of the snow is irreversible, i.e., the snow cannot recover overnight. However, overnight refreezing of the surface layer may increase the specular reflectance

of the surface so that morning albedo may be higher than the albedo of the previous evening.

Long term albedo decay due to the metamorphism of snow has been documented more often than daily albedo variation. Albedo decay trends for deep snowpack (U. S. Army Corps of Engineers 1956) and shallow snowpack (O'Neill and Gray 1973) indicate that the decay for shallow snowpack is much more rapid than that for deeper snow because of the influence of the lower albedo of the ground beneath the shallow snow. Baker et. al. (1990), analyzed data for the albedo of terrestrial snow as it decayed and found that the linear equation

$$\alpha = 77.0\text{-}2.0t \qquad (1.1)$$

where α = albedo given as a percentage and t = number of days after a snowfall, described 90% of the variations in albedo for periods of albedo decay lasting seven days or less in March. They also developed a non-linear decay equation for the same data which described 88% of the variations in albedo:

$$\alpha = 83\text{-}7t^{0.5} \qquad (1.2)$$

Baker and Ruschy (1988, 1989) studied terrestrial snow albedo data from Minnesota for a 19-year period. They found three distinct albedo periods during the months of November to April: (1) introduction to winter when snowfalls begin to occur with low frequency and duration, (2) the high albedo season when fresh snow usually exists on the ground, (3) a transitional period in the late winter and early spring characterized by periods of snowmelt. The albedo decay equation used to describe albedo decay for the entire winter season of November to April by Baker et al. (1990), is

$$\alpha = 85\text{-}6t^{0.5} \qquad (1.3)$$

1.3 Field Study

A 22-day field study was conducted on Ryan Lake, Minnesota, in order to measure the albedo of the snow and/or ice cover of this lake. Ryan Lake (45°N, 93°W) is located in the northwest area of Minneapolis, Minnesota. It has a surface area of 6.1 ha, a mean depth of 5.0m, and a maximum depth of 10.0m.

The radiation sensors used were LI-COR LI-200SA Pyranometer Sensors which are sensitive to wavelengths of about 0.4 to 1.2 μm which includes the photosynthetically active radiation range. The pyranometers were factory calibrated against an Eppley Precision Spectral Pyranometer to an uncertainty of ± 5%.

Two pyranometers were used in the study, one for incident radiation and the other for reflected radiation. These two instruments were calibrated against one another while facing upward. The measurements were within ± 2% prior to the beginning and after the conclusion of the field study. The pyranometers were mounted horizontally with one facing upward and the other downward. The latter was mounted 1.60 m above the lake surface, the height used by Baker and Ruschy (1988, 1989) in their albedo studies over land at a weather station about 13 km from Ryan Lake. The equipment was placed about 40 meters from the eastern shore of the lake. This location was easily accessible from shore, and the ice and snow conditions were representative of the lake surface.

Along with the radiation measurements air temperature measurements were taken and recorded every 5 minutes with a Campbell Scientific CR10 data logger. The 5 minute record represented an average of values taken over that time period. In addition to these continuous measurements, weekly observations of snow depth and lake cover conditions were made during the study.

The faces of the pyranometers were checked during each site visit to insure that snow and/or ice was not collecting on the upright pyranometer. The deposition of snow on the upright pyranometer could have resulted in the reduction of incident radiation measured and, therefore, caused an abnormal increase in albedo. Although such depositions were noted by Baker and Ruschy (1988), the upright pyranometer face was observed to be free of ice and snow during each site visit. This lack of snow deposition on the instrument may have been due to the absence of heavy snowfall during the study period.

1.4 Results

Figs. 1.1a through 1.1d show the variations in albedo for each day of the study. The values plotted are for 5-minute intervals and were obtained by dividing the data from the downward-facing pyranometer by those from the upward-facing pyranometer.

Average daily albedos were calculated in two ways. One method of finding the average daily albedo consisted of averaging the 5-minute interval albedo values between 8:00 AM and 5:00 PM. These daylight hours included 97% of the measured total daily incident radiation and avoided the spikes in albedo which occurred near sunrise and sunset. Such aberrations in the albedo will be discussed later in the paper. The second method used to find the average daily albedo was to divide the total reflected radiation by the total incident radiation measured between 8:00 AM and 5:00 PM. The average daily albedos found using both methods are reported for comparison in Table 1.1. The mean difference between the two average daily albedos for each day of the study period is less than 1%. Throughout the remainder of the paper average daily albedo refers to the average albedo obtained using the first method.

Throughout the study the average daily albedo of the lake cover ranged from a low of 0.30 to a high of 0.88. The first considerable day to day increase in albedo occurred between February 26 and 27 and coincided with a 0.8 cm snowfall on February 27. The albedo again increased the following day when another 0.3 cm of snow fell. The lake remained snow-covered and the daily albedo stayed above 0.79 until March 11 when the air temperature climbed above freezing. A decrease in albedo from 0.70 to less than 0.50 can be seen in Fig. 1.1c for this date. No more snow fell during the remainder of the study period; however, melting and refreezing of the snow, and possibly some lake ice, did result in further variations in daily albedo.

In addition to the day to day variations in albedo, diurnal variations of albedo are also apparent in Figs. 1.1a through 1.1d. An obvious variation in albedo occurred due to instrumental error at low solar angles of incidence. Spikes in the albedo were evident in both the early morning and early evening hours. As noted by Dirmhirn and Eaton (1975) low solar angles of incidence at these times cause an instrumental error due to the deviation from the cosine law. Also, the trees, buildings and other obstacles surrounding the lake may have caused a filtering of the sunlight and, consequently, a variation in the incident radiation measured during the early morning and early evening hours.

Often the albedo decayed throughout the day. This is attributed to the daily metamorphism of the snow cover and can be seen in Figs. 1.1a through 1.1d with the exception of snowfall days and days of melting and refreezing when the albedo increased. These days are identified in Table 1.1 by the amount of daily snowfall and/or the maximum, minimum and average daily air temperatures.

Because the metamorphism of a snow cover has been reported to depend on the amount of radiation received by that snow cover (Dirmhirn and Eaton 1975), a brief investigation was performed to see whether a relationship existed simply between the change in albedo and the total amount of radiation received during the day. From the data collected in this field study the change in albedo of the snow or ice cover throughout the day appeared to be unrelated to either the total daily incident or reflected radiation.

Fig. 1.2 gives the daily average albedos, the daily average air temperatures, and the total daily snowfall depths as a time series. After each significant snowfall a peak and then a decay in albedo over the days following the snowfall occurred. Actually, three types of albedo transitions occurred during the study period from Julian Day 54 (February 23) to Julian Day 75 (March 15). These periods of transition can be identified in Fig. 1.2. The first type is an albedo increase which occurred during a snow accumulation period when air temperatures were below freezing. This type of transition in lake cover albedo appears to have taken only 2 to 3 days beginning on Julian Day 57 (February 26). The albedo increased from 0.38 to 0.86 during that time. The second type of transition occurred after a snowfall when the albedo decayed due to the metamorphism of the snow. Two such albedo decay periods can be seen in Fig. 1.2 -- the first beginning on Julian Day 59 (February 28) and the second beginning on Julian Day 64 (March 4). The third albedo transition type took place between Julian Days 70 and 72 (March 10 and 12) as the

(a)

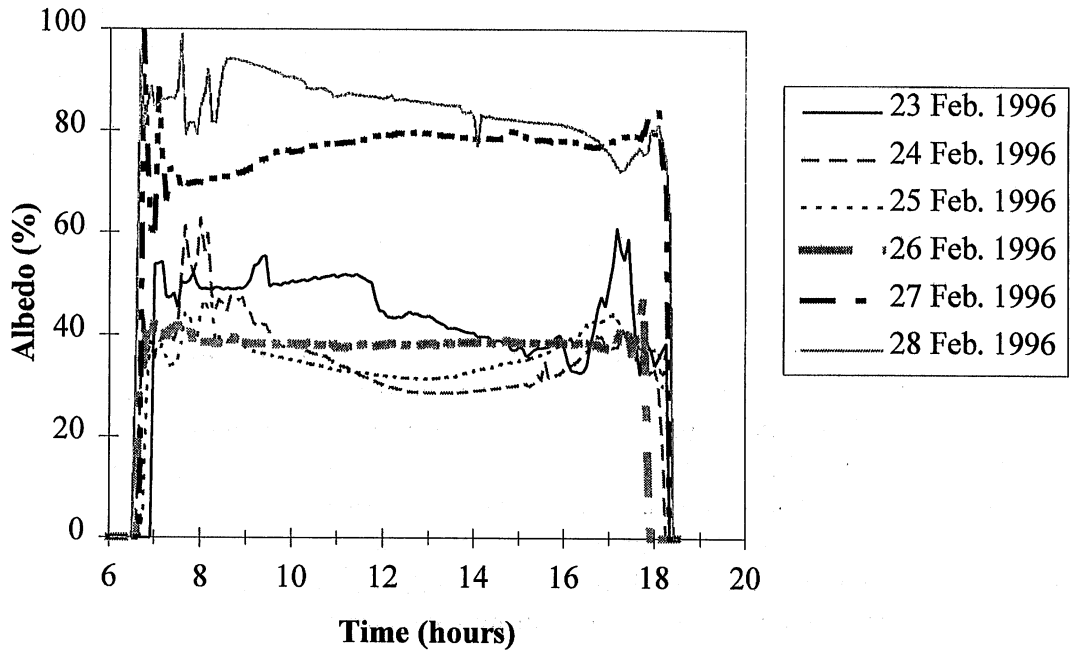

(b)

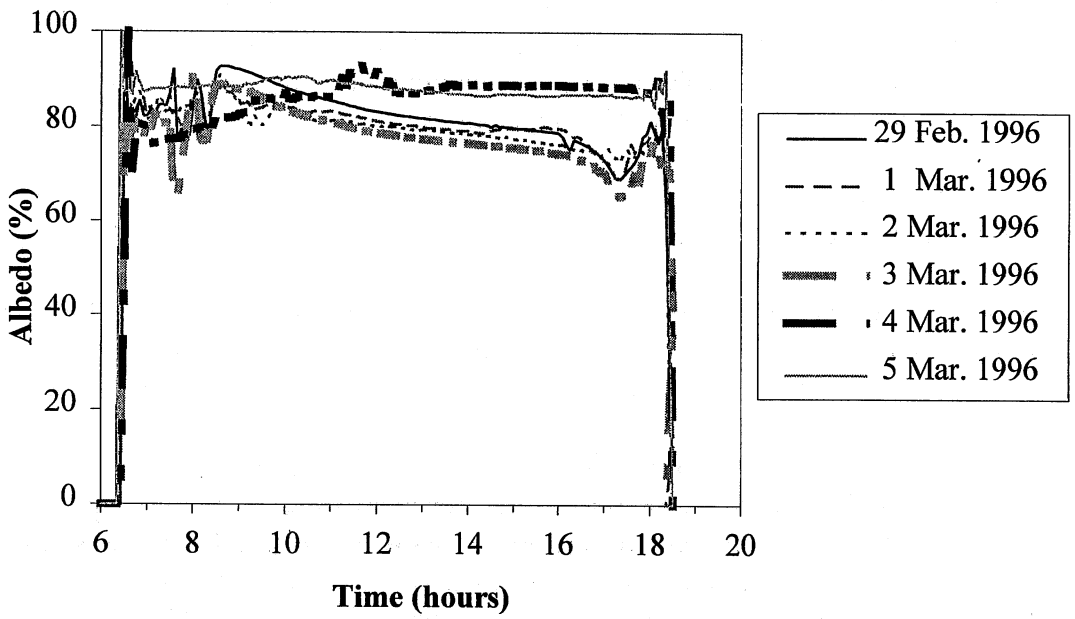

Figure 1.1a and 1.1b Daily variations in snow and ice albedos measured on Ryan Lake from (a) February 23 - 28, 1996 and (b) February 29 - March 5, 1996.

(c)

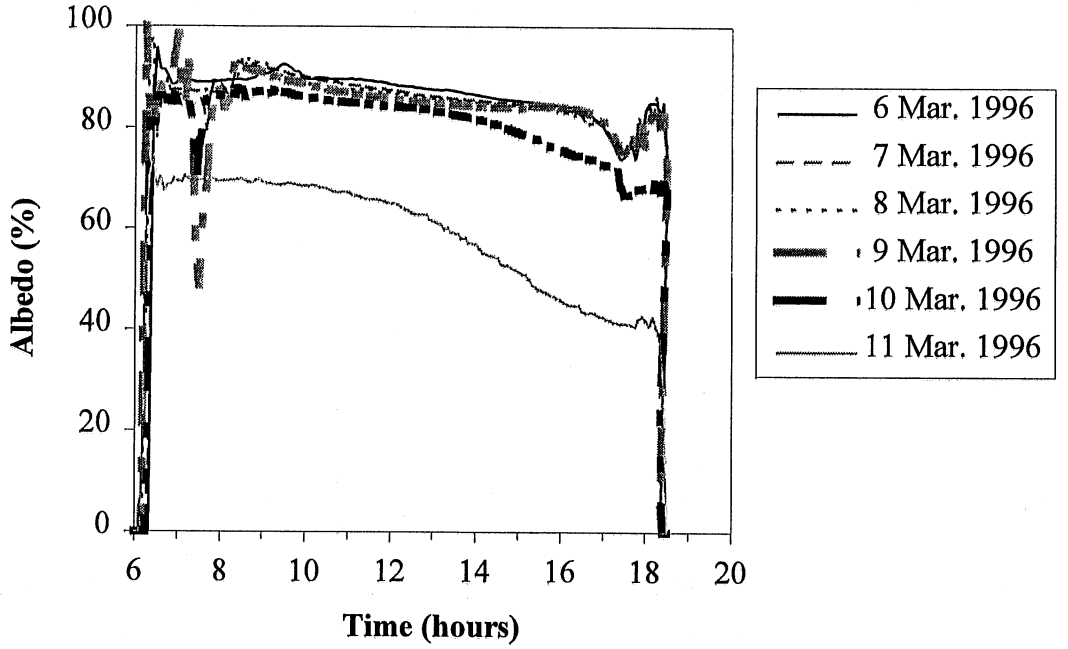

(d)

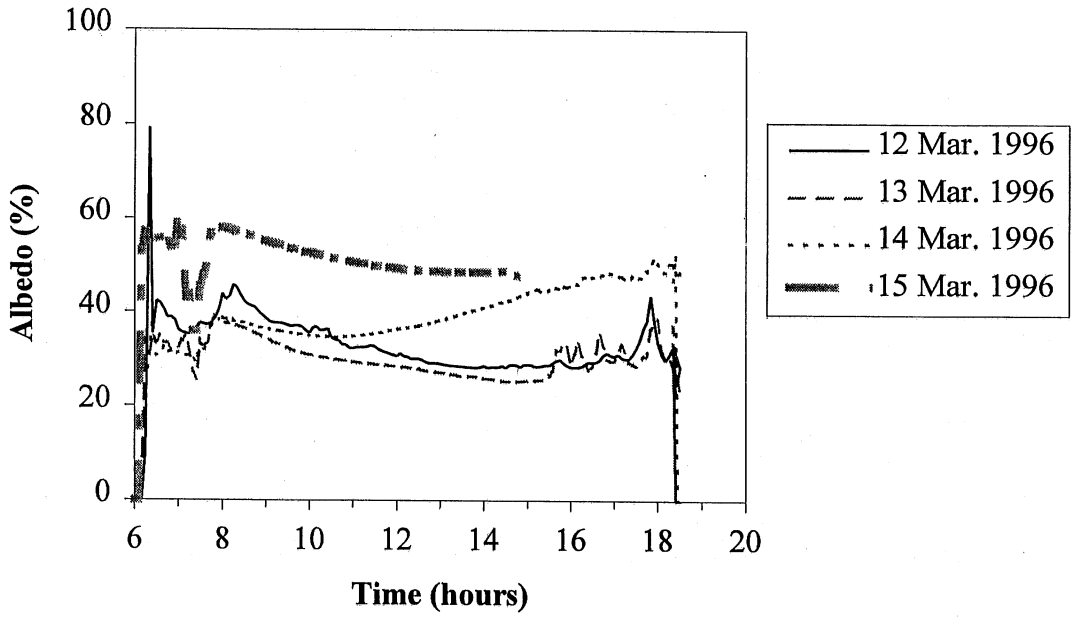

Figure 1.1c and 1.1d Daily variations in snow and ice albedos measured on Ryan Lake from (c) March 6 - 11, 1996 and (b) March 12 - 15, 1996.

air temperature rose to above freezing and the snow cover melted. The resulting rapid change in albedo was of the same magnitude as the albedo transition during the snow accumulation period.

Although the albedo decay data collected in the Ryan Lake field study are limited at this time, snow albedo decay equations were developed for the second and third types of transition described above. For $T_{air}<0^{o}C$ the decay equation

$$\alpha = 86 - 2t^{0.5} \qquad (1.4)$$

where α = albedo given as a percentage and t = the number of days after a snowfall day, describes the albedo decay due to the metamorphism of snow. It is similar to Eqs. 1.2 and 1.3 and to equations which Fang and Stefan (1996) developed based in part on the results of this study. However, the albedo decay occurs more slowly than in the equations developed by Bakeret al. (1990).

For $T_{air}>0^{o}C$ the data are described by the linear equation

$$\alpha = 86 - 25\tau \qquad (1.5)$$

where:
τ = the number of above freezing days following a period when the lake is snow-covered.

It should be noted that the rapid albedo decay described by Equation 5 may be the result of little snow cover on the lake prior to the days with above freezing temperatures.

Fig. 1.3 shows the relationship between average daily albedo and average daily air temperature. Although the snow cover albedos do decay somewhat over time as expressed in Eqs. 1.4 and 1.5 above, it appears that a quasi steady-state can be used as a good approximation for the relationship between albedo and air temperature. However, this relationship between albedo and air temperature may be affected by the limited time period of the field study and the shallow depth of the snow cover on the lake (O'Neill and Gray 1973; Male and Gray 1981).

The quasi steady-state relationship depends mainly on whether the air temperature is above or below freezing ($0^{o}C$) and whether there is snow covering the ice. When the air temperature was below freezing and there was snow covering the ice, the mean of the daily average albedos was 0.84 with a standard deviation of 0.04. This value is slightly higher than the 0.80 mean terrestrial snow albedo found by Baker et al. (1990), for days following a snowfall. (Albedos of snow cover were ignored during transitional periods of snowmelt for the calculations.) In the case where the lake ice was not covered by snow the mean daily average albedo of the ice cover was 0.38 ± 0.07, which is lower than the average ice albedo of 0.43 found by Bolsenga (1977). The larger standard deviation for

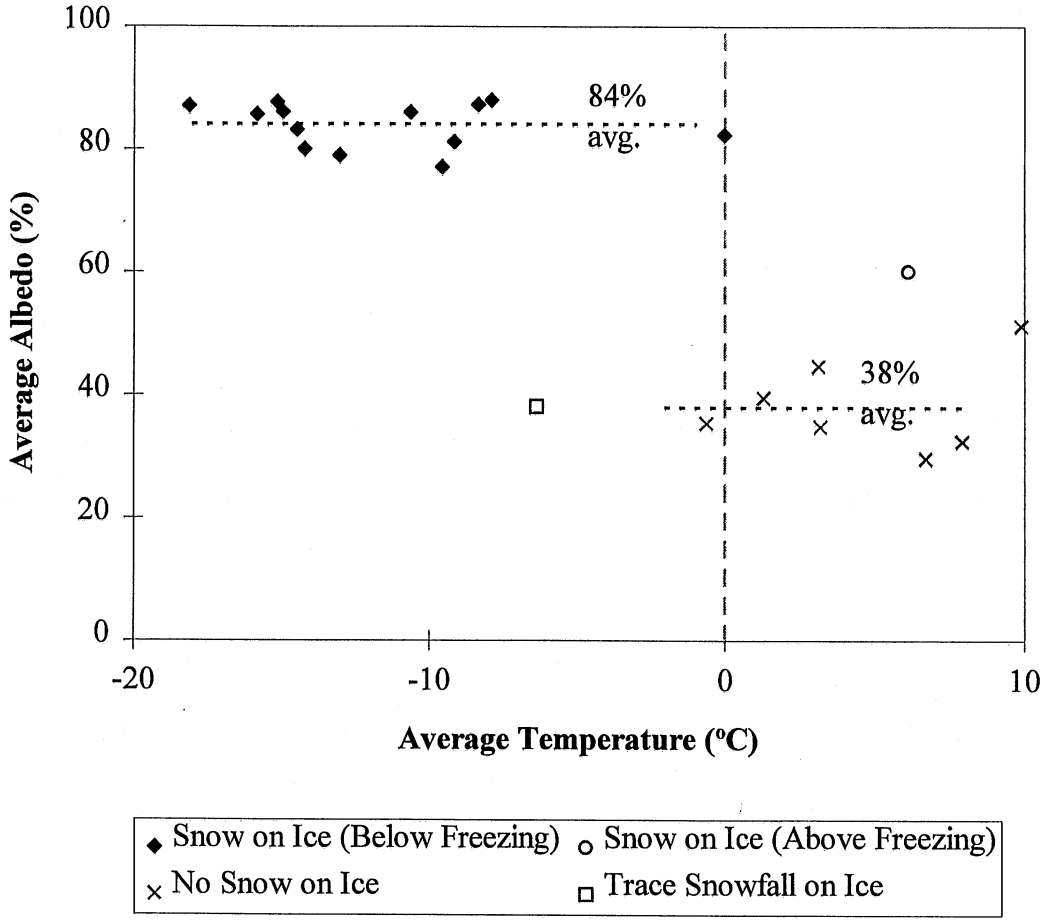

Figure 1.3 Average daily albedo versus average daily air temperature. Different markers indicate when the ice was snow covered. All measurements from Ryan Lake, February 23 to March 15, 1996.

the ice may be due to a larger variation in the type of ice which occurred, e.g., various mixtures of snow and ice.

1.5 Snow and Ice Observations

Snow and ice conditions on the lake were documented weekly throughout the study (See Table 5.1 in Section 5.).

On March 8, 1996, a layer of clean, powdery snow over solidly packed snow covered the lake. A few scattered ice spots were also present. Photos 1 through 3 in Section 5, "Field observations and photographs," show examples of the dry snow cover. The depth of the snow on March 8 ranged from 0 to 15 cm. Trace amounts (<0.25 cm) of snow fell on this date and 2 cm fell two days before on March 6. The March 8 average daily albedo of 0.86 was calculated from measurements collected over a section of the lake which was completely snow-covered.

On March 15, 1996, after five days of above freezing daytime air temperatures, a slush mixture of water, snow and ice covered the lake. Photo 7 shows the snow/ice mixture on the northeast side of the lake. The crack in the photo was approximately 6 cm wide, while the depth of the snow/ice mixture was about 7.5 cm. The March 15 average daily albedo of 0.51 was calculated from measurements collected over an area which was free of cracks in the snow/ice cover.

1.6 Recommendations And Conclusions

The albedos for snow and ice in the MINLAKE95 model were held constant at 0.80 and 0.55, respectively, throughout the entire winter period (Fang and Stefan 1996a). In this field study it was found that the average albedo of the snow cover over a lake is 0.84, or 0.04 greater than the value used in MINLAKE95. The average ice albedo is 0.38, or 0.17 less than in MINLAKE95. All but one of the average daily ice albedos were measured at above freezing air temperatures. Hence, the ice albedos are characteristic of a slushy, rough ice surface occurring in spring rather than of a smooth, clear ice surface which occurs more often in midwinter at below freezing temperatures.

Both snow and ice albedos are somewhat variable depending on a number of factors including air temperature and time after snowfall. In order to better assess variations in snow and ice covers of a freshwater lake over time, e.g., albedo decay following snowfalls, longer-term studies will need to be performed. However, because a quasi steady-state appears to exist between albedo and air temperature, using constant values for snow and ice cover depending on the air temperature and snow cover may be sufficient for an ice cover model at this time. The rapid transition periods, i.e., when the air temperature changes from above freezing to below freezing or vice versa, can perhaps be ignored in order to simplify the modeling.

MINLAKE95 has been modified to include the ice albedo found in this study and the albedo decay due to aging snow and has been renamed MINLAKE96 (Fang and Stefan 1996b). Because the albedo decay equations used in the new model give albedos consistently lower than the measured albedo values and underestimate the magnitude of albedo decay when snow depth on the lake is shallow, it is recommended that the equations be modified. Eqs. 1.5 and 1.6 are suggested to describe snow albedo decay for $T_{air}<0^{o}C$ and $T_{air}>0^{o}C$, respectively.

If constant values for snow and ice albedos are again adopted in the model, snow albedo should be held at 0.84 for below freezing air temperatures and ice albedo at 0.38 for above freezing air temperatures. Sufficient data for ice albedos at below freezing air temperatures were not collected during this study, nor were measurements made for ice conditions other than snow/ice mixtures and refrozen slush (e.g., clear ice). However, based on ice albedo values from Bolsenga (1969, 1977) and the limited data collected here, an ice albedo less than 0.55 should be used when $T_{air}<0^{o}C$. An ice albedo of 0.38 for both above and below freezing air temperatures is recommended at this time.

2. Application of LI-COR Adjustment Equations to 1996 Albedo Data

2.1 Introduction

Snow and ice albedos were measured during a field study conducted on Ryan Lake in northwest Minneapolis from February 23 to March 16, 1996. The pyranometers used to measure incident and reflected radiation were photovoltaic sensors with a spectral sensitivity of 0.4 to 1.1 μm. The pyranometers were manufactured by LI-COR.

Because of the short duration of the 1996 field study, a second albedo study was conducted from December 17, 1996, to March 21, 1997 (Henneman and Stefan, 1997a and 1997b). The LI-COR manufacturer does not recommend that LI-COR pyranometers be used to measure reflected radiation because of their limited spectral response. Therefore, in the more recent study, thermopile pyranometers manufactured by Kipp and Zonen were used to measure incident and reflected radiation. These pyranometers have a spectral sensitivity of 0.3 to 2.8 μm (the total short-wave band).

During the second field study LI-COR pyranometers were also used to measure incident and reflected radiation over Ryan Lake. In this way the data from the LI-COR pyranometers, which have a limited spectral response, could be compared to data from the Kipp and Zonen pyranometers, which have a total short-wave spectral response. Equations were developed from the results of the data comparisons which allow the LI-COR radiation data to be adjusted to the total short-wave band.

Herein, the adjustment equations developed from the data collected during the second field study (December 17, 1996 to March 21, 1997) are used to adjust the LI-COR data collected during the initial field study (February 23 to March 16, 1996). Additionally, predictions by the two albedo models developed in the second field study are compared to the adjusted LI-COR data from the initial study.

2.2 Data Adjustments

Eqs. 2.1 and 2.2 were developed to adjust both incident and reflected total daily radiation values measured by LI-COR instrumentation (Henneman and Stefan, 1997b). The equations adjust the LI-COR data (spectral response of 0.4 to 1.1 μm) to total short-wave radiation data (0.3 to 2.8 μm).

$$I_{incident} = 1.0(\text{LI-COR}_{incident}) - 0.12 \qquad (2.1)$$

$$I_{reflected} = 0.90(\text{LI-COR}_{reflected}) + 0.058 \quad (2.2)$$

where:

$I_{incident}$ = adjusted total daily incident radiation (MJ m^{-2} day^{-1}) for the waveband 0.3 to 2.8 μm;
$I_{reflected}$ = adjusted total daily reflected radiation (MJ m^{-2} day^{-1}) for the waveband 0.3 to 2.8 μm;
$\text{LI-COR}_{incident}$ = total daily incident radiation (MJ m^{-2} day^{-1}) as measured by LI-COR pyranometer for the waveband 0.4 to 1.1 μm;
$\text{LI-COR}_{reflected}$ = total daily reflected radiation (MJ m^{-2} day^{-1}) as measured by LI-COR pyranometer for the waveband 0.4 to 1.1 μm.

Eq. 2.3 gives an adjusted albedo value and is the ratio of total daily reflected radiation (Eq. 2.2) to total daily incident radiation (Eq. 2.1). Eq. 2.3 was used to adjust the LI-COR albedo data collected from February 23 to March 16, 1996.

$$\text{Adjusted Albedo} = 0.90\frac{(\text{LI} - \text{COR}_{reflected}) + 0.058}{(\text{LI} - \text{COR}_{incident}) - 0.12} \quad (2.3)$$

The total daily incident radiation, total daily reflected radiation, albedo, and adjusted albedo are shown in Table 2.1 for each day of the study. Fig. 2.1 shows both the original albedo data and the adjusted albedo as a time series. The adjusted albedos are consistently lower than the measured albedos.

2.3 Model Application

The predictions of the two models developed from the results of the second field study (December 17, 1996 to March 21, 1997) were compared to the adjusted albedo values calculated herein. Model 1 is described by Eqs. 2.4 through 2.6, while Model 2 is described by Eqs. 2.7 through 2.9 (Henneman and Stefan, 1997a).

Eq. 2.4 of Model 1 and Eq. 2.7 of Model 2 were applied from February 23 to March 10, 1996, the nonmelt period. Eqs. 2.5 and 2.6 of Model 1 and Eqs. 2.8 and 2.9 of Model 2 were applied to the remaining days which were within the melt period. The albedo was set to 0.83 on a snowfall day for either model.

2.3.1 Model 1

Nonmelt Period:

For all T_{air} values:

$$\alpha = -0.0015R + 0.84 \quad (2.4)$$

Melt Period:

For $T_{air} > 0^{o}C$:

$$\alpha = 0.0029R - 0.009T + 0.95 \quad (2.5)$$

For $T_{air} \leq 0^{o}C$:

$$\alpha = \alpha_{-1} - 0.00036T \quad (2.6)$$

where:
α_{min} = minimum albedo = 0.38;
α = daily albedo;
α_{-1} = albedo on previous day;
R = accumulated incoming daily solar radiation since last snowfall (MJ/m^2)*;
T = accumulated daily air temperature index since last snowfall (^{o}C)*;
T_{index} = daily air temperature index = $T_{air} - T_{base}$;
T_{air} = average daily air temperature (^{o}C);
$T_{base} = -18^{o}C$;
*Solar radiation and temperature begin accumulating after a snowfall greater than 2.5 mm (0.1 in).

The total daily incoming solar radiation data collected by the LI-COR pyranometer was adjusted by Eq. 2.1 before being used as input to Eqs. 2.4 and 2.5 in Model 1.

2.3.2 Model 2

Nonmelt Period:

For all T_{air} values:

$$\alpha = -0.011d + 0.83 \quad (2.7)$$

Melt Period:

For $T_{air} > 0^{\circ}C$:

$$\alpha = \alpha_{-1} - 0.17 \tag{2.8}$$

For $T_{air} \leq 0^{\circ}C$:

$$\alpha = \alpha_{-1} - 0.013 \tag{2.9}$$

where:
d= number of days after snowfall.

Fig. 2.2 compares the predictions by each model to the adjusted LI-COR albedo. Model 1 overpredicts the albedo during the melt period, and both models overpredict albedo for most days during the nonmelt period.

2.4 Error Analysis

Table 2.2 gives the results of the error analyses performed on the models. These results show that Model 2 does considerably better at predicting the adjusted albedo. The modeling efficiency (EF) of Model 2 is 0.89, compared to only 0.18 for Model 1. Model 2 also has a mean absolute error (MAE) of 0.058 while Model 1 has an MAE of 0.088.

2.5 Summary and Conclusions

Snow and ice albedos were collected on Ryan Lake from February 23 to March 16, 1996, using a LI-COR photovoltaic pyranometer. The albedo data were adjusted using Eq. 2.3. The equation adjusts the spectral-response-limited LI-COR data to total short-wave radiation data.

Albedo predictions by Model 1 and Model 2 developed from a longer-term field study (December 17, 1996 to March 21, 1997) were compared to the adjusted LI-COR albedos. Model 2 predicted albedo with a modeling efficiency of 0.89, while Model 1 only had a modeling efficiency of 0.18.

Because only the LI-COR instrumentation was used during the initial field study, no total short-wave albedo data were collected from February 23 to March 16, 1996, on Ryan Lake. Therefore, comparisons between the adjusted albedo data calculated herein and actual short-wave albedo values for that time period cannot be made. The adjusted albedo values are reasonable, although slightly lower than snow and ice albedos measured during the most recent field study.

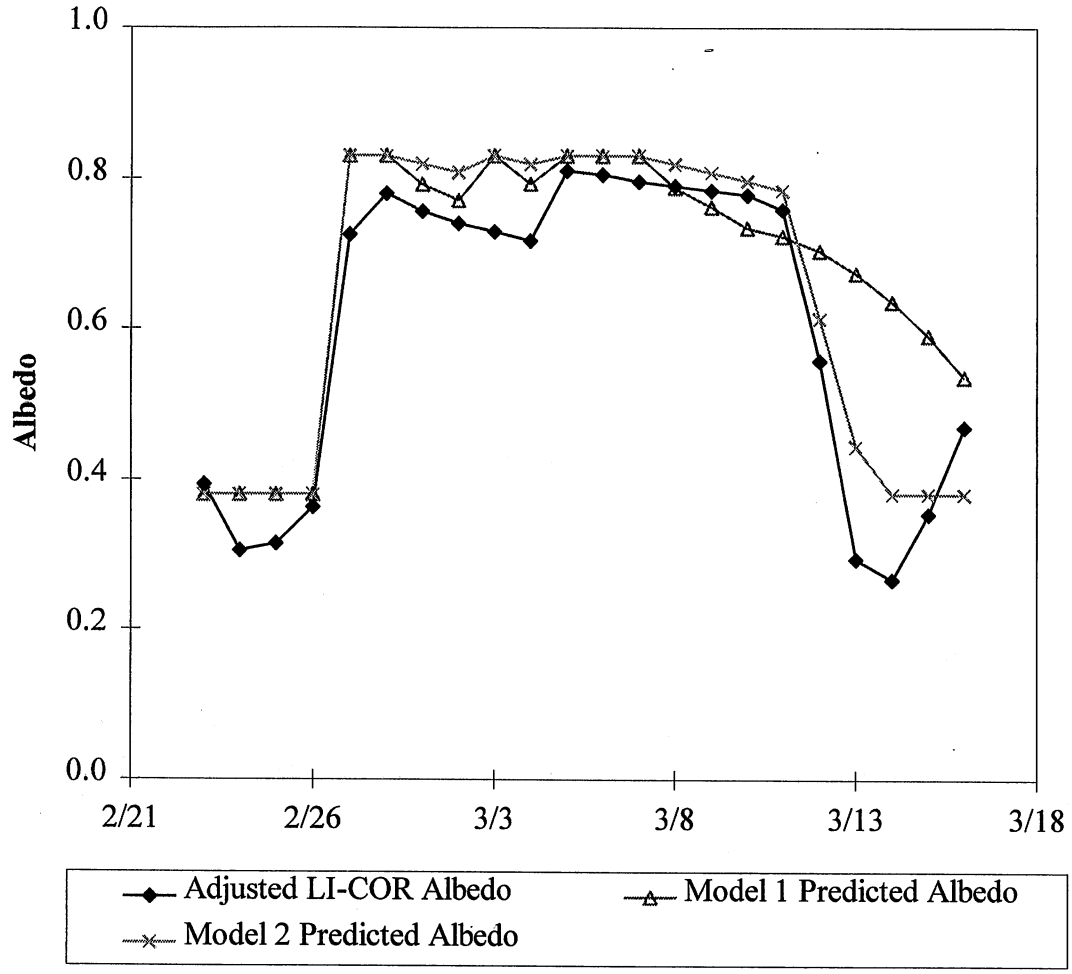

Fig. 2.2 Adjusted LI-COR albedo and predictions from Model 1 and Model 2. Adjusted LI-COR albedo from field data collected on Ryan Lake, February 23 to March 16, 1996.

Table 2.2. Mean absolute error, root mean square error, mean absolute percent error, and modeling efficiency for Model 1 and Model 2. Adjusted albedo from LI-COR albedo data collected on Ryan Lake, February 23 to March 16, 1996.

Statistical Parameter	Model 1	Model 2
MAE	0.088	0.058
RMSE	0.19	0.069
MA%E	23	12
EF	0.18	0.89

Mean Absolute Error (MAE) = $\frac{\sum|y_i - \hat{y}_i|}{n}$

Root Mean Square Error (RMSE) = $\sqrt{\frac{\sum(y_i - \hat{y}_i)^2}{n}}$

Mean Absolute Percent Error (MA%E) = $\frac{100}{n}\sum\frac{|y_i - \hat{y}_i|}{|y_i|}$

Modeling Efficiency (EF) = $1 - \frac{\sum(y_i - \hat{y}_i)^2}{\sum(y_i - \bar{y})^2}$

y_i = adjusted LI-COR albedo

$\hat{y}_i$ = simulated albedo

$\bar{y}$ = mean adjusted albedo

n = number of data points

3. PAR-Total Solar Radiation Partitioning, A Literature Search Summary

3.1 Introduction

Two questions concerning photosynthetically active radiation (PAR) were posed during a recent discussion on solar radiation. First, what portion of global solar radiation is PAR? That is, if the global solar radiation is known or predicted, what value should be used for PAR? Second, what is the albedo of snow and ice across the visible spectrum?

Investigations concerning the first question have been performed around the world, and the results are readily available in the literature. Field studies have also been conducted in an attempt to answer the second question. However, more articles reporting the visible albedo of snow have been published than those reporting ice albedo in the PAR region. In order to answer the questions, a literature search was conducted, and the results are summarized herein.

3.2 Photosynthetically Active Radiation

Photosynthetically active radiation (PAR) is that part of the solar spectrum in the visible region (wavelength range: 0.385 - 0.695 μm). Total, or global, solar radiation refers to the entire solar spectrum from 0.295 to 2.8 μm, including both diffuse and direct beam radiation. Fig. 3.1 shows the solar radiation spectra at the top of the atmosphere and at the earth's surface.

The ratio of PAR to total solar radiation has been measured as (Nagaraja Rao 1984)

$$\frac{\textbf{PAR}}{\textbf{Total Solar Radiation}} = \textbf{0.457}$$

The author compared his results to published values from around the world and found that 0.457 compared well with other results. Table 3.1 shows the ratio of PAR to total solar radiation for varying sky cover conditions measured during the same study by Nagaraja Rao (1984).

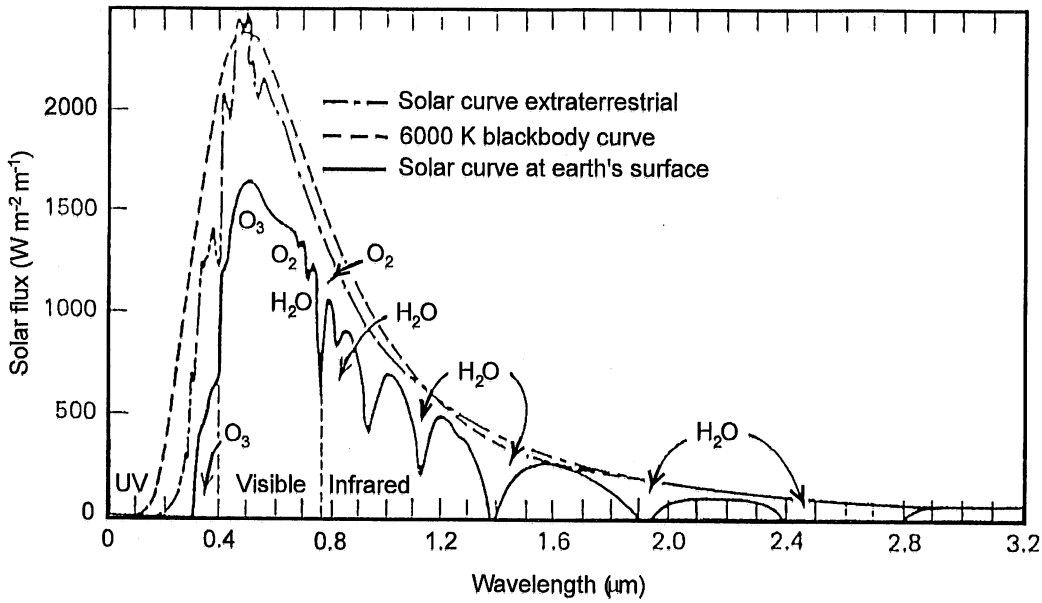

Fig. 3.1 Theoretical and actual spectra of solar radiation at the top of the atmosphere and the actual spectrum at the earth's surface (from Gates 1962).

Table 3.1. Ratios of PAR to total solar radiation for various sky cover conditions.

	Clear (FS*>0.85	Partly Cloudy (0.15≤FS≤0.85)	Cloudy (FS<0.15)
PAR/Total	**0.443**	**0.447**	**0.483**

* Fractional sunshine (FS) is the ratio of hours of bright sunshine to length of day from sunrise to sunset.

The increase in the ratio of PAR to total solar radiation with increasing cloud cover is as expected. Clouds attenuate incoming solar radiation at wavelengths greater than about 0.7 μm by both absorption and scattering, whereas attenuation in the visible spectrum is due to scattering alone. As seen in Fig. 3.1, water vapor absorbs radiation in the infrared region of the spectrum.

3.3 Snow Albedo

A number of field studies have investigated the short-wave albedo of snow in different wavebands, e.g., the ultraviolet (UV), visible, and infrared (IR). Many of the field studies were conducted in the Antarctic; however, the extent of the investigations may allow the conclusions to be applied to other parts of the world.

In one such study at the south pole Grenfell et al. (1994) found

albedo across UV and visible spectrum = **0.96-0.98**

The albedo was found to be nearly independent of snow grain size and solar zenith angle for the visible spectrum. The spectrally averaged albedo, i.e., the albedo over wavelengths 0.3 to 2.8 μm, ranged from 0.80 to 0.85 for solar zenith angles 55° to 72°. These albedo values correspond with values measured on Ryan Lake. The solar zenith angle, the angular distance of the sun from zenith, in Minneapolis ranges from about 68° in January to 40° in March.

In an earlier theoretical study Choudhury (1979) found

albedo across the visible spectrum = **0.95-0.98**

In Figs. 3.2a through 3.2d, four plots of albedo versus wavelength are shown. Note that for changes in snow grain size or solar zenith angle, the albedo in the visible waveband does not change considerably. However, for shallower snow depths and dirty snow, the visible albedo decreases substantially. Snowfall depths less than 25 mm are considered "trace" snowfall events for the MNLAKE albedo model and are not indicative of a new snow cover. Therefore, low visible albedos due to shallow snow depths may be disregarded for new snowfall events. That is, for clean snow the visible albedo remains greater than 0.95 and does not decay significantly with increasing grain size.

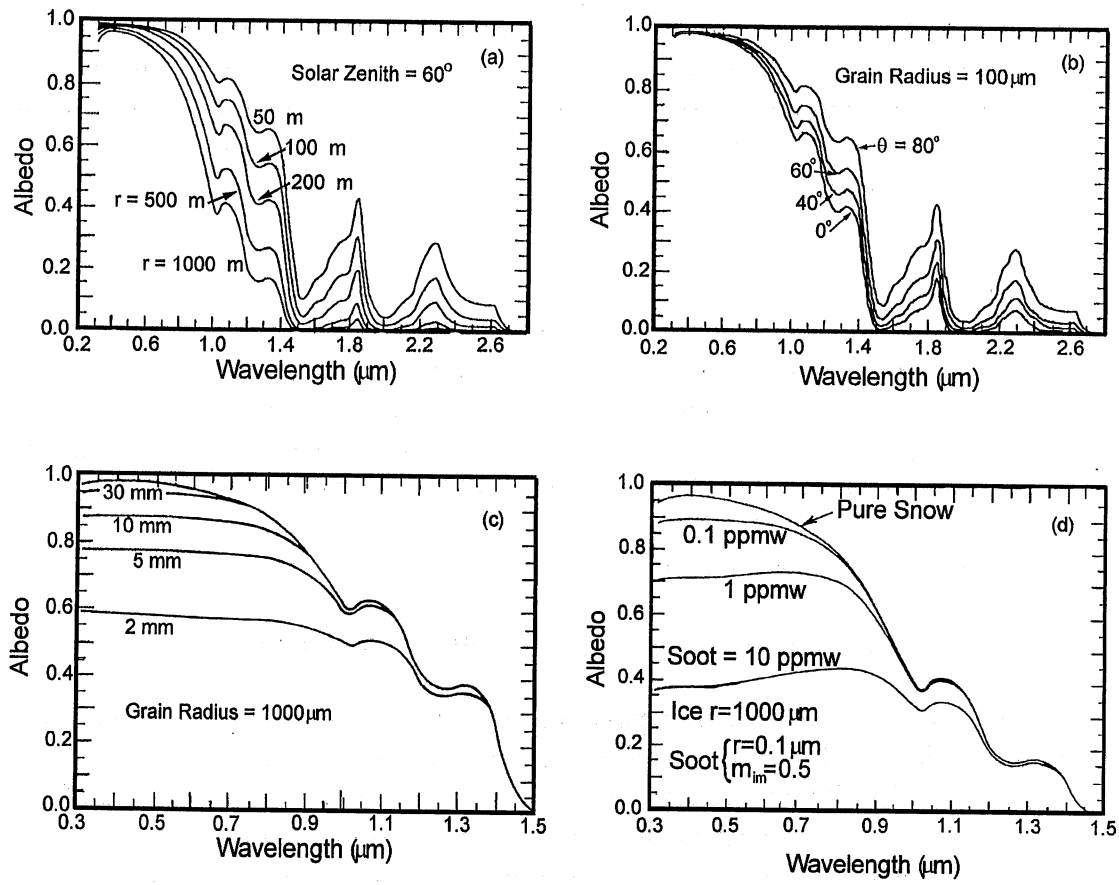

Fig. 3.2 Plots of the effects on the spectral albedo of snow of (a) snow grain size, (b) solar zenith angle, (c) snow cover thickness (from Wiscombe and Warren 1980) and (d) contamination by soot (from Warren and Wiscombe 1980).

3.4 Ice Albedo

As stated previously there are not as many articles on ice albedo across the visible region as there are for snow. Sea ice albedo values were measured in a study conducted in Canada by Perovich (1994). The spectral albedo was measured for a number of wavelengths between 0.4 and 1 μm. Albedo varied across the visible spectrum, and the results are shown below.

albedo across the visible spectrum for bare ice = **0.74-0.78**

albedo across the visible spectrum for blue ice = **0.53-0.68**

The albedo for sea ice across the entire solar spectrum had previously been reported as 0.52 for bare ice and 0.32 for melting blue ice (Perovich et al. 1986).

A study relating ice albedo to bubble size within ice was conducted by Mullen and Warren (1988); however, the data collected was limited to direct beam albedo. Since diffuse radiation was not included, their results are not particularly useful for our purposes.

4. Comparison of Snow Depths on a Lake to Snow Depths on Land

4.1 Introduction

The depth of snow covering the ice on a northern lake in winter affects (1) lake ice thickness, (2) energy transmitted between the atmosphere and the underlying lake water by radiation and conduction, (3) lake oxygen budgets in winter, and (4) winterkill of fish in lakes. When snow depths are more than half the thickness of lake ice, the weight of the snow can depress the lake ice so that the lake water can seep through cracks in the ice and wet the snow adjacent to the ice surface. This slush layer subsequently freezes into snow ice, also referred to as white ice (Nelson 1990). The depth of snow on the lake is, thereby, decreased, while the ice thickness is increased. The fraction of radiative solar and atmospheric energy transmitted to lake water during the winter depends strongly on the depth of the snow covering the lake. Snow depth can also affect the fraction of radiation which is reflected from the snow surface and, hence, the energy available for transmittance (Baker et al. 1990, Gray and Landine 1987). Radiation transmitted through the snow and ice cover of a lake is an energy source for lake water temperatures and for photosynthesis of plants in a lake (Ellis and Stefan 1989). Winterkill of fish, or fish mortality resulting from oxygen depletion under lake ice, may indirectly result from a thick snow layer covering a lake. Snow removal from an ice surface has been used as a natural means of increasing oxygen levels through increased light penetration that boosts photosynthesis (Barica et al. 1983).

Snow depth data are useful for winter-lake water quality modeling, snowmelt modeling and winter lake management. Snow depth data may be used to validate the predictions of winter-lake snow and ice cover models and snowmelt models. They may also be used for predicting snowmelt runoff in watershed modeling. The amount of snow covering a lake may influence whether artificial lake aeration is used to help prevent winterkill.

In order to obtain unbiased, reliable snow depth data, it has been recommended that climate stations locate their snow courses in areas which are well protected from wind movement (Peck 1997). Snow depths measured on land in areas sheltered by forests or buildings, however, are often drastically different from snow depths measured in open areas, e.g. prairies. A study in Canada showed that snow depths measured on Knob Lake were much less than those measured on surrounding "open" land areas characterized by occasional trees and relatively abundant shrubs. The difference between mean snow depths of the lake and of the "open" areas was about 60 cm (Adams and Rogerson 1968).

Presented herein are snow depths measured on a small urban lake in Minnesota along with snow depths measured at the nearest National Weather Service station. The data are compared and tentative interpretations about the differences in data are given.

4.2 Data

4.2.1 Lake Measurements of Snow Depth

Snow depth measurements were taken during a winter field study conducted on Ryan Lake in northwest Minneapolis from December 17, 1996, to March 21, 1997. Average snow depth for a particular day was obtained from a circular snow course on the lake. The snow course encircled the instrumentation used during the field study. The instrumentation was located approximately 45 m from the shore of Ryan Lake. Twelve snow depth measurements were taken with a ruler at regular intervals around the circular snow course (radius about 6.1 m). These measurements were averaged to obtain an average snow depth for each day that a snow course was conducted. Average snow depths were obtained for 19 days during the study. These depths are shown in Table 4.1.

On two days, January 10 and 29, 1997, a linear snow course was also conducted. The linear snow course extended 165 m across the lake in a northwesterly direction from the instrumentation site. Snow depth measurements were taken every 5 m. The average snow depths for these two days are included in Table 4.1.

4.2.2 Land Measurements of Snow Depth

Snow depth data were obtained from the National Weather Service station at the Minneapolis-St. Paul International Airport which is located approximately 20 km from Ryan Lake. Snow depths were measured at random points on a vacant lot located in an area exposed to wind.

Snow depths were also obtained from a volunteer climate site located less than 5 km from Ryan Lake in New Hope, Minnesota. Snow depths were measured at the same location(s) throughout the winter in an area sheltered from the wind.

4.3 Results and Discussion

The lake snow depth data and the land snow depth data are plotted in Fig. 4.1. It is obvious from the graph that the depths measured on land are much greater than those measured on Ryan Lake. The differences between measurements on the lake and at the airport range from 2 to 37 cm, with an average difference between snow depths of 21 cm. The differences between measurements on the lake and at New Hope range from 10 to

Table 4.1. Snow depth data from Ryan Lake, 1996-1997.

Date	Average Snow Depth (cm)	Linear Snow Course Depth (cm)
12/17/96	2.5	
12/27/96	9.1	
12/31/96	8.9	
1/3/97	8.3	
1/6/97	7.6	
1/10/97	8.3	11.7
1/21/97	7.2	
1/23/97	9.2	
1/29/97	10.4	8.4
2/4/97	7.0	
2/11/97	5.9	
2/12/97	8.4	
2/19/97	2.6	
2/24/97	2.5	
3/3/97	0	
3/7/97	7.5	
3/18/97	4.5	
3/19/97	1.8	
3/21/97	0	

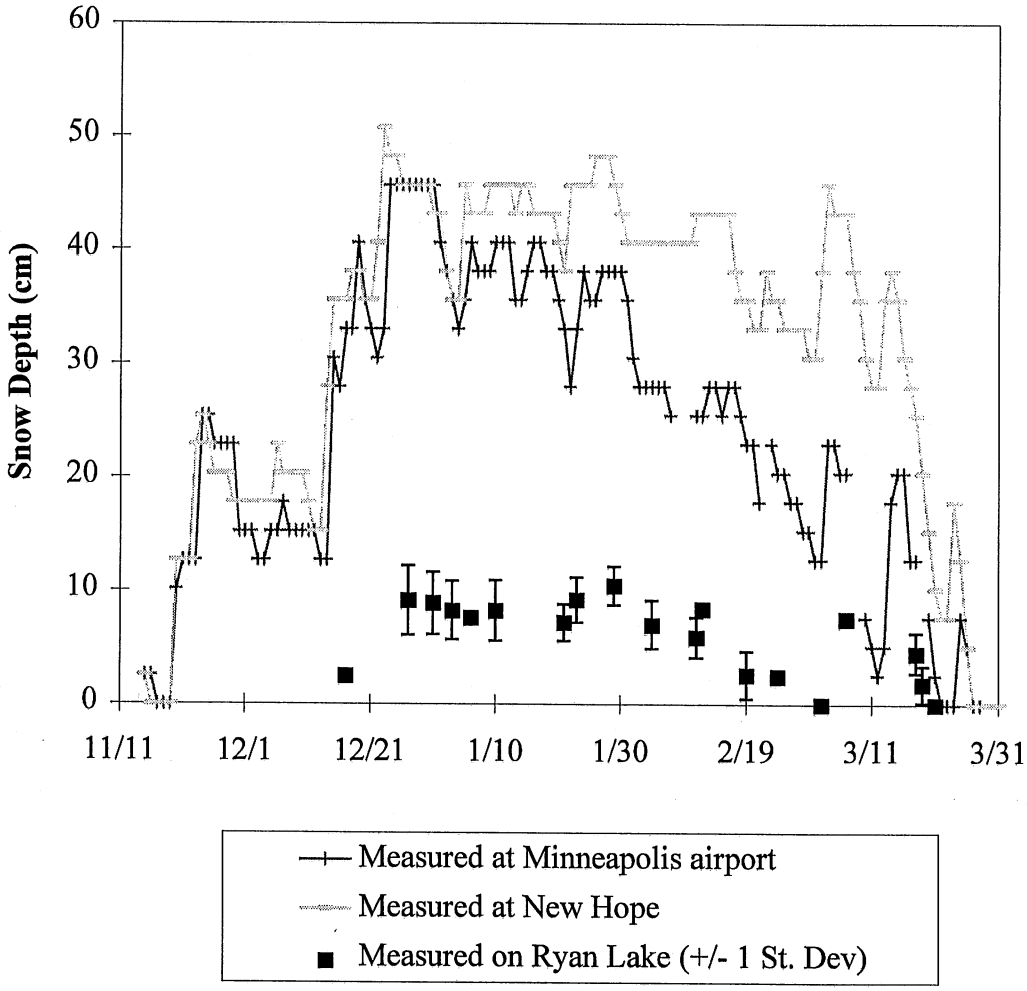

Figure 4.1 Snow depths measured at Minneapolis-St. Paul airport, New Hope volunteer climate site, and Ryan Lake during the winter of 1996-1997.

38 cm, with an average difference between snow depths of 32 cm. The standard deviations for the snow depth measurements along the circular snow course on Ryan Lake are included in Fig. 4.1 as error bars.

The most obvious cause for the dramatic difference in snow depths is wind sheltering. The relatively open area of a lake and its smooth surface make its snow cover susceptible to wind drifts. Snow is also more readily compacted when exposed to wind.

Another reason for the decrease in snow depths on a lake is the conversion of snow to white ice by the process of slushing as described in the introduction. This process decreases the snow depth while simultaneously increasing the ice thickness. Adams and Rogerson (1968) adjusted the snow depths measured on Knob Lake by the thickness of the white ice layer. Even then, they report that a large difference remained between snow depths measured in "open" areas and on the lake surface.

4.4 Conclusions

Snow depths are highly dependent on the terrain over which they are measured. Users of snow depth data obtained at climate stations need a method for adjusting those snow depth data to estimate snow depth on nearby lakes or in areas characteristically different from those where the snow depths were measured.

5. Field Observations and Photographs

Ryan Lake was visited throughout both winter field studies and observations were made on the lake cover and weather conditions at least once per week. The observations for the first field study, February 23 to March 15, 1996, are included in Table 5.1. More frequent and detailed observations were made during the second field study, December 17, 1996, to March 21, 1997, and these observations are listed in Table 5.2.

Photographs were taken during both winter field studies. Twenty-two representative photographs are included herein from the two studies. Each photo is clearly labeled.

Table 5.1 Field study observations for Ryan Lake, Minnesota. February 23 to March 15, 1996.

Day of Year	Date	Site Visit Time	Lake Cover	Avg. Snow Depth (cm)	Miscellaneous
53*	Feb. 22, 1996	17:00	Standing water on lake	< 5	1st day on lake
59	Feb. 28		Clean, powdery snow. Scattered drifts. Drifts around platform deeper than the rest.	2-10	
60	Feb. 29		No change in snow conditions		Data dumped since yesterday's attempt unsuccessful.
68	Mar. 8		Few scattered ice spots on lake. Snow packed under powdery top layer. Snow/ice mixture of ice.	0-2 away from equip.; 10-15 near base of equip.	Photos 1-4
75	Mar. 15		Water out from shore ~ 10 - 15 m. Slush covering lake with some standing water on ice.	0.0	Photos 5-8

*Ryan Lake was visited on highlighted days.

Table 5.2 Field study observations for Ryan Lake, Minnesota. December 17, 1996 to March 21, 1997.

Day of Year	Date	Site Visit Time	Lake Cover	Sky Cover	Weather	Instrumentation	Avg. Snow Depth (cm)	Comments
352*	Dec. 17, 1996	12:00					2.5	1st day on lake
362	Dec. 27	10:00	Snow covered with slightly wind-packed, dry snow. Powdery top layer. *Rough, snow-ice beneath snow.	100% cloud cover (cc)	Light snowfall in AM and early afternoon	No snow on any instrument. (2-3 frost flakes on upward-facing K&Z.) All level.	9.1	
365	Dec. 30			100% cc	Afternoon sleet/freezing rain			
366	Dec. 31	11:00		100% cc		Ice on instruments cleaned off with tissue	8.9	
3	Jan. 3, 1997	10:00	Snow has melted and compacted after a few days of below 0°C temp's. Snow is crystalline "sno-cone" ice. Milky snow-ice beneath snow.	100% cc	Late evening rain	Level and free of ice or frost	8.3	Footprints surround equip. (more under K&Z). Ice thickness = 19"
4	Jan. 4				Rain turned to sleet until late afternoon/early evening when light snow fell			
5	Jan. 5				Light snow in AM			Snow

*Ryan Lake was visited on highlighted days.

Table 5.2 (continued) Field study observations for Ryan Lake, Minnesota. December 17, 1996 to March 21, 1997.

6	Jan. 6	12:45	Light, powdery snow drifted across lake. Snow/ice ice below snow cover.	<5% cc		K&Z free of ice/snow. LICOR face free, but ice covers black portion surrounding white face.	7.6	Photos 9-11
7	Jan. 7			100% cc	No snow			
8	Jan. 8			Clear	Warmer temp's			
9	Jan. 9			100% cc	~11:00 light snow changing to flurries ~13:00			
10	Jan. 10	11:00	Clean, dry, powdery snow covers lake. Snow is not densely packed (easily moved). Some drifting and small ridges. Ice is milky, bubbly and, at places, grainy.	8:00/100% cc 11:00/10% cc	Snow in early morning. Winds from NW.		8.3	A straight snow course was conducted for ~ 165m.
21	Jan. 21	12:15	Dense, moist snow covers lake (snowball snow). Light wind, but snow remains packed. Ice is milky, white, rough snow/ice. (Some slush below upper snow layer.)	100% cc	Foggy	K&Z instruments had condensed liquid drops on them. Level on K&Z adjusted slightly. LICOR level.	7.2	Data @ 12:15 & 12:30 deleted due to fisherman standing underneath
22	Jan. 22				Snowfall beginning at ~10:00.			
23	Jan. 23	10:00	Light, powdery, dry snow over a crusty bottom layer. Ice very grainy, rough (Possibly frozen snow slush of 2 days earlier?)	90-100% cc	Snowfall from ~13:00 to 14:30	Cleaned frost off of upper K&Z. Cleaned all remaining.	9.2	

Table 5.2 (continued) Field study observations for Ryan Lake, Minnesota. December 17, 1996 to March 21, 1997.

24	Jan. 24			100% cc	Snowfall ~ 8:45 <50% cloud cover ~10:00			
28	Jan. 28			Clear				
29	Jan. 29	11:00	Slightly wet, snow cover crusty layer. Ice rough and milky.	100% cc; 12:30/40%; 13:30/clear	Both sensors free of ice/snow and level.		10.4	
32	Feb. 1			80-100% cc				
33	Feb. 2			0-20% cc				
35	Feb. 4	10:30	Snow crusty and well-packed; wet, granular; hard top layer (ice top layer in places). Ice milky, white (probably refrozen melted snow).	90-100% cc		Cleaned both sensors; K& Z had some moisture condensed on them. Both level.	7.0	Some footprints show only ice, i.e., snow melted.
36	Feb. 5			100% cc	9:00-10:00 - light snow drizzle			
37	Feb. 6	8:30	Snow as Feb. 4	90-100% cc; 12:00/10-20%		All sensors free of moisture, but wiped clean anyway.		
38	Feb. 7			8:00/100% cc; 12:00/80-90%; 13:00/40-50%	Light snowfall in AM which ends by 12:00			
39	Feb. 8			0-20% cc				
40	Feb. 9			0-10% cc				
41	Feb. 10			100% cc	Light snow in AM			
42	Feb. 11	11:50	Snow has rough surface and is crusty/ well-packed. <0.1" powdery snow over old snow. Granuals compsed of larger ice crystals frozen toether, still white, however. Ice is milky.	90-100% cc	Snow flurries in AM with intermittent light snow around noon.	Moisture droplets on K&Z. All level.	5.9	

Table 5.2 (continued) Field study observations for Ryan Lake, Minnesota. December 17, 1996 to March 21, 1997.

43	Feb. 12	10:00	Powdery, dry, newly fallen snow.	Clear		Ice crystals on K&Z dome.	8.4	Photos 12-14. Neglect data collected before 10:30 due to cleaning
44	Feb. 13			9:00/80-100% cc; 12:00/100%	Light snowfall from 14:00-16:30			
45	Feb. 14	9:00 % 11:15	Light powdery, drifted snow	8:00/100% cc; 9:00/clear; 11:15/60-80%	Light snow before 9:00	No frost on instruments, but cleaned. Levelled lower LICOR on 2nd visit.		
46	Feb. 15			100% cc	Light snow in evening			
47	Feb. 16			20-30% cc until ~ 13:00 then 100%				
48	Feb. 17	9:15	Snow packed and moist. Some very smooth and icy patches covering snow. Textured w/valleys (not really drifts) in snow. Ice cracks in places below snow.	70-80% cc; 11:00/100%; 14:00/50-60%		Small amount of moisture on both K&Z domes. All level.		
49	Feb. 18			10-20% cc in AM w/incr clouds in PM				
50	Feb. 19	10:30	Snow is well-packed where present. Open patches on lake where only ice is present. Milky, snow-ice.	Clear; 13:45/<10% cc		Clean and level	2.6	Photos 15-17.
51	Feb. 20			9:00/0-10% cc; 14:00/10-20%				

Table 5.2 (continued) Field study observations for Ryan Lake, Minnesota. December 17, 1996 to March 21, 1997.

52	Feb. 21			100% cc				
55	Feb. 24	AM	Dry, powdery snow and milky, white ice.	Clear		Few flakes of frost on K&Z. All level.	2.5	
56	Feb. 25	9:30	Snow cover as Feb. 24	Clear; 11:45/<10%cc	No frost and all level.			
57	Feb. 26			8:45/50%; 9:30/30%; 12:00/0-10%; 14:15/90-100%				
58	Feb. 27	8:30	Well-packed snow. Some ice patches show.	100% cc until 13:00; 14:00/50%; 15:00/30-40%; 16:30/70%	Snow flurries or light snow until 13:00	Clean and level.		
59	Feb. 28			100% cc	Snow flurries from AM changed to sleet by 14:20.			
62	Mar. 3	8:30	No snow. 95% of lake is bare ice; smooth and bumpy portions.	100% cc	Snow @ 13:30	Lower K&Z had a small piece of dirty ice on it. All instruments wiped clean (very little dust & no ice).	0	Under sensors there are places with white ice.
63	Mar. 4			100% cc	Very light snowfall @ 9:30 becoming heavier before ceasing in afternoon.			
64	Mar. 5			9:30/100% cc; 10:15/<20%	Light snowfall @ 9:30			
65	Mar. 6			0-10% cc				

Table 5.2 (continued) Field study observations for Ryan Lake, Minnesota. December 17, 1996 to March 21, 1997.

66	Mar. 7	10:30	Clean, powdery snow covers lake.	90-100% cc		No frost & minimal dust (but cleaned)	7.5	Possible battery problems & only dumped 2 days of data.
69	Mar. 10	12:15	Hard slush (water+ice+snow) covers lake. Water in places.	(AM clear) 90-100% cc		Cleaned of dust		Batteries changed
70	Mar. 11			Clear				
71	Mar. 12			90-100% cc (high alt.)				
72	Mar. 13			100% cc	8:00 - Light snowfall becoming heavy in afternoon.			
73	Mar. 14		Snow covers lake in drifts.	10-20% cc	Light snowfall in AM & windy.	Clean and level.		
76	Mar. 17			100% cc				
77	Mar. 18	8:15	Snow covers lake (packed on top). Wet snow	100% cc; 13:00/50-60%		Clean and level.	4.5	
78	Mar. 19	9:00	Wet snow & some bare, milky ice patches cover lake.	20-30% cc; 14:00/10-20%; 15:30/90-100%		Clean and level.	1.8	Photos 18-20. More footprints near K&Z than
79	Mar. 20	PM	Standing water on lake. Some snow patches remain.	9:00/10-20%; 11:00/80-90%; 16:20/50-60%				Photos 21-22. Storm sewer/drainage into lake flows
80	Mar. 21	PM	Standing water over slush.	9:15/80-100%; 10:00/20-30%; 13:00/100%			0	Removed equipment from lake.

Ryan Lake Photos

March 8, 1996 (Photos 1-4)

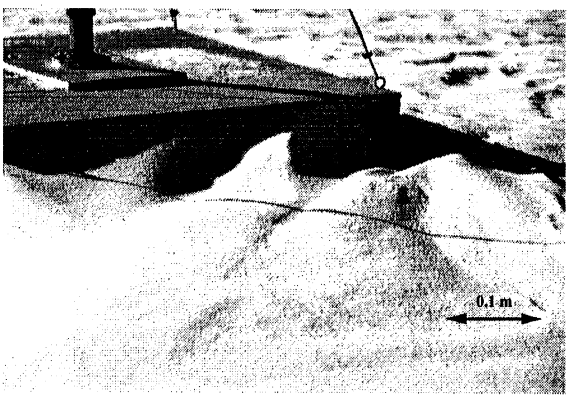

Photo 1. Drifted snow at base of equipment. Snow depth range: 10-15 cm near base.

Photo 2. Bare ice spots visible and snow is drifted. Snow depth range: 0-2 cm.

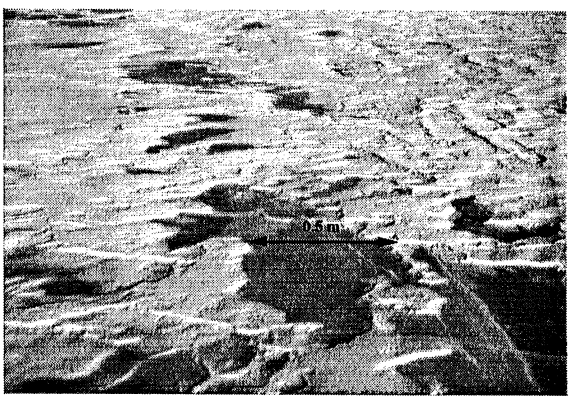

Photo 3. Closer view of bare ice spots in Photo 2.

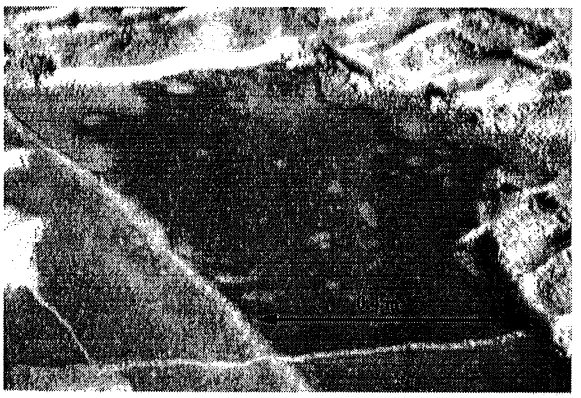

Photo 4. Zoom view of bare ice spot.

March 15, 1996 (Photos 5-8)

Photo 5. Water out from shore ~10 m.

Ryan Lake Photos

March 15, 1996 (Photos 5-8)

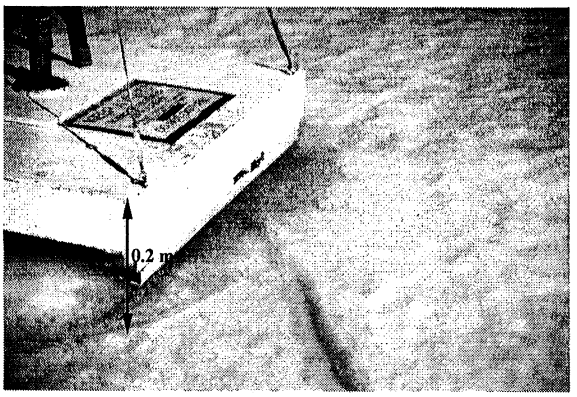

Photo 6. Slush mixture of snow, water, and ice near base of equipment. Slush mixture 7-8 cm deep.

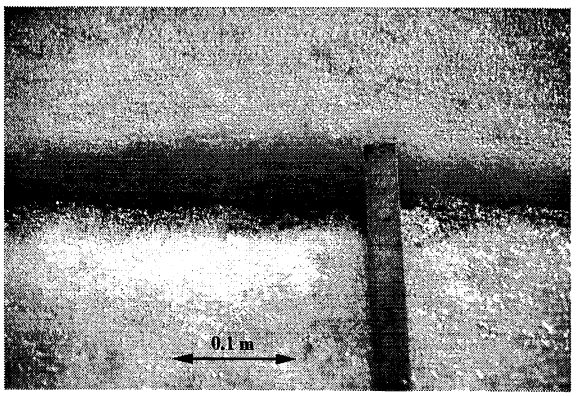

Photo 7. Crack in ice and slush.

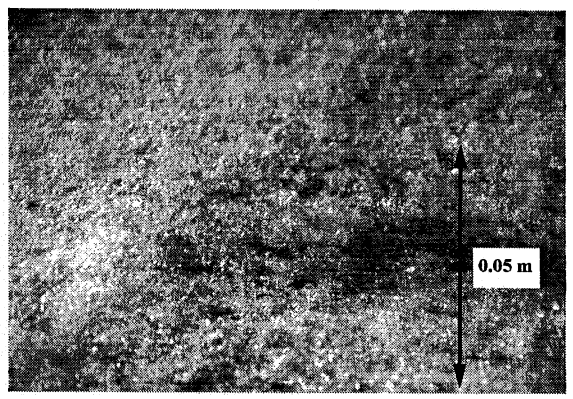

Photo 8. Zoom view of ice/snow mixture.

January 6, 1997 (Photos 9-11)

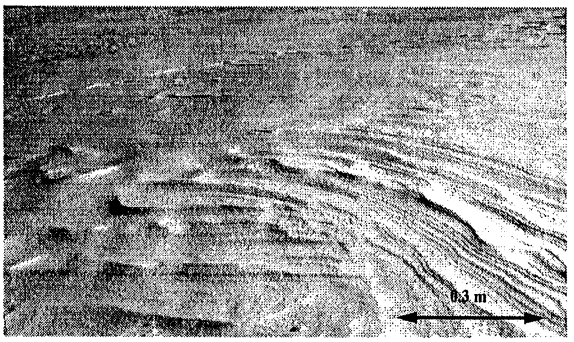

Photo 9. Light, powdery snow drifted across lake. Average snow depth ~8 cm.

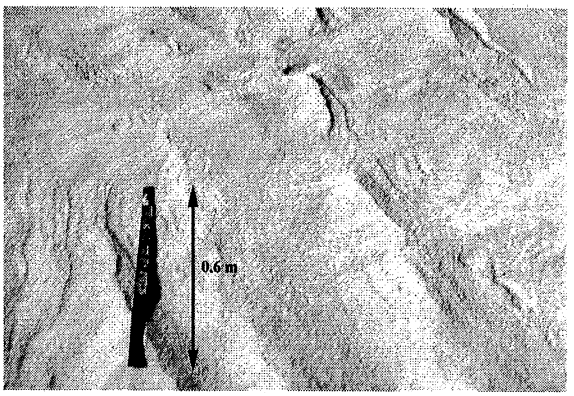

Photo 10. Note wind-blown snow cover.

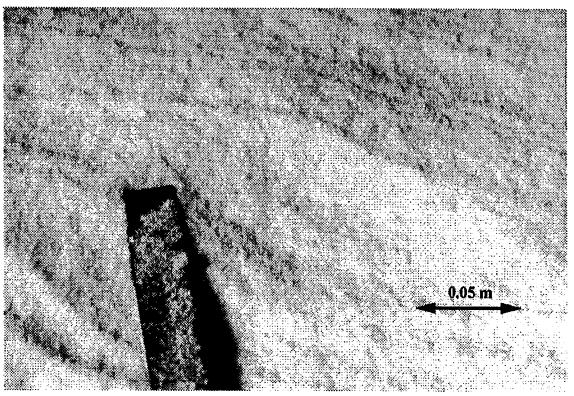

Photo 11. Zoom view of snow.

Ryan Lake Photos

February 12, 1997 (Photos 12-14)

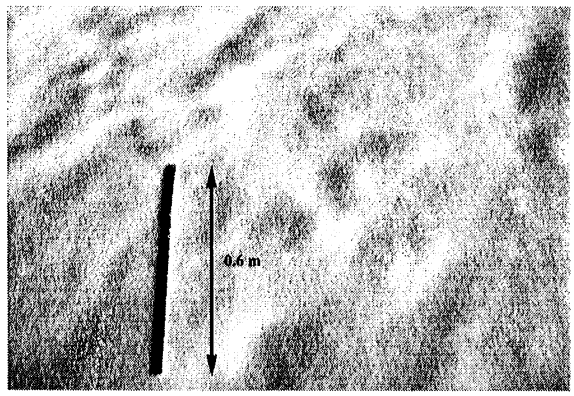

Photo 12. New snow cover. Average snow depth ~ 8 cm.

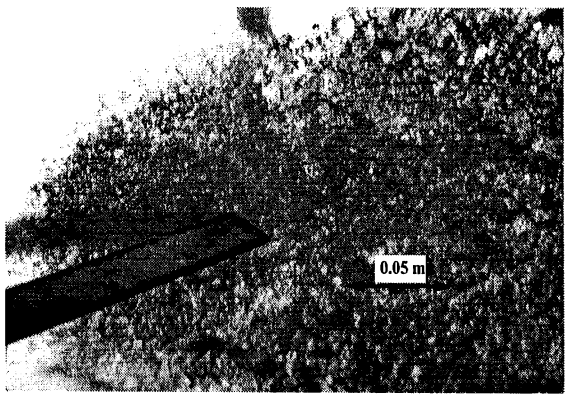

Photo 13. Ice below manually removed snow. Large ice granules.

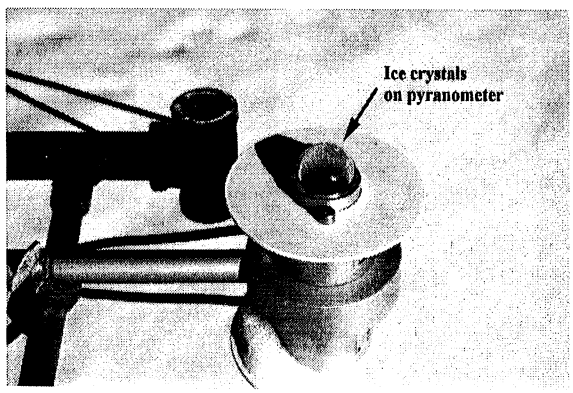

Photo 14. Ice crystals cover the surface of the Kipp and Zonen pyranometer. The ice was removed before 10:00 am.

February 19, 1997 (Photos 15-17)

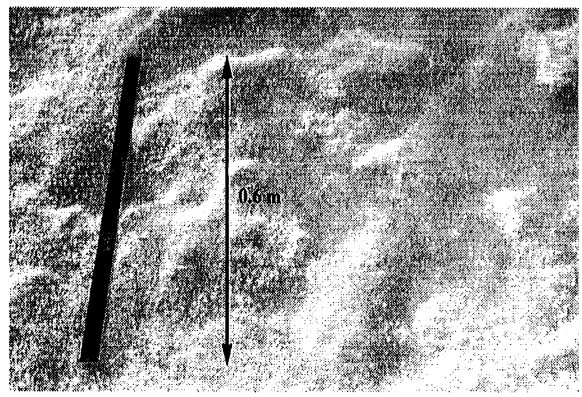

Photo 15. Milky, snow-ice patches and some snow.

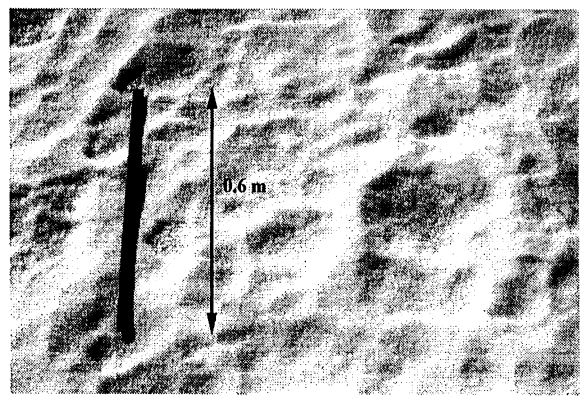

Photo 16. Well-packed snow, where present. Average snow depth ~3 cm.

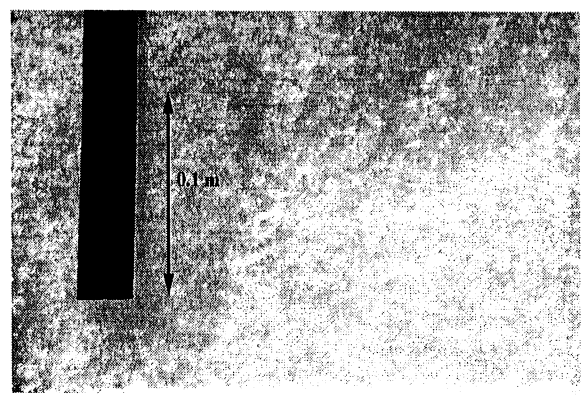

Photo 17. Zoom view of snow-ice.

Ryan Lake Photos

March 19, 1997 (Photos 18-20)

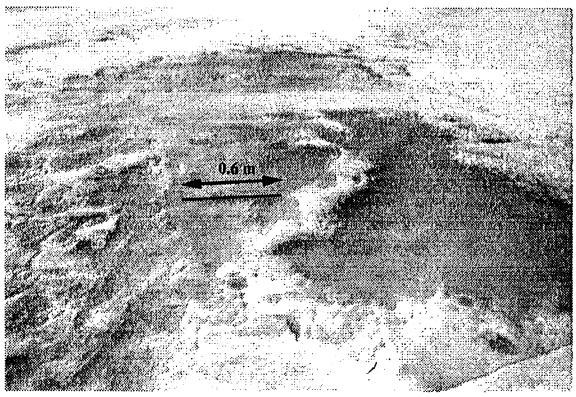

Photo 18. Wet snow and some bare, milky ice patches cover lake.

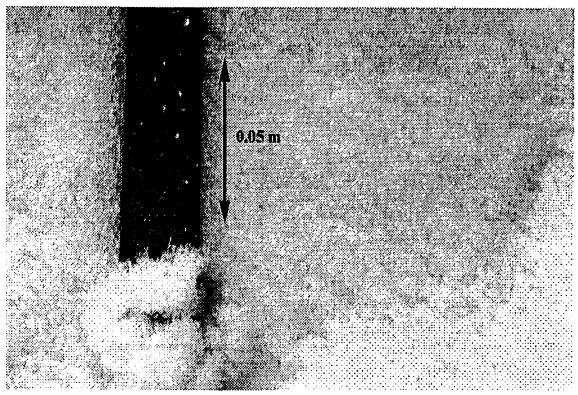

Photo 19. Zoom view of snow. Note water droplets on ruler. Average snow depth ~2 cm.

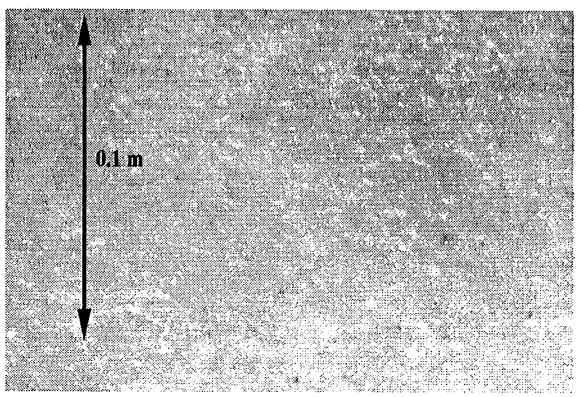

Photo 20. Zoom view of milky ice. Note dirt particles in ice.

March 20, 1997 (Photos 21-22)

Photo 21. Storm water inflow melted a snow in the near shore snow and ice cover.

Photo 22. Standing water on lake. A few snow patches remain with depths less than 1 cm.

References

Adams, W. P., and R. J. Rogerson, 1968. Snowfall and snowcover at Knob Lake, Central Labrador-Ungava. *In:* Proceedings of the Annual Eastern Snow Conference Meeting, Boston, Massachusetts, pp. 110-139.

Baker, D. G., and D. L. Ruschy, 1988. Historical albedo values at St. Paul, Minnesota, 1969-85. *Journal of Applied Meteorology* 27:244-253.

Baker, D. G., and D. L. Ruschy, 1989. Winter albedo characteristics at St. Paul, Minnesota. *Journal of Applied Meteorology* 28(3):227-232.

Baker, D. G., D. L. Ruschy and D. B. Wall, 1990. The albedo decay of prairie snows. *Journal of Applied Meteorology* 29(2):179-187.

Barica, J., J. Gibson, and W. Howard, 1983. feasibility of snow clearing to improve dissolved oxygen conditions in a winterkill lake. *Canadian Journal of Fisheries and Aquatic Sciences* 40:1526-1531.

Bergen, J. D., B. A. Hutchinson, R. T. McMillen, A. D. Ozmenty, and G. J. Gottfried, 1983. Observations on the relation of the shortwave reflectivity of recently deposited snow to its physical properties. *Journal of Climate and Applied Meteorology* 22:193-200.

Bolsenga, S. J., 1969. Total albedo of Great Lakes ice. *Water Resources Research* 5(5):1132-33.

Bolsenga, S. J., 1977. Preliminary observations on the daily variation of ice albedo. *Journal of Glaciology* 18(80):517-521.

Choudhury, B. J., 1979. Radiative properties of snow for clear sky solar radiation. Report CSC/TR-79/6025, Computer Science Corporation, Silver Spring, MD.

Conway, H. A. Gades, and C. F. Raymond, 1996. Albedo of dirty snow during conditions of melt. *Water Resources Research* 32(6):1713-1718.

Curry, J. A., J. L. Schramm, and E. E. Ebert, 1995. Sea ice-albedo climate feedback mechanism. *Journal of Climate* 8:240-247.

Dirmhirn, I., and F. D. Eaton, 1975. Some characteristics of the albedo of snow. *Journal of Applied Meteorology* 14:375-379.

Ellis, C. R., and H. G. Stefan, 1989. Oxygen demand in ice covered lakes as it pertains to winter aeration. *Water Resources Bulletin* 25(6):1169-1176.

Fang, X., and H. G. Stefan, 1996a. Long-term lake water temperature and ice cover simulations/measurements. *Cold Regions Science and Technology* 24:289-304.

Fang, X., and H. G. Stefan, 1996b. Development and validation of the water quality model MINLAKE96 with winter data. Project Report No. 390, St. Anthony Falls Laboratory, University of Minnesota, Minneapolis, MN.

Gates, D. M., 1962. *Energy Exchange in the Biosphere*. Harper & Row, New York, 151 pp.

Gray, D. M., and P. G. Landine, 1987. Albedo model for shallow prairie snow covers. *Canadian Journal of Earth Sciences* 24:1760-1768.

Grenfell, T. C., S. G. Warren, and P. C. Mullen, 1994. Reflection of solar radiation by the Antarctic snow surface at ultraviolet, visible and near-infrared wavelengths. *Journal of Geophysical Research* 99(D9):18,669-18,684.

Gu, R. and H. G. Stefan, 1990. Year-round temperature simulation of cold climate lakes. *Cold Regions Science and Technology* 18(2):147-160.

Henneman, H. E., and H. G. Stefan, 1997a. Albedo decay models for snow and ice on a freshwater lake. Submitted to *Journal of Applied Meteorology.*

Henneman, H. E., and H. G. Stefan, 1997b. Pyranometer comparison study. Submitted to *Cold Regions Science and Technology.*

Male, D. H., and D. M. Gray, 1981. Snowcover ablation and runoff. *In*: Handbook of snow: Principles, Processes, Management & Use. D. M. Gray and D. H. Male (Editors), Pergamon Press, Toronto.

Male, D. H., and R. J. Granger, 1981. Snow surface energy exchange. *Water Resources Research* 17(3):609-627.

Mullen, P. C., and S. G. Warren, 1988. Theory of the optical properties of lake ice. *Journal of Geophysical Research* 93(D7):8403-8414.

Nagaraja Rao, C. R., 1984. Photosynthetically active components of global solar radiation: measurements and model computations. *In.* Archives for Meteorology, Geophysics, and Bioclimatology Series B, 34(4):353-364.

Nelson, W. G., 1990. Formation and growth of lake ice. *In:* Cold Regions Hydrology and Hydraulics, L. W. Ryan and R. D. Crissman (Editors), American Society of Civil Engineers, pp. 459-467.

O'Neill, A. D. J., and D. M. Gray, 1973. Spatial and temporal variations of the albedo of prairie snowpack. *In*: The Role of Snow and Ice in Hydrology: Proceedings of the Banff Symposium. Sept. 1972, UNESCO - WMO-IAHS, Geneva-Budapest-Paris, Vol 1, pp. 176-186.

Peck, E. L., 1997. Quality of hydrometeorological data in cold regions. *Water Resources Bulletin* 33(1):125-134.

Perovich, D. K., 1994. Light reflection from sea ice during the onset of melt. *Journal of Geophysical Research* 99(C2):3351-3359.

Perovich, D. K., G. A. Maykut, and T. C. Grenfell, 1986. Optical properties of ice and snow in the polar regions, I: Observations. *In.* Proceedings SPIE Ocean Optics VIII 637:232-241.

U. S. Army Corps of Engineers, 1956. *Snow Hydrology.* North Pacific Division, Corps of Engineers: Portland, Oregon, 437 pp.

Warren, S. J., 1982. Optical properties of snow. *Reviews of Geophysics and Space Physics* 20(1):67-89.

Warren, S.G., and W.J. Wiscombe, 1980. A model for the spectral albedo of snow. II. Snow containing atmospheric aerosols. *Journal of Atmospheric Sciences* 37:2734-2745.

Wiscombe, W. J., and S. G. Warren, 1980. A model for the spectral albedo of snow. I. Pure snow. *Journal of Atmospheric Sciences* 37:2712-2733.

APPENDIX A

Albedo Models for Snow and Ice on a Freshwater Lake

by

Heather E. Henneman and Heinz G. Stefan

ALBEDO MODELS FOR SNOW AND ICE ON A FRESHWATER LAKE

by

Heather E. Henneman and Heinz G. Stefan
University of Minnesota, St. Anthony Falls Laboratory
Department of Civil Engineering, Minneapolis, MN 55414

ABSTRACT: Snow and ice albedo measurements were taken over a freshwater lake in Minnesota for three months during the winter of 1996-97 for use in a winter lake water quality model. The mean albedo of new snow was measured as 0.83 ± 0.028, while the mean ice albedo was measured as 0.38 ± 0.033. The period from December 17, 1996 to February 17, 1997, was marked as the nonmelt, or high albedo, season when albedo decayed at an average rate of 0.02 per day. The melting, or rapid albedo decay, season began on February 18 and continued until the end of the study on March 21. During the melt season the albedo decay rate varied from 0.10 to 0.20 per day.

Two albedo models were developed for the entire winter season; they use separate equations for the nonmelt and melt periods. The input data for both models are readily available climatic data. The first model requires daily incident solar radiation, air temperature, and snowfall data as input, while the second model requires daily air temperature and snowfall data only. The first model predicts albedo with a modeling efficiency of 0.94 for the entire three month period, and the second model predicts albedo with a modeling efficiency of 0.89. The mean absolute error between values observed on the lake surface and values predicted by the model was 0.023 for the first model and 0.029 for the second model.

Albedo predictions made by three albedo models given in the literature were also compared to the observed lake surface data. The two models developed herein predicted albedo better than the three existing surface albedo models because the two new models were calibrated to the observed lake surface data.

Albedo predictions from both new models and the three existing models were also compared to 11 years of observed surface albedo data collected over land. (No other lake surface observations were available.) The new models reasonably predicted albedo during those winters when the total snowfall depth was greater than 60 cm. The new model predictions for the land data were as good, if not better, than those by the three existing models.

1. Introduction

Radiation transmitted through the ice and snow cover of a lake is an energy source for lake water temperatures and for photosynthesis of plants in the lake (Ellis and Stefan 1989). The fraction of incident radiation transmitted through the ice and snow cover depends in part on the depth of these covers and on the albedo of the snow and/or ice. Deterministic year-round lake water quality simulation models, such as MINLAKE95 (Fang and Stefan 1996), use albedo in the winter energy balance to help predict ice cover growth over fresh water lakes (Gu and Stefan 1990). Because the ice is at times snow-covered during the winter months, albedo values for both ice and snow are needed in the models.

What particular values to use for snow and ice albedos is not easily determined. Research on surface albedo has been conducted for decades, and a wide range of albedo values have been reported for snow and ice. Albedos for freshly fallen, dry snow on land typically range from 0.80 to 0.87 (Perovich 1986; Baker et al. 1990; Conway et al. 1996). Melting snow albedo values decrease to values below 0.50 (U.S. Army Corps of Engineers 1956). Ice albedos, depending on the ice type, are reported to vary from 0.10 to 0.58 (Bolsenga 1977; Perovich 1986).

Given the broad range of albedo values, an albedo decay model in place of constant values may be more appropriate for use in the surface energy budget of a winter lake. Several such models exist, however, it is not apparent which of the albedo models found in the literature should be used for a freshwater lake. A summary of some of the available snow albedo models found in the literature is given in Table 1.

Of the existing snow albedo models, a number are empirical models which require easily obtainable climatic data (Gray and Landine 1987; Kondo and Yamazaki 1990; Baker et al. 1990; Winther 1993; Rogers et al. 1995); however, the albedos predicted by these models for freshly fallen snow range from 0.84 to over 0.90. Most of the existing empirical models were developed for snow over land, not for snow over a lake. Also, empirical albedo models are generally developed for only a portion of the winter season. Theoretical, or physically-based, spectral albedo models (Wiscombe and Warren 1980; Choudhury and Chang 1981) often require multiple inputs, some of which are not readily available to a water quality or snowmelt modeler. Snow albedo models developed for use on a large or even global scale (Lindsay and Rothrock 1994; Marshall and Oglesby 1994), at times, require satellite input data and may not be suitable for use over a comparatively small-scale lake.

An all-winter albedo model requiring readily available input data was needed for use with a year-round winter lake water quality model. On the following pages we describe a field study which was conducted to measure the albedo of the snow and/or ice cover of a freshwater lake, and how the data obtained were used to develop two albedo decay models. An error analysis section is included in which both models are evaluated. Additionally, the predictions of the two albedo models are compared to 11 years of winter surface albedos measured over land. Also presented are the comparisons of the two albedo models with three snow albedo models found in the literature.

2. Background

Total, or spectrally integrated, albedo (α_t) is defined as (Perovich 1996)

$$\alpha_t = \frac{\int \alpha(\lambda) F_d(0,\lambda) d\lambda}{\int F_d(0,\lambda) d\lambda} \quad (1)$$

where

$\alpha(\lambda)$ = spectral albedo at wavelength $\lambda = \frac{F_u(\lambda)}{F_d(\lambda)}$

$F_u(\lambda)$ = upwelling spectral irradiance from the surface

$F_d(\lambda)$ = downwelling spectral irradiance, or radiance integrated over downward directions

$F_d(0,\lambda)$ = downwelling irradiance at the surface (0 designates surface)

Equation 1 basically states that albedo is the ratio of reflected to incident solar energy. The limits of integration for total albedo, hereafter referred to only as albedo, depend upon the response of the measuring device.

The albedo of a surface depends on both the reflective properties of that surface and on atmospheric parameters which can alter the spectral distribution of incident irradiance. The reflective properties of snow vary widely depending on wetness, impurities (Conway et al. 1996), snow grain size (Grenfell et al. 1994), density and composition, and surface roughness (Dirmhirn and Eaton 1975). The albedo of snow has been more widely studied than that of ice; however, many of the determinants of snow albedo may also be applicable to ice albedo. The reflective properties of lake ice have been found to depend on the bubble content of ice (Mullen and Warren 1988); ice type, e.g., white ice, clear ice, or refrozen slush (Bolsenga 1977, 1983); surface roughness; and

ice thickness (Mullen and Warren 1988; Bolsenga 1983). Parameters affecting incident radiation include solar angle (Dirmhirn and Eaton 1975; Warren 1982); cloud characteristics, e.g., thickness and distribution (Male and Granger 1981; Warren 1982); and atmospheric parameters like precipitable water and turbidity.

Snow and ice albedos have been observed to undergo both daily variations and long term decay. Albedo decay has previously been studied on snow-covered land (U.S. Army Corps of Engineers 1956; Dirmhirn and Eaton 1975; Baker et al. 1990), on sea ice (Curry et al. 1995) and on freshwater ice (Bolsenga 1977). Long-term albedo decay trends for deep snowpack (U.S. Army Corps of Engineers 1956) and shallow snowpack (O'Neill and Gray 1973) indicate that the decay for shallow snowpack is much more rapid than that for deeper snow because of the influence of the lower albedo of the ground beneath the shallow snow.

Baker and Ruschy (1988, 1989) collected and analyzed a 19-year time series of prairie snow albedo data from Minnesota. They found three distinct albedo "seasons" during the months of November to April: (1) introduction to winter, or accumulation season, when snowfalls begin to occur with low frequency and duration, (2) the high albedo season when fresh snow usually exists on the ground, and (3) a transitional, or melt, period in the late winter and early spring characterized by periods of snowmelt. They also found similarities between albedo decay during the accumulation and melt seasons (Baker et al. 1990). Gray and Landine (1987) further broke down the melting period of prairie snow covers and the corresponding decreases in albedo into premelt,

melt and postmelt periods. All three of these melt periods occur during the third albedo period noted by Baker and Ruschy.

3. Field Study/Data Collection

A three-month (December 17, 1996 - March 21, 1997) field study was conducted on Ryan Lake, Minnesota, in order to measure the albedo of the snow and/or ice cover of this lake. Ryan Lake (45°N, 93°W) is located in the northwest area of Minneapolis, Minnesota. It has a surface area of 6.1 ha, a mean depth of 5.0m, and a maximum depth of 10.0m.

The radiation sensors used were Kipp & Zonen CM3 pyranometers which are sensitive to wavelengths of about 0.3 to 2.8 μm. Two pyranometers were used in the study, one for incident radiation and the other for reflected radiation. The instruments were checked against each other to see that they measured the same amount of solar radiation. The measurements were within ±2% prior to the beginning and after the conclusion of the field study. At the field study site the pyranometers were mounted horizontally with one facing upward and the other downward. The latter was mounted 1.60 m above the lake surface to avoid shading effects and to promote spatial averaging. The equipment was placed about 40 meters from the eastern shore of the lake. This location was easily accessible from shore, and the ice and snow conditions were representative of the lake surface.

Incident and reflected radiation were measured throughout the field study at one-minute intervals. These one-minute measurements were averaged and stored every 15

minutes by a Campbell Scientific CR10 data logger. Along with the radiation measurements, air temperature measurements were taken at a height 2.2 m above the lake surface. As with the radiation measurements, the 15-minute record of air temperature represented an average of values taken over that time period. In addition to these continuous measurements, observations of snow depth and lake cover conditions were made two to three times per week during the study.

The faces of the pyranometers were checked during each site visit to insure that snow and/or ice was not collecting on the upright pyranometer. The deposition of snow could result in the reduction of incident radiation measured and, therefore, cause an abnormal increase in albedo. When ice or snow did accumulate on either pyranometer, the equipment was carefully cleaned. The equipment was ice or snow-covered for seven of the 95 days of the field study, and the data from those days were eliminated from the analysis. The eliminated days were December 22 and 23, 1996, January 4 and 5, February 22, and March 3 and 4, 1997.

4. Data

Figure 1 gives the incoming solar radiation, maximum and minimum air temperatures, snowfall and albedo for each day of the study. Average daily albedo was calculated by dividing the total daily reflected solar radiation by the total daily incoming solar radiation. Total daily incoming and reflected solar radiation values were obtained by integrating the 15-minute radiation measurements over the daylight hours.

The albedo increased after each new snowfall. The average new snow albedo was 0.83 $\pm$ 0.028. Increases in albedo are most obvious near the end of the field study when three peaks in albedo correspond to three snowfall events in late February and early March. Also apparent in Fig. 1 are the rapid decreases in albedo following the aforementioned albedo peaks.

In Figure 2 the measured albedo values are reproduced with a higher resolution, and the average daily air temperatures are shown for each day of the study. Two of the three albedo "seasons" noted by Baker and Ruschy (1988, 1989) are apparent in Fig. 2. The high albedo season, or nonmelt season, when average daily air temperatures generally remained below 0°C, occurred from December 17, 1996, to February 17, 1997. The albedo decayed during this period at a rate of about 0.02 per day. The remainder of the study period, from February 18 to March 21, 1997, appears to be in the transitional, or melt, season. Four distinct events of rapid albedo decay occurred during the melt period, which was characterized by a number of days with average daily air temperatures above 0°C and the melting of the existing snow cover. Albedo decreased at a rate of 0.10 to 0.20 per day during the melt period. The average minimum value of surface albedo was 0.38 $\pm$ 0.033, which was measured during times when no snow covered the lake ice. The periods of melt and nonmelt are indicated in Fig. 2.

5. Model Development

In order to model daily albedo decay, the data were divided into a nonmelt decay period and a melt decay period. Initially, an analysis was performed over the entire

period of study without dividing the data into these two periods. However, the resulting albedo model did not capture the rapid decay in albedo which occurred during the final weeks of the field study. Therefore, the data were divided into two periods.

December 17, 1996 to February 17, 1997, was designated the nonmelt period, while the remainder of the study period until March 21, 1997, was considered the melt period (Fig. 2). A change in the albedo curve was evident near February 17, when albedo began to decay at a more rapid rate than earlier in the study. The decision to start the melt period on February 17 was made based upon air temperature data and upon the obvious change in the rate of albedo decay after this date. During the nonmelt decay period the average daily air temperatures generally remained below $0^{\circ}C$, and the decay of albedo was slow. The melt decay period was characterized by maximum daily air temperatures above $0^{\circ}C$ for the majority of the days and a substantial or complete melting of the snow cover.

The duration of the nonmelt and melt periods will vary by the location of the site to be modeled and the meteorological conditions at that site. When to begin the rapid decay, or melt, period is discussed further in the model application section of the paper.

A correlation analysis between albedo and a number of climate variables was performed for the entire study period and for both the nonmelt and melt periods separately. The Pearson correlation coefficient was calculated between albedo and the following variables: incident solar radiation, accumulated solar radiation, air temperature, accumulated air temperature, days after snowfall and fractional cloud cover. (Fractional cloud cover was measured at the Minneapolis-St. Paul International Airport

and was obtained from the Minnesota State Climatology Office.) The choice of these variables as possible predictors of albedo was made based primarily on previously developed albedo models (See Table 1.). Also, easily obtainable or calculated input data were preferred for the albedo model. The Pearson correlation coefficients for the nonmelt period, the melt period, and the entire field study period are shown in Table 2.

The accumulation of solar radiation and of air temperature restarted on each new snowfall day. A new snowfall day is one on which the snowfall is greater than 2.5 mm (0.1 in), i.e., a snowfall greater than a trace snowfall. On a snowfall day the accumulated solar radiation (MJ m^{-2} day^{-1}) is set to the total daily incident radiation for that day. The accumulated solar radiation for each subsequent day is then calculated by simply adding the total daily incident radiation to the previous day's accumulated solar radiation until the next new snowfall day. Accumulated air temperature is calculated using a degree day method with a calibrated base temperature, T_{base}. A temperature index, T_{index}, for each day is calculated from

$$\mathbf{T_{index} = T_{air} - T_{base}} \qquad \mathbf{(2)}$$

where

T_{air} = average daily air temperature (°C)

T_{base} = -18°C.

On each new snowfall day the accumulated air temperature is set to the temperature index for that day. As with accumulated solar radiation, the accumulated temperature is calculated for each day by adding the temperature index for that day to the accumulated temperature from the previous day.

The strongest correlations shown in Table 2 are between albedo and three variables: accumulated solar radiation, accumulated temperature, and days after snowfall. During the nonmelt period the highest negative correlations are between albedo and accumulated solar radiation and between albedo and days after snowfall. However, during the melt season the strongest correlation by far is between albedo and accumulated temperature. Since days after snowfall is itself highly correlated with accumulated solar radiation and accumulated air temperature, a regression analysis was not performed using all three of these variables. Rather, two separate sets of analyses were performed, resulting in two albedo models. One model predicts albedo based on accumulated solar radiation and accumulated air temperature, while the second model predicts albedo based on days after snowfall.

Air temperature is accounted for in the albedo models in the following manner. During the nonmelt period, one equation describes the albedo decay for all air temperatures. However, during the melt period the albedo is described by two equations: one for average air temperatures greater than $0^{o}C$ and a second for average air temperatures less than $0^{o}C$.

Theoretically, albedo should also depend on cloud cover since clouds affect the incident solar radiation. Clouds absorb a higher portion of infra-red than visible radiation. Thus, a relatively high portion of visible radiation reaches the surface under cloudy conditions. Because the visible snow albedo is high (> 0.90) compared to the near-infra-red albedo (~ 0.50), an increase in surface albedo is to be expected during overcast weather (Male and Granger 1981; Warren 1982). However, available cloud

cover data are usually restricted to fractional cloud cover. Without data on optical cloud depth and other cloud parameters, it is difficult to relate cloud cover to surface albedo. The correlation coefficient between albedo and cloud cover was insignificant (< 0.3), and the addition of cloud cover to either of the following two models was not useful in simulating albedo.

a. Model 1

Equations 3 to 5 represent Model 1 and predict albedo over the entire study period. The model requires average daily air temperature, accumulated solar radiation and accumulated air temperature as inputs. Daily snowfall data are also required. Equation 3 predicts albedo decay during the nonmelt period (December 17, 1996 to February 17, 1997, in the Ryan Lake study), and Eqs. 4 and 5 predict albedo during the melt period (February 18 to March 21, 1997, in the Ryan Lake study). On snowfall days the albedo was set to 0.83 for either the nonmelt or melt period. Additionally, the minimum albedo, which depends upon the surface beneath the snow layer, was limited to the value 0.38.

Nonmelt Period:

For all T_{air} values:

$$\alpha = -0.0015R + 0.84 \qquad (3)$$

Melt Period:

For $T_{air} > 0^{o}C$:

$$\alpha = 0.0029R - 0.009T + 0.95 \quad (4)$$

For $T_{air} \leq 0^{o}C$:

$$\alpha = \alpha_{-1} - 0.00036T \quad (5)$$

α_{min} = minimum albedo = 0.38

α = daily albedo

α_{-1} = albedo on previous day

R = accumulated incoming daily solar radiation since last snowfall (MJ m^{-2})*

T = accumulated daily air temperature index since last snowfall (^{o}C)*

T_{index} = daily air temperature index = $T_{air} - T_{base}$

T_{air} = average daily air temperature (^{o}C)

$T_{base} = -18^{o}C$

*Solar radiation and temperature begin accumulating after a snowfall greater than 2.5 mm (0.1 in).

b. Model 2

Model 2 requires only snowfall and average air temperature data to predict albedo. Equation 6 predicts albedo during the nonmelt period, and Eqs. 7 and 8 predict albedo during the melt period. The albedo is set to 0.83 for snowfall days and the minimum albedo is 0.38.

Nonmelt Period:

For all T_{air} values:

$$\alpha = -0.011d + 0.83 \quad (6)$$

Melt Period:

For $T_{air} > 0^{o}C$:

$$\alpha = \alpha_{-1} - \mathbf{0.17} \tag{7}$$

For $T_{air} \leq 0^{o}C$:

$$\alpha = \alpha_{-1} - \mathbf{0.013} \tag{8}$$

d= number of days after snowfall

6. Model Fit and Error Analysis

Error analyses were performed on both models with the results shown in Table 3. Model 1 predicts albedo over the entire three-month period with a modeling efficiency (EF) of 0.94, while Model 2 predicts albedo with an EF of 0.89. The root mean square error (RMSE) and mean absolute error (MAE) are 0.031 and 0.023, respectively, for Model 1. For Model 2 the RMSE is 0.042, and the MAE is 0.029.

Modeling efficiency is a dimensionless statistic which directly relates model predictions ($\hat{y}$) to observed data (y) and is defined as:

EF = 1 – (Sum of squares about $y = \hat{y}$)/(Corrected sum of squares of y)

$$= 1 - \sum(y_i - \hat{y}_i)^2 / \sum(y_i - \bar{y})^2 \tag{9}$$

where

$\bar{y}$ = average observed value.

Modeling efficiency is an overall indicator of goodness of fit. Negative values are possible since predicted data are compared with the fixed line $y = \hat{y}$; however, any model

giving a negative value cannot be recommended. The closer EF is to one, the better the model fit.

Figures 3a and 3b show albedos simulated by Model 1 and Model 2, respectively, against the observed albedo data. A one to one line is included on each graph for comparison. The goodness of fit of Model 1 is 0.94, and the goodness of fit for Model 2 is 0.89. When the two points highly overpredicting albedo (Figs. 3a and 3b) are included in the error analysis, the goodness of fit is 0.71 for Model 1 and 0.68 for Model 2. Although these are significantly lower EF values, they do indicate that the models still reasonably predict albedo.

The two outlying days, March 1 and 2, followed a snowfall day on which albedo was predicted as 0.83. The average air temperature remained below 0°C on these two days. Therefore, Model 1 predicted an albedo decay of about 0.015 per day, and Model 2 predicted a decay rate of 0.013 per day. The observed albedo, however, decreased on these days at a rate of about 0.20 per day, a much more rapid decay than predicted by either model. One reason for the discrepancy between observed and simulated albedo may have been that only a small amount of snow fell (5 mm) on February 28. The snow probably melted quickly by radiative energy, resulting in a rapid albedo decay, but the models could not account for this at air temperatures below 0°C. It may be necessary to add another snowfall depth criterion to the model; however, this data set includes only one such small snowfall occurrence during the melt period which is insufficient for making a definite conclusion about albedo response to small snowfall depths during the melt period.

In order to determine what minimum snowfall depth best signaled an increase in albedo, another set of regression analyses was performed. New snowfall periods were defined at different depths of snowfall greater than 2.5 mm. The additional new snowfall depths tested were 5, 10 and 25 mm. The results of these analyses showed that the highest model EF and lowest model errors were for new snowfalls marked by any depth greater than 2.5 mm.

Equations 3 and 5 (Model 1) require only accumulated solar radiation and accumulated air temperature, respectively. Neither the addition of an accumulated air temperature term to (3) nor the addition of an accumulated solar radiation term to (5) increased the modeling efficiency of Model 1. However, the addition of the accumulated air temperature term in (4) increased the modeling efficiency dramatically from 0.38 to 0.94.

Albedo values for the nonmelt period were further analyzed to determine whether either model was improved by differentiating between air temperatures above or below $0^{o}C$. The analysis showed that the use of two equations during the nonmelt period (one for air temperatures greater than $0^{o}C$ and one for air temperatures less than $0^{o}C$) did not decrease albedo model errors or increase modeling efficiency. Therefore, only one equation is used during the nonmelt period in each model.

7. Model Applications

a. Determination of Nonmelt and Melt Periods

That albedo decays over time at substantially different rates has previously been documented (Gray and Landine 1987; Baker and Ruschy 1988, 1989; Winther 1993); the exact criteria used to distinguish between the nonmelt period and the melt period are, however, not evident in the literature. Gray and Landine (1987) with 14 years of albedo data remark that the beginning of the melt period remains subject to an arbitrary decision. Missing the actual onset of the melt period by a few days and using a rapid albedo decay equation during that "erroneous" melt period will, however, yield better results than ignoring the melt season altogether. In both Minnesota and Saskatchewan the melt period usually begins in either February or March (Gray and Landine 1987; Baker and Ruschy 1988, 1989). Gray and Landine determine the transition to the melt period based upon net radiation, Q_N; a threshold melt temperature, MT; and minimum and maximum air temperatures, T_{min} and T_{max}. The threshold melt temperature, is defined by the day of the year and is obtained from

$$\mathbf{MT = -0.064(Day\ of\ year) + 6.69} \qquad \mathbf{(10)}$$

Gray and Landine begin the melt period when any one of the following three conditions is true: (1) $T_{min} > -4^{\circ}C$, (2) $Q_N > 1$ MJ/m^2-day and $T_{max} \geq 0^{\circ}C$, or (3) $T_{max} > MT$ and $Q_N > -0.5$ MJ/m^2-day.

In order to use either of the albedo models presented here, it is necessary to have some sort of guidelines or criteria for choosing the time periods of nonmelt and melt. Since the Ryan Lake field study on albedo decay was conducted for only one year,

general rules for determining the nonmelt and melt periods cannot be formulated from the Ryan Lake data alone. However, the information from this study, in addition to those guidelines noted from previous albedo studies, is useful in determining the periods of nonmelt and melt.

For the Ryan Lake field study, it was obvious from the albedo depletion curve that the albedo decay rate changed considerably after February 17. February 18 was designated as the starting date of the melt period. Average air temperatures remained below 0°C for the majority of the nonmelt period, and incoming solar radiation remained below 10 MJ/m^2-day until a few days before the melt period. Albedo decay during the nonmelt period was slow (< 0.05/day). During the melt period, on the other hand, the albedo decay rate generally exceeded 0.05 per day. The melt period began after the incoming solar radiation had been greater than 10 MJ/m^2-day for more than two days and average air temperature exceeded 0°C. Incoming solar radiation remained above 10 MJ/m^2-day for most of the melt period.

b. Comparisons of Model 1 and 2 Predictions to Measured Prairie Snow Albedos

In order to see how well Model 1 and Model 2 predicted snow albedo, the results of model simulations were compared to 11 years of albedo data collected at a terrestrial climate station (albedo data are rarely collected on lakes) at the University of Minnesota, St. Paul. Only the surface albedos from November to April (winter months) were simulated. Because Baker et al. (1990) had found similar albedo decay rates during the fall snow accumulation season and the spring melt season, the melt period equations ((4),

(5), (7) and (8)) were used to simulate albedo also during the snow accumulation season in the early winter. The nonmelt period began in late November/early December after average daily air temperatures had dropped to below 0°C for at least two days. The spring melt period was designated to begin after daily incoming solar radiation remained above 10 MJ/m^2-day for more than two days and average daily air temperature was greater than 0°C. Once the spring melt period had begun, the melt period equations were applied until the end of the designated winter period (April).

Figure 4 documents the modeling efficiencies (EF) for Model 1 and Model 2 for each of the 11 years. Also shown for each year is the total snowfall depth for the winter season. The EF values are consistently better for high snowfall years than for low snowfall years (total snowfall less than 60 cm). Model 1 has a slightly higher EF than Model 2 for seven of the 11 winter seasons. The results show that Model 1 and Model 2, developed for data collected over a lake, can be used to simulate snow albedo over land as long as the total annual snowfall is high.

c. Comparisons of Model 1 and 2 to Existing Albedo Models

Two sets of analyses were performed in order to determine how well Model 1 and Model 2 compared to three existing snow albedo models (Table 1): Baker et al. (1990), Gray and Landine (1987) and Rogers et al. (1995). First, the predictions of the existing albedo models were compared to 11 years (1979-1990) of daily albedo data collected at a terrestrial climate station at the University of Minnesota, St. Paul. In the second set of analyses, the three existing albedo models were used to predict albedo during the Ryan

Lake field study (December 17, 1996 to March 21, 1997), and the results were related to the albedo data collected. To conclude the comparison of the models, the results of the three existing models were compared to the results of Model 1 and Model 2 for the terrestrial and the Ryan Lake data sets.

1) ALBEDO PREDICTIONS FOR THE UNIVERSITY OF MINNESOTA, ST. PAUL SITE, 1979-1990

The Baker et al. (1990), Gray and Landine (1987) and Rogers et al. (1995) models were used to predict daily albedos for the entire winter season (November to April) for 11 years (1979-1990). The predictions were compared to albedo data collected at St. Paul, Minnesota. None of the models tested were developed for the entire winter season. The applications were, however, performed from the first snowfall until the end of April in order to determine how well albedo could be predicted for the whole winter season.

The Baker et al. (1990) model gives different equations for each month of the winter season (November through April). Instead of the overall equation in Table 1, a separate equation was applied for each month:

$$\alpha_{NOV} = 0.878 - 0.0744d^{1/2} \quad \textbf{(11a)}$$

$$\alpha_{DEC} = 0.824 - 0.0126d \quad \textbf{(11b)}$$

$$\alpha_{JAN} = 0.847 - 0.0447d^{1/2} \quad \textbf{(11c)}$$

$$\alpha_{FEB} = 0.809 - 0.0372d^{1/2} \quad \textbf{(11d)}$$

$$\alpha_{MAR} = 0.798 - 0.0291d \quad \textbf{(11e)}$$

$$\alpha_{APR} = 0.887 - 0.0326d \quad \textbf{(11f)}$$

where:

α_{month} = daily albedo during specified month

d = days after snowfall.

This model was developed primarily for the high albedo, or nonmelt, season when snow depths are greater than 10 cm. Herein the equations were applied even when depths were less than 10 cm in order to obtain albedo values for the entire winter.

The Gray and Landine (1987) model was developed in Saskatchewan for the period from February until the end of the winter season. It includes predictions for the nonmelt period. The model requires net radiation data which were not available; therefore, only the temperature criteria were used as conditions for the melt period determination.

The Rogers et al. (1995) model used was altered from that shown in Table 1. The original model includes adjustments for cloud cover and solar noon angle; however, with these adjustments the model, at times, predicts albedo values greater than one. Such albedo values are theoretically impossible; therefore, the sky condition adjustments (cloud cover and solar noon angle) were omitted, resulting in predictions of albedo values less than one.

Figures 5a through 5d show the mean absolute error, the root mean square error, the mean absolute percent error and the modeling efficiency, respectively, for Model 1, Model 2 and the three existing models for each of the 11 winter seasons (1979-1990). The winter season begins in November of the year shown on the abscissa of each figure.

Model 1, Model 2 and the Gray and Landine (1987) model predict albedo with the highest modeling efficiencies for all years tested (Fig. 5d). During the high snowfall seasons Model 1 and Model 2 had lower mean absolute errors and higher modeling

efficiencies than the other models tested. The winter seasons of 1980, 1986 and 1989 had total snowfall depths less than 60 cm. During these low snowfall seasons, only the Gray and Landine model gave reasonable albedo predictions. All other models tested had negative modeling efficiencies. The Gray and Landine model computes the increase in albedo after a new snowfall as a function of the amount of snowfall; therefore, in low snowfall seasons, the Gray and Landine model tends not to overpredict albedo as do the other models.

2) Albedo Predictions for Ryan Lake, 1996-1997

Figures 6a through 6c show comparisons of the albedos predicted by the three existing models with the albedos measured at Ryan Lake. A one to one line is included in each figure. These figures may be compared to Figs. 3a and 3b, which are for Model 1 and Model 2, respectively. The highest modeling efficiency of the existing models is 0.47 for the Gray and Landine (1987) model (Fig. 6a). The Baker et al. (1990) model in Fig. 6b consistently overpredicted albedo during the melt season. The Rogers, et al (1995) model generally underpredicted new snowfall albedos throughout the study period and also underpredicted snow albedos during the melt season (Fig. 6c).

An error analysis was performed on the albedo predictions by each of the three existing models, and the results are given in Table 4. Included in Table 4 are the statistical parameters for Model 1 and Model 2 (reprinted from Table 3) for comparison purposes. Not surprisingly the predictions by Model 1 and Model 2 are better since these models were calibrated against the Ryan Lake data, while the existing models were not.

The mean absolute error, the root mean square error, and the mean absolute percent error are nearly identical for the three existing models. The MAE is less than 0.10 for all three existing models, and the average RMSE of the existing models is 0.11.

The errors of the existing models in predicting the albedos measured on Ryan Lake (Table 4) are lower than the errors in predicting the prairie snow albedos measured at the University of Minnesota, St. Paul, climate station. The lower error values are most likely due to two reasons: (1) The Ryan Lake study period from December 17, 1996, to March 21, 1997, excluded the fall snow-accumulation season and the final portion of the spring melt period. (2) The total snowfall during the period of study was high (111 cm).

8. Summary

Snow and ice albedos were measured on a lake in southeastern Minnesota for 95 days during the winter of 1996-97. The average albedo measured after a new snowfall was 0.83, and the average measured ice albedo after the snow had melted was 0.36. The highest albedo measured was 0.90 (snow) and the lowest was 0.33 (ice). Two daily snow albedo models were developed from the collected data. One model uses accumulated solar radiation and accumulated air temperature to predict albedo. The second model predicts albedo based on days after snowfall. Data for those three independent variables are available from weather stations. Both models divide the winter period into a nonmelt period and a melt period based on average daily air temperature and total daily incoming solar radiation. Model 1 and Model 2 predicted albedos for Ryan Lake (1996-97) with modeling efficiencies of 0.94 and 0.89, respectively.

Predictions by both models were compared to 11 years (1979-1990) of daily winter surface albedos measured over snow-covered grassland in St. Paul, Minnesota. Each model predicted winter albedos with modeling efficiencies greater than 0.50 for six of the eight high snowfall (total snowfall greater than 60 cm) seasons. Three existing albedo models were also applied to predict snow albedos for the same 11 years. Model 1 and Model 2 developed herein consistently predicted surface albedos with higher modeling efficiencies than either the Baker et al. (1990) model or the Rogers et al. (1995) model. The third model, Gray and Landine (1987), predicted surface albedo with modeling efficiencies greater than either Model 1 or Model 2 during winters when the total snowfall was less than 60 cm. However, during high snowfall winters, Model 1 and Model 2 predicted albedo with modeling efficiencies greater than or comparable to the Gray and Landine model.

The predictions of the three existing models were also compared to the albedo data collected during the Ryan Lake field study. The modeling efficiencies of the three models ranged from 0.31 for the Rogers et al. (1995) model to 0.47 for the Gray and Landine (1987) model, much lower than the modeling efficiencies Model 1 and Model 2 developed herein.

9. Recommendations

Further studies need to be performed to see how the period prior to the nonmelt period, i.e., the snow-accumulation period, should be modeled. For now it is suggested that the equations used during the melt season be used also during the accumulation

season. Additional work needs also be done on albedo decay for very shallow snow depths (< 1 cm). However, considering the length of the entire winter season, errors incurred when snow depths are small may be insignificant. Finally, more specific criteria need to be developed for determining the division between melt and nonmelt periods.

Acknowledgments

The authors would like to thank David Ruschy of the Department of Soil, Water and Climate, University of Minnesota, St. Paul, for providing the terrestrial surface albedo data and informational support for this field study. The authors also thank Greg Spoden, Minnesota State Climatology Office, for providing climate data.

This study was supported partially under a grant from the U.S. Environmental Protection Agency, Office of Research and Development, Washington, DC. Barbara M. Levinson was the project officer.

O'Neill, A. D. J., and D. M. Gray, 1973: Spatial and temporal variations of the albedo of prairie snowpack. *The Role of Snow and Ice in Hydrology: Proc. Banff Symposia*, Vol. 1, UNESCO - WMO-IAHS, 176-186.

Perovich, D. K., G. A. Maykut, and T. C. Grenfell, 1986: Optical properties of ice and snow in the polar regions, I: Observations. *Proc. SPIE Ocean Optics VIII*, **637**, 232-241.

Perovich, D. K., 1996: The optical properties of sea ice. *CRREL* Monograph, 96-1.

Petzold, D. E., 1977: An estimation technique for snow surface albedo. *Climatol. Bull.*, McGill University, **21**, 1-11.

Rogers, C. K., G. A. Lawrence, and P. F. Hamblin, 1995: Observations and numerical simulation of a shallow ice-covered midlatitude lake. *Limnol. Ocean.*, **40(2)**, 374-385.

U. S. Army Corps of Engineers, 1956: *Snow Hydrology*. North Pacific Division, Corps of Engineers,. Portland, OR, 437 pp.

Warren, S. J., Optical properties of snow, *Reviews of Geophysics and Space Physics*, *20*(1), 67-89, 1982.

Wiscombe, W. J., and S. G. Warren, 1980: A model for the spectral albedo of snow. I: Pure snow. *J. Atmos. Sci.*, **37**, 2712-2733.

Winther, J., 1993: Short-and long-term variability of snow albedo. *Nordic Hydrol.*, **24**, 199-212.

Table 1. Summary of snow albedo models found in the literature.

Albedo Model	Inputs Required	Reference
$\frac{\int R(\alpha)G_C(\alpha)d\lambda}{\int G_C(\alpha)d\lambda}$ where *R(α) =spectral reflectance of snow* *G(α)=incident flux*	(1) Clear sky atmospheric parameters: ozone path length, precipitable water, turbidity, and surface pressure (2) cloud optical thickness, (3) grain size of snow	Choudhury and Chang (1981)
base albedo = 0.84 (for new snow) Aging adjustments: $\Delta\alpha = -10^{-(1.22+0.69d)}$ (accumulating) $\Delta\alpha = -10^{-(0.95+0.07d)}$ (melting) *d=# days since last snowfall (1,2...)* Sky condition adjustments: $\Delta\alpha = -0.019 + .0.248[\exp(-\beta/15.5)]$ $\Delta\alpha = 0.00449 + 0.097C^3$ *β = solar noon angle (degrees)* *C= fractional cloud cover* If rain and albedo > 0.8, then subtract 0.05 before other adjustments..	(1) Days after snowfall (2) Solar noon angle (3) Fractional cloud cover (4) Precipitation	Rogers et al. (1995) follows Petzold (1977).
$\alpha_{min} + (\alpha(0)-\alpha_{min})e^{-n/K}$ *α(0) = albedo on snowfall day (0.85)* *α_{min}= converged albedo value* *n= # days after snowfall (0,1,2...)* *K= rate of decrease parameter*	(1) Days after snowfall	Kondo and Yamazaki (1990)
$0.90 - 9.21\text{x}10\text{-}4\ T_{acc} - 0.0042\ SR$ (melting season) *T_{acc}=accumulated daily maximum temperature index (^0F)* *SR=solar radiation (mW/cm^2)*	(1) Temperature (2) Solar radiation	Winther (1993)
$0.839 - 0.0473\ n^{1/2}$ *n= # days after snowfall*	(1) Days after snowfall	Baker et al.. (1990)
$\alpha_{(t-1)}$-**DR** **Maximum albedo = 0.85** *$\alpha_{(t-1)}$ = albedo from preceding day* *DR = decay rate* Model algorithm included in reference. The decay rate changes depending on snow depth and whether a defined melt period has begun.	(1) Snowfall (2) Maximum temperature (3) Net radiation (4) Starting albedo (5) Snow depth	Gray and Landine (1987)

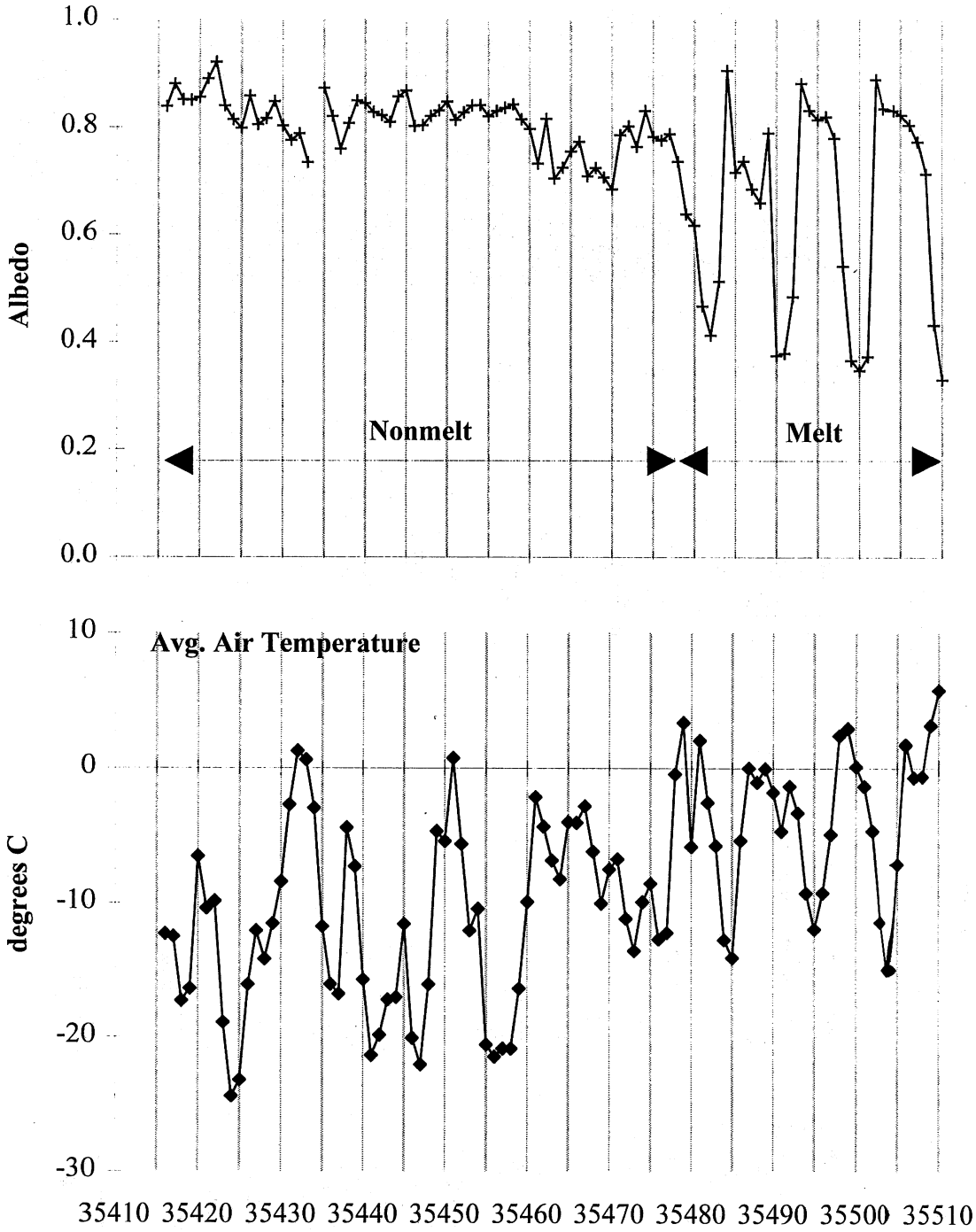

Figure 2. Measured daily albedo values during nonmelt period (December 17, 1996 to February 17, 1997) and melt period (February 18 to March 21, 1997).

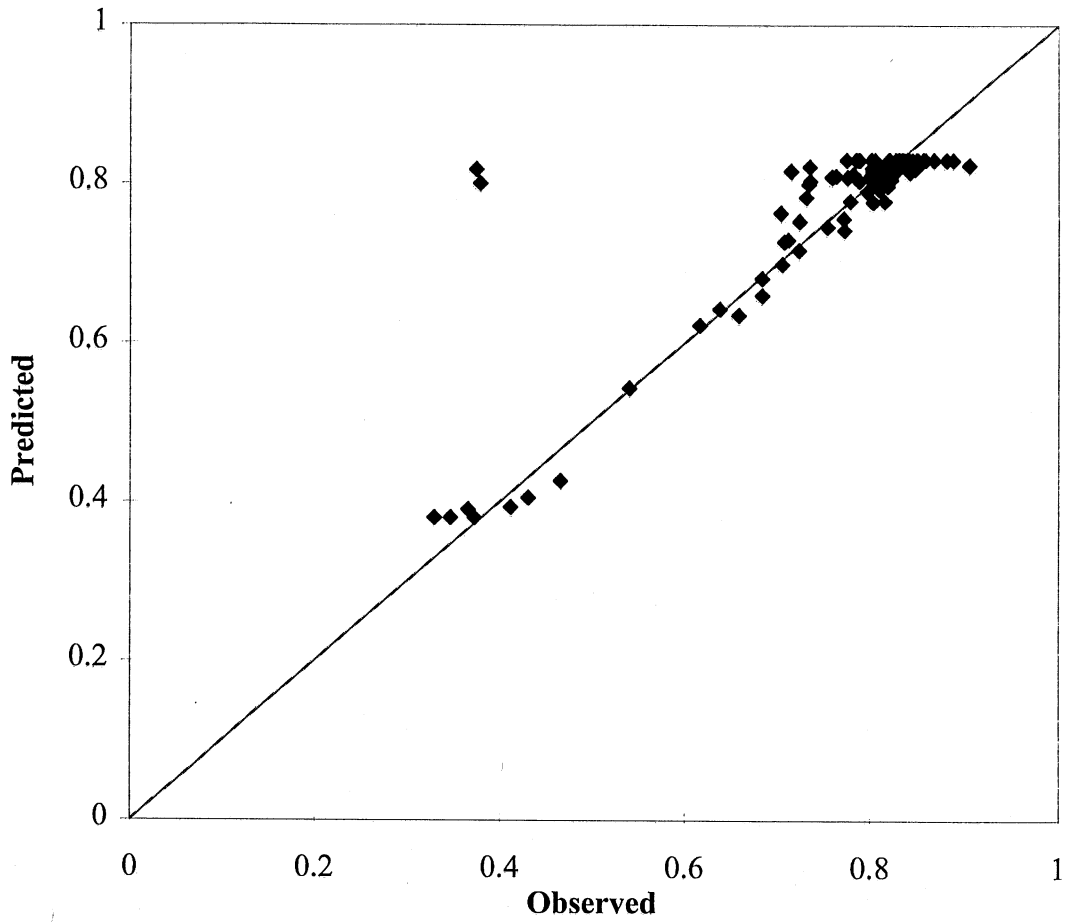

Figure 3a. Predicted albedos (Model 1) versus observed albedos from Ryan Lake, December 17, 1996, to March 21, 1997.

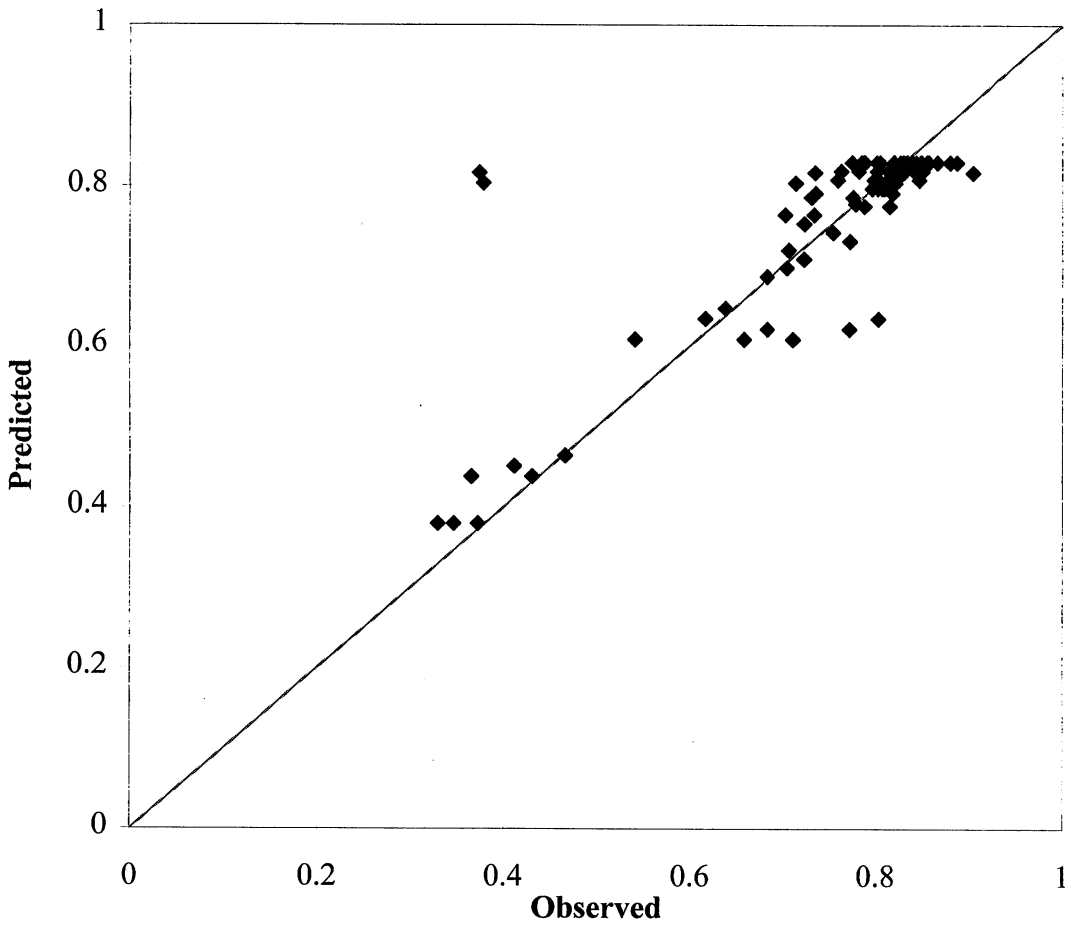

Figure 3b. Predicted albedos (Model 2) versus observed albedos from Ryan Lake, December 17, 1996, to March 21, 1997.

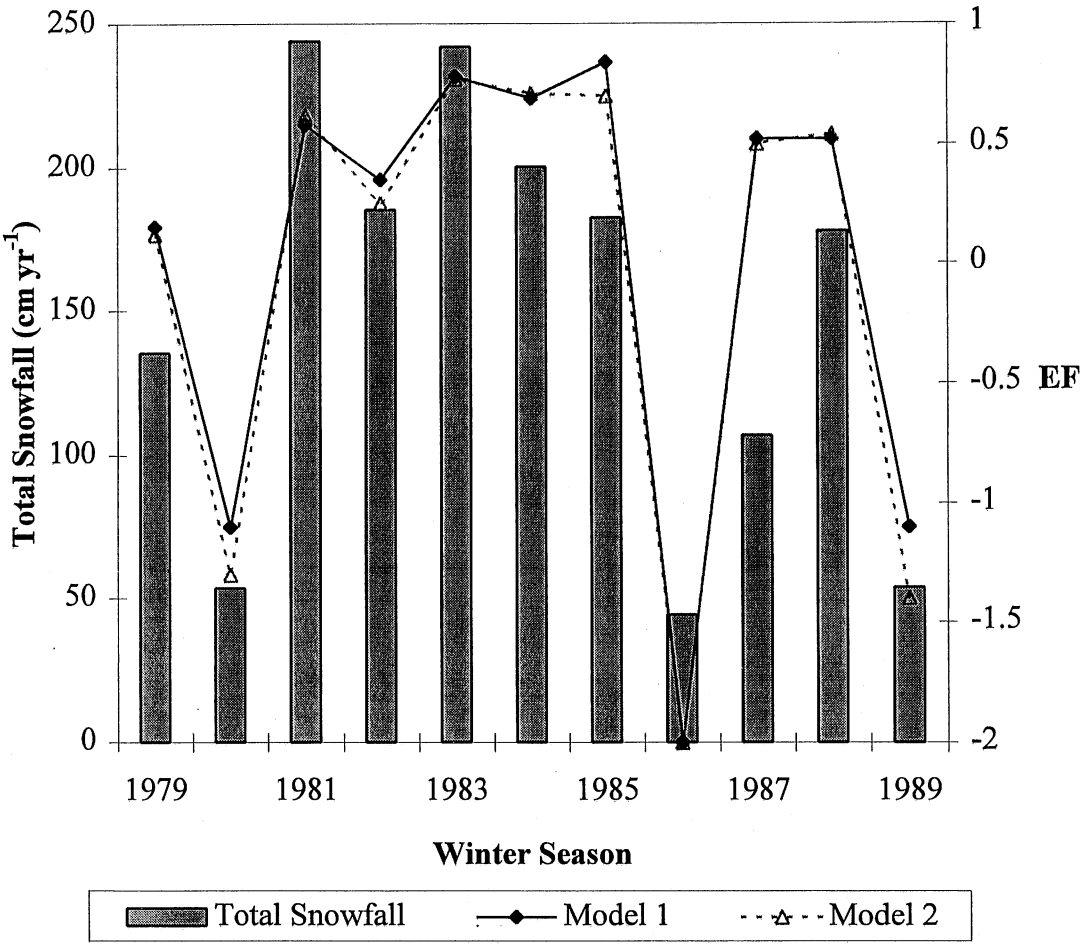

Figure 4. Total snowfall depths and modeling efficiencies of Model 1 and Model 2 in predicting prairie snow albedo for the winter seasons 1979 to 1989. Observed albedo values were measured at the University of Minnesota, St. Paul.

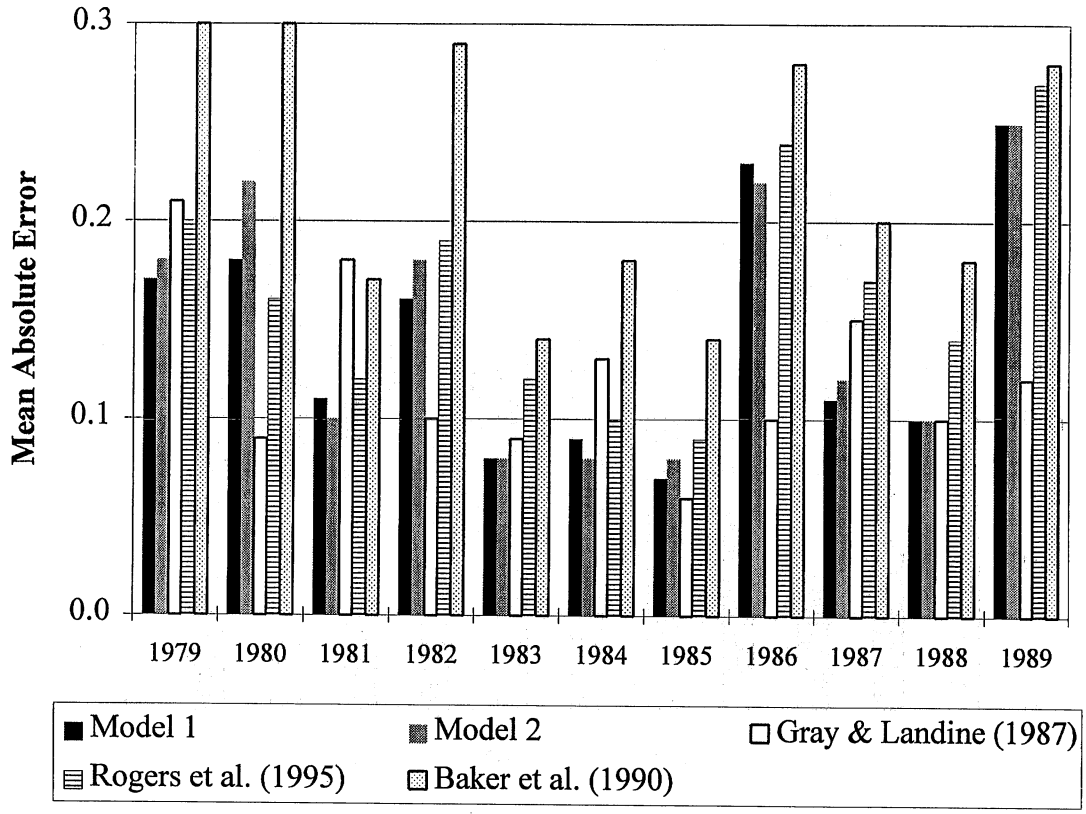

Figure 5a. Comparison of mean absolute errors between five model predictions and measured prairie snow albedos at the University of Minnesota, St. Paul (1979-1989).

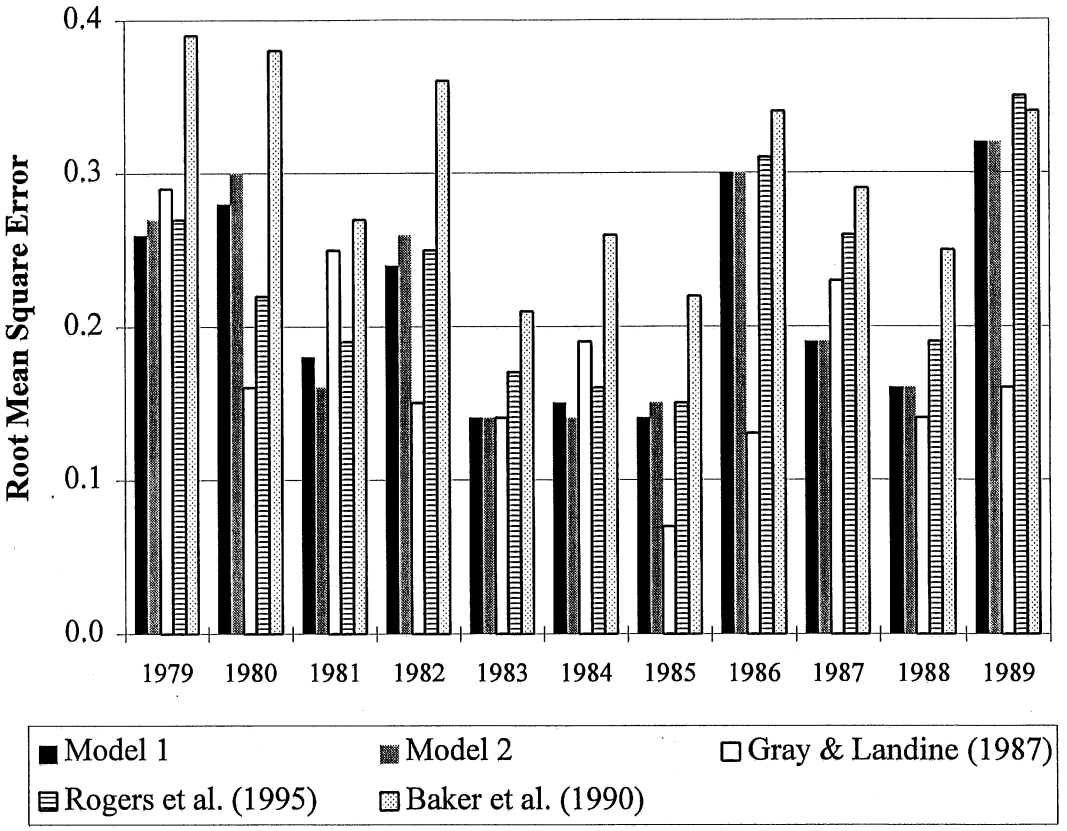

Figure 5b. Comparison of root mean square errors between five model predictions and measured prairie snow albedos at the University of Minnesota, St. Paul (1979-1989).

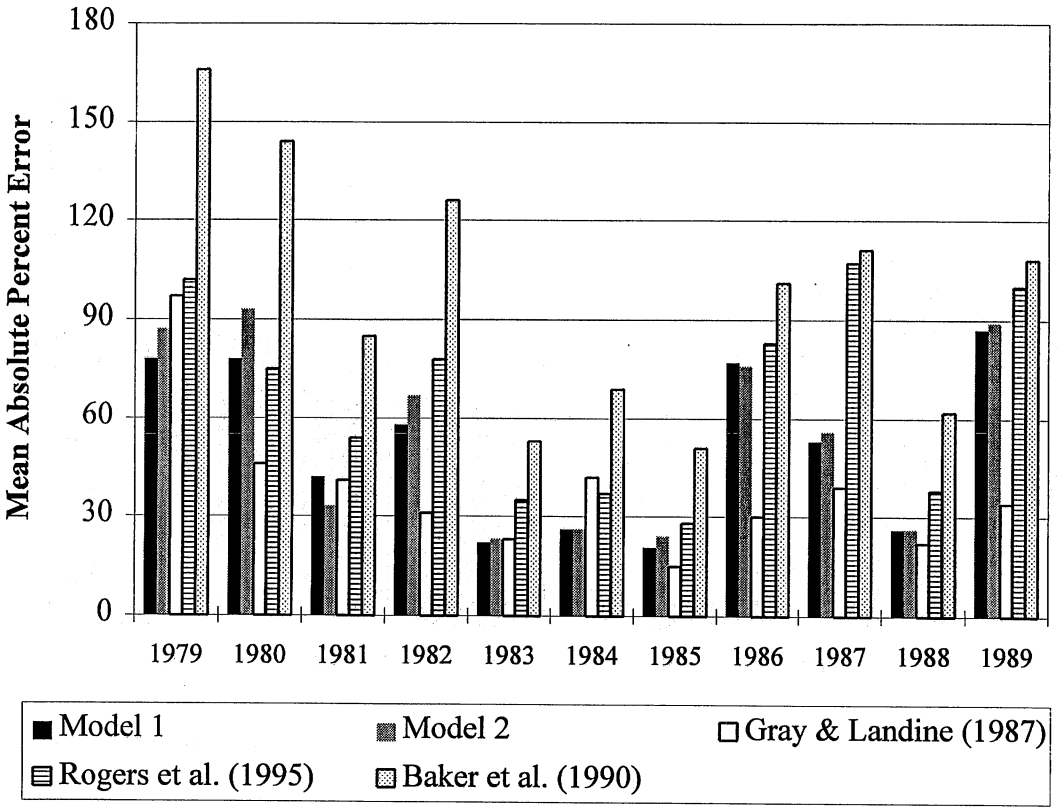

Figure 5c. Comparison of mean absolute percent errors between five model predictions and measured prairie snow albedos at the University of Minnesota, St. Paul (1979-1989).

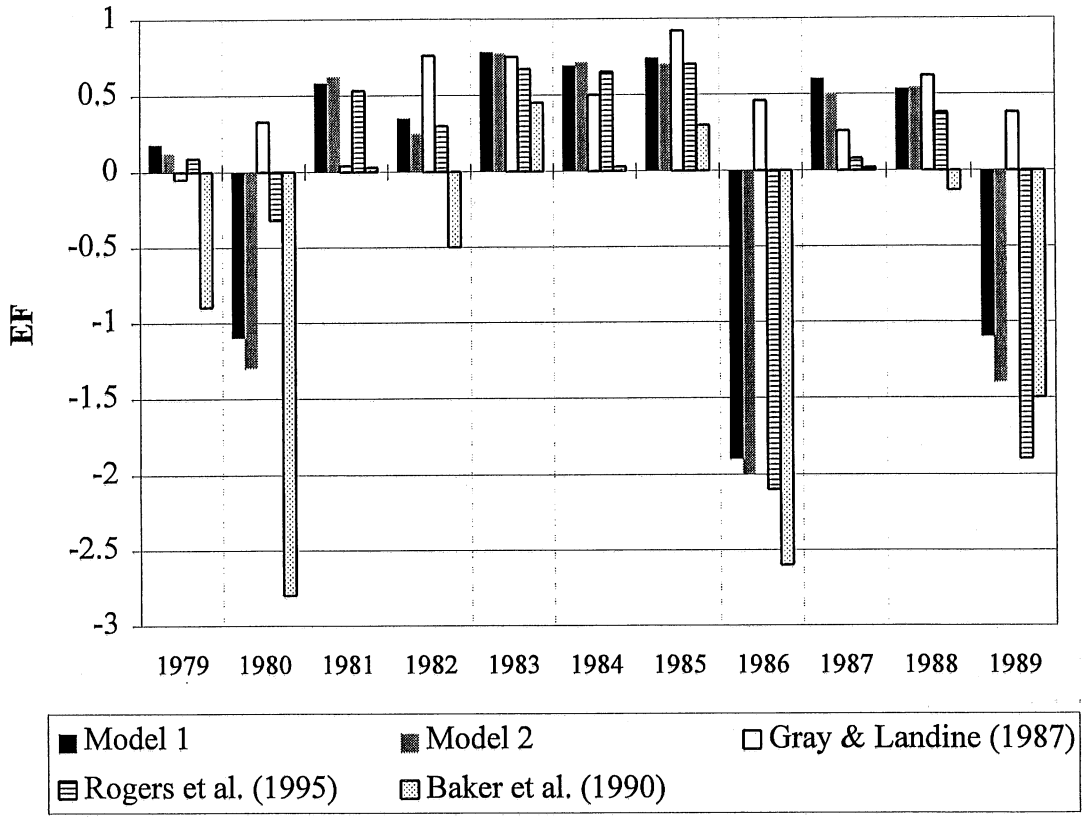

Figure 5d. Comparison of modeling efficiencies between five model predictions and measured prairie snow albedos at the University of Minnesota, St. Paul (1979-1989).

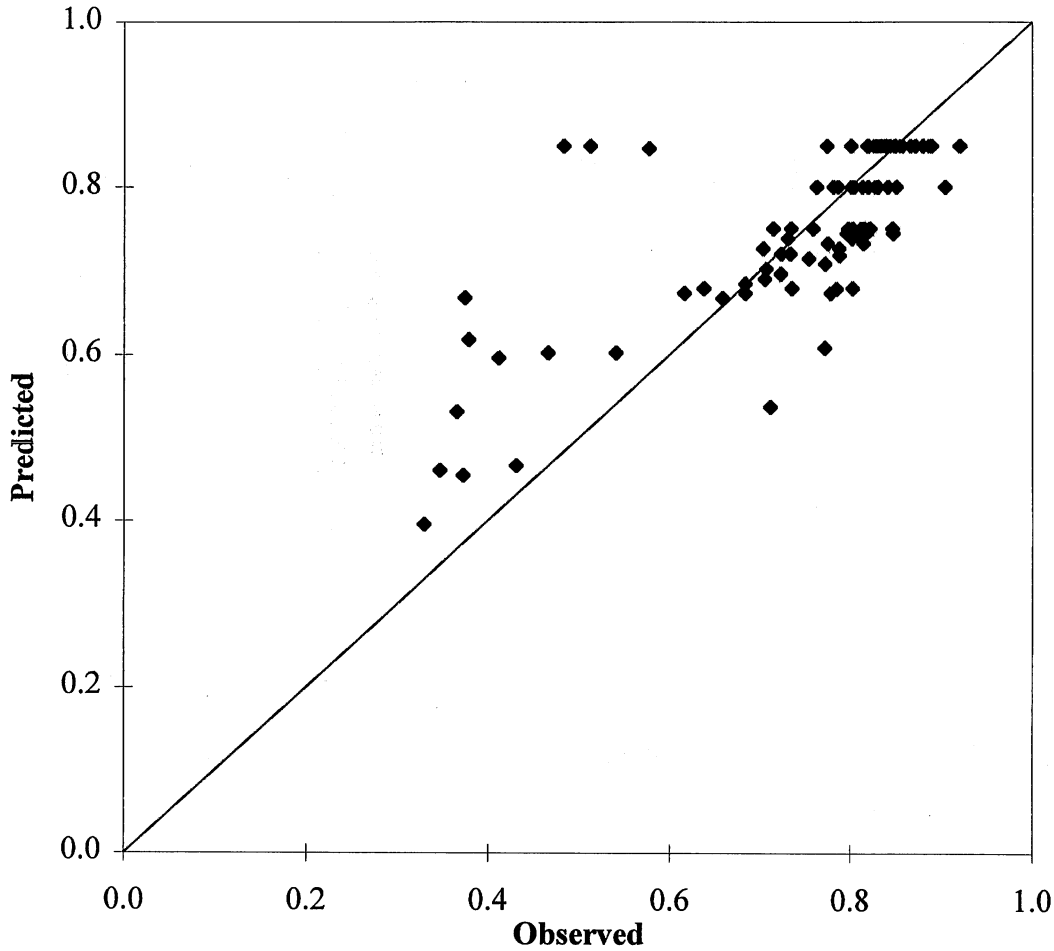

Figure 6a. Predicted albedos (Gray and Landine 1987 model) versus observed albedos from Ryan Lake, December 17, 1996, to March 21, 1997.

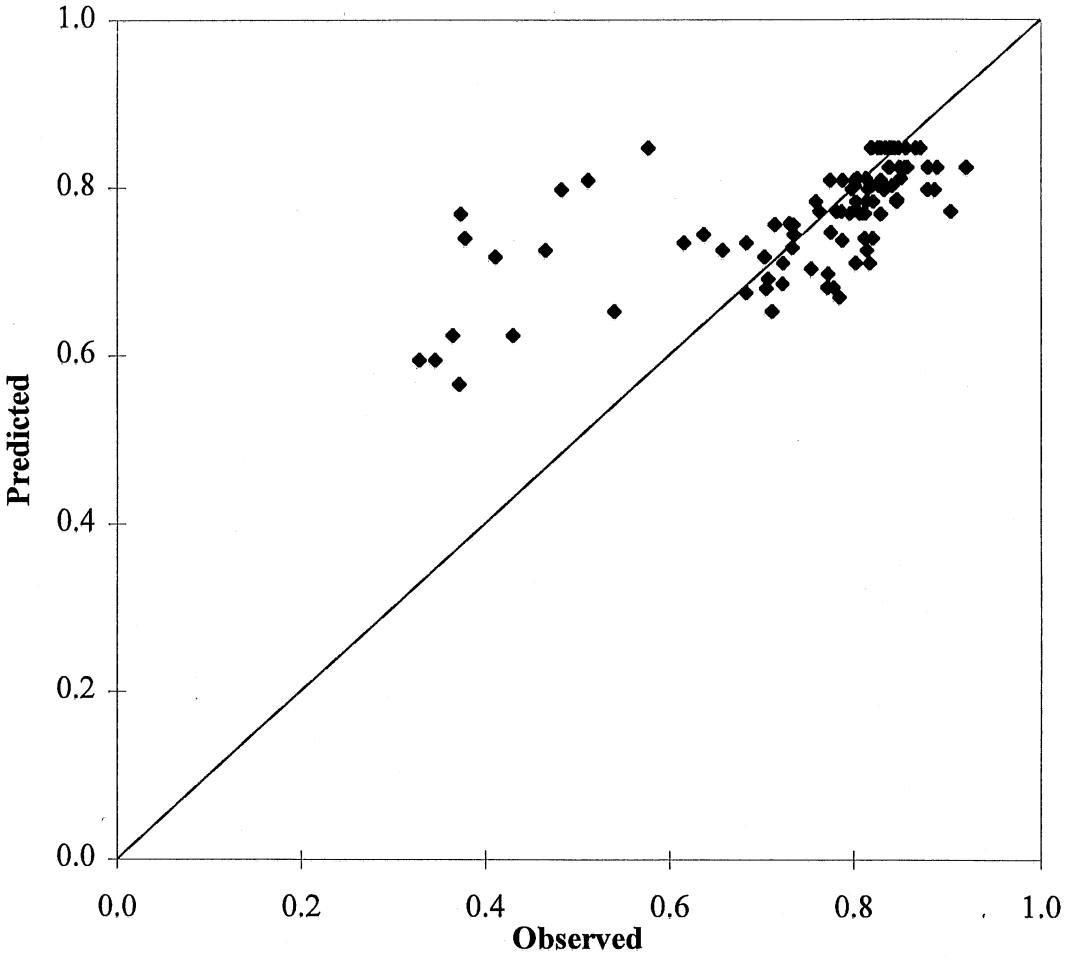

Figure 6b. Predicted albedos (Baker et al. 1990 model) versus observed albedos from Ryan Lake, December 17, 1996, to March 21, 1997.

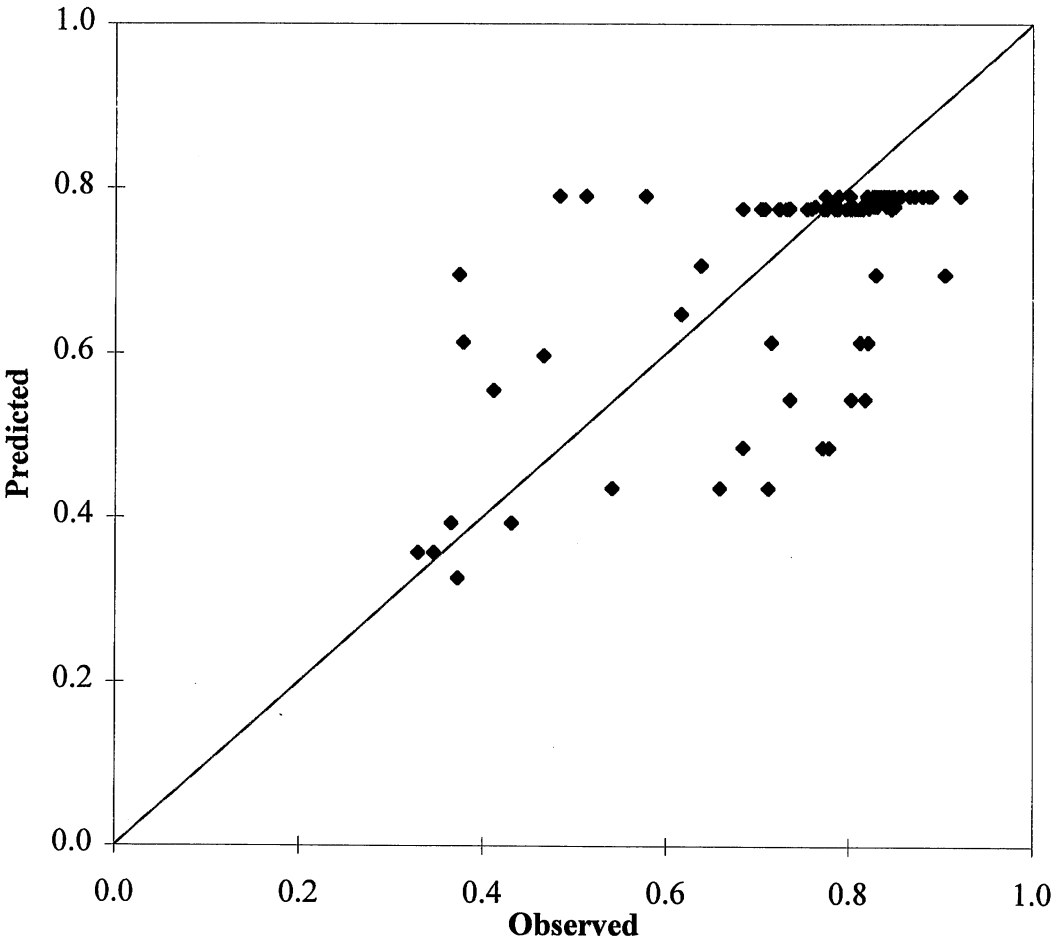

Figure 6c. Predicted albedos (Rogers et al. 1995 model) versus observed albedos from Ryan Lake, December 17, 1996, to March 21, 1997.

APPENDIX B

Pyranometer Comparison in Measuring Snow and Ice Albedo

by

Heather E. Henneman and Heinz G. Stefan

PYRANOMETER COMPARISON IN MEASURING SNOW AND ICE ALBEDO

by Heather E. Henneman and Heinz G. Stefan

ABSTRACT: In order to obtain total short-wave albedos of snow and ice, both incident and reflected solar radiation were measured over a frozen lake surface using two different types of radiation measurement devices: a Kipp and Zonen thermopile pyranometer with a spectral sensitivity of 300 to 2800 nm and a LI-COR photovoltaic pyranometer with a spectral sensitivity of 400 to 1100 nm.. The spectral response of the LI-COR pyranometers limits its use as a short-wave radiation measurement device. Therefore, two equations were developed to adjust both the daily incident radiation data and the daily reflected radiation data measured by the LI-COR instrument to total short-wave radiation values, i.e., to the waveband of 300 to 2800 nm. The LI-COR data were then adjusted, and a total short-wave adjusted albedo was calculated with a modeling efficiency of 0.97.

Keywords: snow and ice albedo, solar radiation, pyranometer, thermopile, photovoltaic

1. Introduction

Total short-wave albedo refers to the ratio of reflected solar radiation to incident solar radiation at a surface. Albedo is a critical parameter for the surface heat balance in any part of the world. Radiative fluxes dominate the surface energy balance of many snow- and ice-covered regions, and the albedo has a controlling influence on the absorption of radiative energy in those regions (Conway et al., 1996). Snow and/or ice albedos are needed for global climate models (Marshall and Oglesby, 1994), snowmelt predictions (Kondo and Yamazaki, 1990), and winter lake water quality models (Fang and Stefan, 1996; Rogers et al., 1995).

Pyranometers are instruments used to measure global solar radiation (the combination of direct-beam and diffuse-sky radiation) arriving from the whole hemisphere (Garg and Garg, 1993a). Two types of pyranometers are commonly used to measure global solar radiation. Thermopile sensors, which thermodynamically convert solar radiation into a measurable electrical energy, are the most widely accepted pyranometer type because of their long-term stability and because their response is not strongly wavelength dependent (Böer and Duffie, 1985). The second pyranometer type, the photovoltaic sensor, directly converts solar radiation into electrical energy at the quantum level. This second type of radiometer is generally less expensive and has a more rapid response to changes in solar radiation (e.g., due to cloud cover changes) than the thermopile type; however, because of the quantum electronical transitions involved, the photovoltaic sensor is wavelength dependent and generally has a limited spectral response (Suehrcke, et al., 1990; Garg and Garg, 1993a).

The total short-wave surface albedo of snow and ice was measured during a field study conducted on Ryan Lake in Minneapolis, Minnesota, during the winter of 1996-97 (Henneman and Stefan, 1997). Incoming and reflected solar radiation were measured by two different sets of instruments. Two of the pyranometers were thermopile pyranometers manufactured by Kipp and Zonen. The other two were photovoltaic sensors manufactured by LI-COR.

Although the manufacturer does not recommend that LI-COR sensors be used for measuring reflected radiation due to their limited spectral response, the substantial price difference between the two types warranted a study to ascertain whether LI-COR radiation measurements could be adjusted to give a reasonable estimate of total short-wave surface albedo. Additionally, photovoltaic sensors are generally easier to maintain than thermopile sensors, allowing for longer-term studies and data acquisition at remote sites without frequent manual checks. The measurements by the Kipp and Zonen thermopile sensors and the LI-COR photovoltaic sensors are related to each other in this paper. The general features, specifications, spectral response curves, installation and maintenance, and output of the different types of pyranometers are compared.

2. Instrumentation

2.1 Kipp and Zonen thermopile pyranometer

The Kipp and Zonen (K&Z) CM3 pyranometer measures solar irradiance over the wavelengths of 305 to 2800 nm. The pyranometer consists of a thermopile sensor, a housing for the sensor, a glass dome, a radiation shield to protect the instrument housing from direct sunlight, and a cable to which a voltmeter may be connected. A diagram of

the K&Z pyranometer is shown in Fig. 1. Generally, thermal radiation sensors use the temperature difference between a (black) surface exposed to solar radiation and the ambient temperature as a measure for the incident radiation. The thermopile in the CM3 pyranometer is coated with a black absorbent coating. The radiation is absorbed by the paint and is converted to heat. The resultant energy flow is converted to a current by the thermopile which consists of multi-junction thermocouples. Because the thermopile is shunted by a resistance, a voltage output is generated.

2.2 LI-COR photovoltaic pyranometer

The LI-COR LI-200SA (LI-COR) pyranometer measures solar irradiance over the wavelengths of 380 to 1100 nm. This pyranometer operates using the photoelectric effect. The photodiode is made of a semiconducting material like silicon. In a semiconductor a p-n junction is formed by joining an electron-deficient material (p-type) to a hole-deficient material (n-type), where a "hole" is an electron vacancy. Light energy, or in this case, solar radiation, absorbed by the electrons causes a movement of electrons and holes, thereby, resulting in an electrical current (Merrigan, 1982). The LI-COR pyranometer consists of a high stability silicon photovoltaic detector, an acrylic diffuser, a housing and a cable. A diagram of the LI-COR pyranometer is shown in Fig. 2. A resistance recommended by the manufacturer is used to generate a voltage output.

2.3 Specifications

The main specifications for each type of pyranometer are shown in Table 1. The reference manual for each type of instrument contains a more extensive list of

specifications. A definition of each specification listed and a brief comparison of the two instrument types are given below.

Definitions of the specifications listed in Table 1:

(a) Sensitivity—the ratio of the output signal of the pyranometer to the received irradiance. This is sometimes called the calibration constant.

(b) Response time—the time for the output signal to reach 90% of the final value after an abrupt change in irradiance.

(c) Temperature dependence of sensitivity—the variation of sensitivity with a change in ambient temperature.

(d) Linearity—the ideal pyranometer should provide an output signal that is directly proportional to the radiation received over a normal range of irradiance levels. The deviation from this ideal is indicated by the linearity specification.

(e) Tilt response—the change in sensitivity of the instrument depending on the orientation of the detector with respect to the horizontal.

(f) Stability—a measure of the change in sensitivity of the instrument due to time and exposure to radiation.

Of the specifications listed in Table 1, the most substantial differences are between the sensitivities and the response times of the two instrument types. The differences in these specifications are, however, not critical for the following reasons. The sensitivity of the data logger used with both instrument types is limited to millivolts. Therefore, although the K&Z sensor has a higher resolution, the precision is limited by the data logger, and the sensitivity difference between the two instrument types is effectively reduced. The photovoltaic sensor responds nearly instantaneously to changes in the incident photon flux, while the thermopile sensor's response time is much slower. However, when the radiation measurements are integrated over sufficiently long periods

of time (e.g., one day), such a response time error may be ignored (Suehrcke, et al., 1990).

The differences between the remaining specifications of the two instrument types were negligible. The third specification listed in Table 1, the temperature dependence of the sensitivity of the instrument, is nearly the same for both types of pyranometers. For the linearity specification, the LI-COR sensor deviates slightly less from the ideal than the K&Z sensor. The tilt response error is minimized by keeping the pyranometers level with the horizon. Because both sets of instruments were less than two years old and, therefore, had been recently factory calibrated, stability differences were also negligible.

2.4 Cosine errors

In addition to the instrumental errors specified in Table 1, an important source of error is that caused by deviation from the cosine law. The reflectance/absorptance of any surface is dependent on the angle at which the radiation strikes the surface. Cosine errors are caused by the failure of the instrument response to correspond with the theoretically required cosine response to radiation at any angle. Ideally, the vertical component of the radiation is accepted by the detector according to the Lambert cosine law, which is as follows:

$$\mathbf{I = I_0 \cos\gamma} \qquad (1)$$

where:

γ = angle between radiant beam and normal

I = radiant flux density

I_0 = maximum radiant flux density.

The cosine error (%) is measured as (Garg and Garg, 1993b)

$$\textbf{cosine error} = \frac{\textbf{output of the pyranometer}}{\mathbf{I_0 \cos\gamma}} \times \mathbf{100} \qquad (2)$$

A perfect cosine response will show maximum sensitivity at $\gamma=0^\circ$ and zero sensitivity at $\gamma=90^\circ$, when the radiation passes over the sensor surface. Reasons for deviations from the ideal response include striations or optical defects in the pyranometer covering, unevenness in the detector surface, and, in the case of the K&Z pyranometer, internal reflections within the glass dome. Incorrect leveling of the sensor can also contribute to cosine errors (Böer and Duffie, 1985; Garg and Garg, 1993b)

For the K&Z pyranometer, the cosine error is specified by the manufacturer as being less than $\pm 2\%$ for angles less than 60° from the normal axis of the sensor ($\gamma < 60^\circ$). At 70° the cosine error is about $\pm 4\%$, and the error increases to $\pm 6\%$ for incident angles greater than 80°. The LI-COR sensor is cosine corrected by the manufacturer so that cosine errors are typically less than $\pm 5\%$ for angles less than 80° from the normal axis of the sensor.

2.5 Spectral response

The solar spectrum at sea level (Kasten, 1983) and the manufacturer-specified spectral response curves for both types of instruments are shown in Fig. 3. The spectral response of the K&Z thermopile pyranometer is almost "ideal" in that it has a nearly

uniform response at all wavelengths. An ideal instrument for measuring solar radiation would have a uniform sensitivity, or "flat" response, and not detect radiation outside the solar spectral region. The spectral response of the LI-COR photovoltaic pyranometer has a spectral response curve limited to the range of 400 to 1100 nm. As shown in Fig. 3, the LI-COR curve is not uniform over this range.

The spectral albedo of snow, or the albedo as a function of wavelength, remains above 0.90 in the range of wavelengths from 300 to about 900 nm. The spectral albedo then falls to an average of approximately 0.35 for the range 1500 to 2500 nm (Grenfell, et al., 1994). It follows that the LI-COR sensor with a spectral response limited to the range 400 to 1100 nm will measure a higher total albedo (wavelength-integrated albedo) than the K&Z sensor, which is sensitive to the wavelength range of 300 to 2800 nm.

3. Experiment

3.1 Installation and maintenance

In order to determine the total albedo, hereafter referred to simply as albedo, of a winter lake surface, an albedometer was constructed by vertically mounting two pyranometers of the same type above the surface of the lake. One pyranometer was oriented with its collecting surface facing upward to collect incident radiation, while the other pyranometer was positioned facing downward to collect reflected radiation. Both a K&Z and a LI-COR albedometer were constructed and used to collect incident and reflected radiation over Ryan Lake in the Minneapolis/St. Paul metropolitan area. The equipment was mounted so that the lower pyranometer of each albedometer was 1.6 m

from the lake surface. This is the height recommended by the manufacturer to avoid shading effects and to promote spatial averaging. A spirit level mounted on each type of pyranometer allowed the instruments to be leveled with respect to the horizontal. Figs. 4a and 4b show photos of both albedometer types at the field site. Fig. 5 shows the entire collection apparatus.

While installed at the field study site, each instrument was wiped free of dirt or cleaned of ice or frost at least twice a week. Additional cleanings were made after snow or rainfall events. After cleaning, the instruments were also checked to make sure they remained level. The K&Z instrument had to be cleaned of ice more often than the LI-COR instrument, most likely because moisture collected more easily on the larger glass dome of the K&Z pyranometer than on the flat acrylic surface of the LI-COR sensor.

3.2 Data collection

Before installing the equipment at the lake site, the two pyranometers of each type were checked to make sure their output was synchronized. To do this the output of the pyranometers, placed with collecting faces oriented upward, was collected for a period of seven hours. During that time the instruments were closely monitored to insure that the instruments remained level with respect to the horizontal. The average percent difference between the readings of the two K&Z instruments was $0.2 \pm 1.8\%$ (mean $\pm$ std. dev.), while the average percent difference for the LI-COR instruments was $0.4 \pm 1.2\%$.

Because of the small differences in the output of the pyranometers, no adjustments were made to the instruments.

The instruments were also checked at the conclusion of the field study. The average percent difference between the readings of the K&Z pyranometers was $1.7 \pm 0.7\%$, and the average percent difference for the LI-COR pyranometers was $1.6 \pm 0.7\%$. The differences between measurements taken by like instruments had increased, while the standard deviations had decreased. Additionally, at the end of the study, one instrument of each type consistently measured higher values than the other. For both instrument types, the instrument which at the end of the study measured higher values was the instrument which had been inverted throughout the study. Of note is that, prior to the study, the instruments which were to be inverted generally measured lower values than the second instrument of the same type. Whether the reason for the increase in error was due to the instrument being inverted for three months is not known; however, future investigators might watch to see if such trends exist.

The field study was conducted from December 17, 1996 to March 21, 1997. Incident and reflected radiation were measured throughout the field study at one-minute intervals. These one-minute measurements were averaged and stored every 15 minutes by a Campbell Scientific CR10 data logger. The total daily radiation for either incident or reflected solar radiation was then obtained by integrating the output of each pyranometer over the daylight hours. Average daily albedo was calculated from these integrated radiation measurements as the ratio of total reflected to total incident solar radiation.

4. Results and discussion

4.1 Data

Figs. 6 and 7 show, respectively, the total daily incident solar radiation and total daily reflected solar radiation values integrated from the output of each pyranometer type. As shown in Fig. 6 the total incoming solar radiation measured by K&Z and LI-COR pyranometers for each day of the study are very similar. Further inspection shows that the total daily incoming solar radiation measured by the LI-COR pyranometer was slightly higher than that measured by the K&Z pyranometer for the majority of the days studied. Fig. 7 shows that the reflected radiation measured by each instrument followed the same temporal pattern, however, the measurements recorded by the LI-COR sensor are consistently higher than those of the K&Z sensor.

The average daily albedo calculated from the total daily radiation values of both sets of pyranometer types is shown in Fig. 8. As could be predicted from the incoming and reflected radiation data, the albedos measured by both sets of instruments follow the same temporal trends. For the most of the time the albedo measured by the LI-COR instrumentation is higher than the albedo measured by the K&Z instrumentation. The spectral response of the LI-COR pyranometer is limited to that range of wavelengths where spectral albedo is highest; therefore, the albedo measured by LI-COR was expected to be higher.

4.2 Data Validation

In order to determine whether the K&Z instrumentation measured reasonable solar radiation values, the K&Z daily incoming solar radiation data were compared to data collected at a climatological station at the University of Minnesota St. Paul campus. The station is located 12 km from Ryan Lake. An Eppley pyranometer with a spectral sensitivity of 280 to 2800 nm is used at that station to measure incident radiation. The mean absolute percent error between daily incident radiation measurements made by the K&Z and Eppley pyranometers was 2.2% for the field study period, indicating that the K&Z data were reasonable.

4.3 Error Between Instruments

Seven of the 95 days of the study were omitted from the data analysis. On the omitted days snow or ice covered one or both of the upward-facing instruments for part of the day, resulting in erroneous incident radiation measurements. These days were eliminated from all calculations. The eliminated days were December 22 and 23, 1996, January 4 and 5, February 22, and March 3 and 4, 1997. Table 2 summarizes the errors between the measurements taken by the LI-COR and K&Z instruments. The errors were calculated from total daily radiation measurements.

The mean absolute error (MAE) between the measurements of the two instrument types is 0.19 MJ m^{-2} day^{-1} for total daily incident solar radiation. This corresponded to a mean absolute percent error (MA%E) of 2.6%. The root mean square error (RMSE) between instrument measurements of daily incident radiation is 0.31 MJ m^{-2} day^{-1}. Both RMSE and MAE give a measure of the deviations between data measured by the two

types of instruments. The RMSE value is greater than the MAE value because the difference between measured values is squared when calculating RMSE.

The errors between measurements of total daily reflected radiation are greater than those of incident radiation. The MAE between daily measured values is 0.61 MJ m^{-2} day^{-1}. The MA%E between the two daily reflected radiation totals is 8.9%, much higher than for the incident radiation. The RMSE of 0.73 MJ m^{-2} day^{-1} is also much higher.

For daily albedo, the MA%E between measurements is 7.2%, while the mean absolute error (MAE) between measurements is 0.057. The RMSE is 0.064. Again, the daily albedo measurements calculated from LI-COR data were greater than those from K&Z data for the majority of the field study days.

The difference between radiation measurements generally increased with an increase in cloud cover. This was most likely due to the slight shift in the solar spectrum on cloudy days. Clouds absorb a higher portion of infra-red than visible radiation. Thus, a relatively high portion of visible radiation reaches the surface under cloudy conditions. (Male and Granger, 1981; Warren, 1982). Because of the limited spectral response curve of the LI-COR sensor, its response to such shifts in the solar spectrum is small, and the error in measurements increases on overcast days. On the other hand, the K&Z sensor has a nearly ideal spectral response allowing the instrument to respond to shifts in the solar spectrum. Hence, the difference between K&Z pyranometer data and LI-COR pyranometer data generally increases when a cloud cover exists.

4.4 LI-COR Data Adjustments

The total albedo measured by LI-COR instrumentation is limited to wavelengths of 400 to 1100 nm. Because LI-COR instrumentation is less costly and is also easier to maintain, an analysis was performed to determine whether an adjustment could be made to LI-COR radiation data to obtain total short-wave albedo. Since the K&Z pyranometers used are sensitive to wavelengths from 300 to 2800 nm and have nearly ideal spectral responses, the K&Z data were used as the standard to which the LI-COR measurements were compared.

The total daily incoming radiation measured by the K&Z pyranometer is plotted against that measured by the LI-COR pyranometer in Fig. 9a. Fig. 9b shows the total daily reflected radiation values measured by K&Z versus those measured by LI-COR. Simple linear regression analyses were performed on both the incoming and reflected radiation data, and the results of these analyses are included in Figs. 9a and 9b, along with the coefficients of determination (r^2) for each linear relationship.

Eqs. (3) and (4) were found to predict from LI-COR measurements the incident and reflected total daily short-wave radiation measured by the K&Z instrumentation. Both equations predict the incident and reflected daily solar radiation with modeling efficiencies (EF) greater than 0.99. Whereas r^2 is interpreted as the proportion of variation explained by a fitted regression line, EF is a measure of variation about a set line of $y = \hat{y}$, where y = observed value and $\hat{y}$ = predicted value. It is a measure of goodness of fit, and its equation is shown in Table 3.

$$I_{incident} = 1.0(\text{LI-COR}_{incident}) - 0.12 \quad (3)$$

$$I_{reflected} = 0.90(\text{LI-COR}_{reflected}) + 0.058 \quad (4)$$

where:

$I_{incident}$ = adjusted total daily incident radiation (MJ m^{-2} day^{-1}) for the waveband 300 to 2800 nm

$I_{reflected}$ = adjusted total daily reflected radiation (MJ m^{-2} day^{-1}) for the waveband 300 to 2800 nm

$\text{LI-COR}_{incident}$ = total daily incident radiation (MJ m^{-2} day^{-1}) as measured by LI-COR pyranometer for the waveband 400 to 1100 nm

$\text{LI-COR}_{reflected}$ = total daily reflected radiation (MJ m^{-2} day^{-1}) as measured by LI-COR pyranometer for the waveband 400 to 1100 nm

The results of Eqs. (3) and (4) were used to compute an adjusted total albedo from the LI-COR data, i.e., the adjusted albedo was simply calculated as the ratio of adjusted reflected radiation to adjusted incident radiation.

$$\text{Adjusted Albedo} = 0.90\frac{(\text{LI}-\text{COR}_{reflected}) + 0.058}{(\text{LI}-\text{COR}_{incident}) - 0.12} \quad (5)$$

Error analyses were performed between the measured K&Z data and adjusted incident radiation, adjusted reflected radiation, and adjusted albedo. The results are shown in Table 3. The MA%E between the reflected radiation measured by K&Z and the adjusted LI-COR data is 2.1%. Before adjusting the LI-COR data, the MA%E between reflected radiation measurements of the two instrument types was 8.9% (See Table 2.)

Using the K&Z measurements of albedo as a reference, Eq. (5) predicted total short-wave albedo with an EF of 0.97. The RMSE for the differences between measured and predicted albedo is only 0.026. Fig. 10 shows the predicted (adjusted) albedo values plotted against the measured K&Z albedo values and a one to one line for comparison.

5. Summary

Snow and ice albedos were measured over a freshwater lake during the winter of 1996-97. A comparison study was conducted between the two types of solar radiation measurement devices used to obtain albedo values. A Kipp and Zonen thermopile pyranometer and a LI-COR photovoltaic pyranometer were used to measure incident and reflected solar radiation. The K&Z sensor has a spectral sensitivity of 300 to 2800 nm, while the LI-COR sensor responds to the waveband of 400 to 1100 nm.

Average daily albedo was calculated from the measurements of both instrument types. The LI-COR instrumentation measured higher daily albedo values than the K&Z instrumentation for the majority of the study.

Eqs. (3) and (4) were developed to adjust both the incident and reflected LI-COR data so that total short-wave radiation values could be calculated (300 to 2800 nm). The adjusted radiation values were used to compute total short-wave albedo. The adjustment Eq. (5) predicted total short-wave albedo with a modeling efficiency of 0.97.

6. Conclusions

Although the spectral response of a LI-COR pyranometer is limited, the developed adjustment equations (Eqs. (3) to (5)) allow LI-COR equipment to be used for obtaining a measure of short-wave albedo for snow and ice surfaces. The low cost and ease of maintenance make such instrumentation favorable for similar winter studies, or for studies in remote locations.

The adjustment equations (Eqs. (3) to (5)) may not be applicable over all terrain. The study was conducted over a snow and/or ice surface; therefore, the adjustment equations developed here may not be suitable for reflected radiation from other surfaces. Additionally, the radiation adjustment equations may not be appropriate for use at locations where the solar angle is much different. At lower or higher solar angles the adjustment equations may not be reliable. Longer term comparison studies and studies at different sites would need to be conducted in order to determine whether the equations could be more generally applied. A longer study might also ascertain whether the inversion of pyranometers measuring reflected solar radiation does contribute to an increase in instrumental error with time as suggested by this study.

Acknowledgments

David Ruschy of the Department of Soil, Water and Climate at the University of Minnesota, St. Paul, provided solar radiation data for the winter of 1996-97. Greg Spoden at the Minnesota State Climatology Office provided cloud cover data for 1997.

The study was supported by a grant from the U.S. Environmental Protection Agency, Office of Research and Development. Barbara M. Levinson was the project officer.

References

Böer, K. W., and J. A. Duffie, eds., 1985. Advances in Solar Energy: An Annual Review of Research and Development. Vol. 2, ASES, pp. 1-49.

Conway, H., A. Gades, and C. F. Raymond, 1996. Albedo of dirty snow during conditions of melt. Water Resources Research, 32(6): 1713-1718.

Fang, X., and H. G. Stefan, 1996. Long-term lake water temperature and ice cover simulations/measurements. Cold Regions Science and Technology, 24: 289-304.

Garg, H. P., and S. N. Garg, 1993a. Measurement of solar radiation—I. Radiation instruments. Renewable Energy, 3(4/5): 321-333.

———, 1993b. Measurement of solar radiation—II. Calibration and standardization. Renewable Energy, 3(4/5): 335-348.

Grenfell, T. C., S. G. Warren, and P. C. Mullen, 1994. Reflection of solar radiation by the Antarctic snow surface at ultraviolet, visible, and near-infrared wavelengths. Journal of Geophysical Research, 99(D9): 18,699-18,684.

Henneman, H. E., and H. G. Stefan, 1997. Albedo models of snow and ice over a freshwater lake. Submitted to Journal of Applied Meteorology.

Kasten, F., 1983. Measurement and analysis of solar radiation data. In: G. Beghi, (Editor), Performance of Solar Energy Converters: Thermal Collectors and Photovoltaic Cells. Lectures at Joint Research Centre, Ispra, Italy, pp. 1-64.

Kondo, J., and T. Yamazaki, 1990. A prediction model for snowmelt, snow surface temperature and freezing depth using a heat balance method. Journal of Applied Meteorology, 29: 375-384.

Male, D. H., and R. J. Granger, 1981. Snow surface energy exchange. Water Resources Research, 17(3): 609-627.

Marshall, S. E., and R. J. Oglesby, 1994. An improved snow hydrology for GCMs. Part 1: snow cover fraction, albedo, grain size, and age. Climate Dynamics, 10: 21-37.

Merrigan, J. A., 1982. Sunlight to Electricity: Photovoltaic Technology and Business Prospects. MIT Press, Cambridge, Massachusetts.

Rogers, C. K., G. A. Lawrence, and P. F. Hamblin, 1995. Observations and numerical simulation of a shallow ice-covered midlatitude lake. Limnology and Oceanography, 40(2): 374-385.

Suehrcke, H., C. P. Ling, and P. G. McCormick, 1990. The dynamic response of instruments measuring instantaneous solar radiation. Solar Energy, 44(3): 145-148.

Warren, S. J., 1982. Optical properties of snow. Reviews of Geophysics and Space Physics, 20(1): 67-89.

Table 1. Specifications of Kipp and Zonen and LI-COR pyranometers

Specification	Kipp and Zonen CM3	LI-COR 200SA
Sensitivity	18-19 $\mu V\ W^{-1}m^{-2}$	69-73 $mV\ W^{-1}m^{-2}$
Response time	95% in 18s	10μs
Temperature dependence of sensitivity	6% from -10 to +40°C or ~± 0.12% per °C	± 0.15% per °C maximum
Linearity	± 2.5% (< 1000 W/m^2)	± 1% (< 3000 W/m^2)
Tilt response	<± 2%	No error induced from orientation.
Stability	< 1% change per year	< 2% change per year

Table 2. Errors between Kipp and Zonen data and LI-COR data

Statistical Parameter	Incident Radiation	Reflected Radiation	Albedo
MAE[1]	0.19 $MJm^{-2}day^{-1}$	0.61 $MJm^{-2}day^{-1}$	0.057
RMSE[2]	0.31 $MJm^{-2}day^{-1}$	0.73 $MJm^{-2}day^{-1}$	0.064
MA%E[3]	2.6	8.9	7.2

[1]Mean Absolute Error (MAE) = $\frac{\sum|y_1 - y_2|}{n}$

[2]Root Mean Square Error (RMSE) = $\sqrt{\frac{\sum(y_1 - y_2)^2}{n}}$

[3]Mean Absolute Percent Error (MA%E) = $\frac{100}{n}\sum\frac{|y_1 - y_2|}{|y_1|}$

y_1 = K&Z value
y_2 = LI-COR value
n = number of data points

Table 3. Errors between K&Z data and adjusted LI-COR measurements of incident radiation, reflected radiation, and albedo.

Statistical Parameter	Adjusted Incident Radiation	Adjusted Reflected Radiation	Adjusted Albedo
MAE	0.15 MJ/m^2/day	0.12 MJ/m^2/day	0.018
RMSE	0.29 MJ/m^2/day	0.18 MJ/m^2/day	0.026
MA%E	1.8	2.1	2.7
EF[1]	0.996	0.998	0.97

[1]Modeling efficiency (EF) = $1 - \frac{\sum (y_1 - y_{adj})^2}{\sum (y_1 - \bar{y})^2}$

y_1 = K&Z value
y_{adj} = adjusted LI-COR value
$\bar{y}$ = average K&Z value

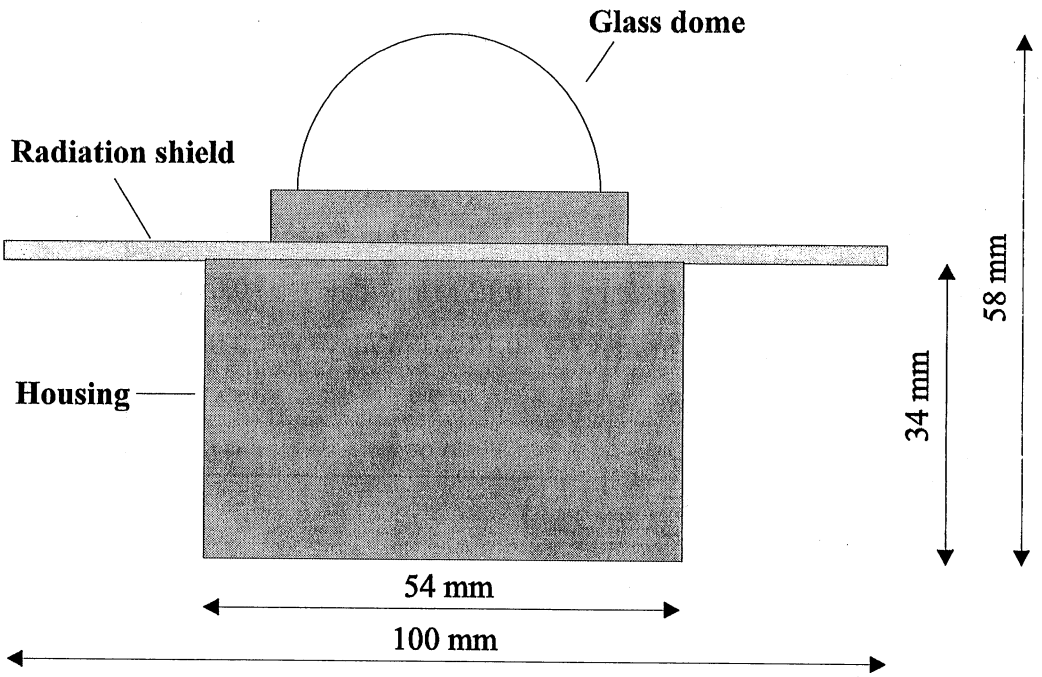

Figure 1. Schematic of Kipp and Zonen CM3 pyranometer.

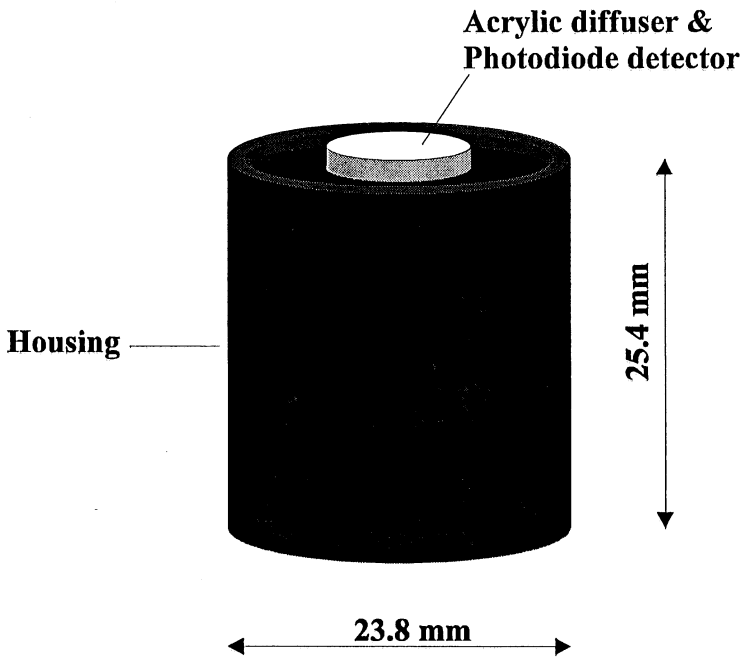

Figure 2. Schematic of LI-COR LI-200SA pyranometer.

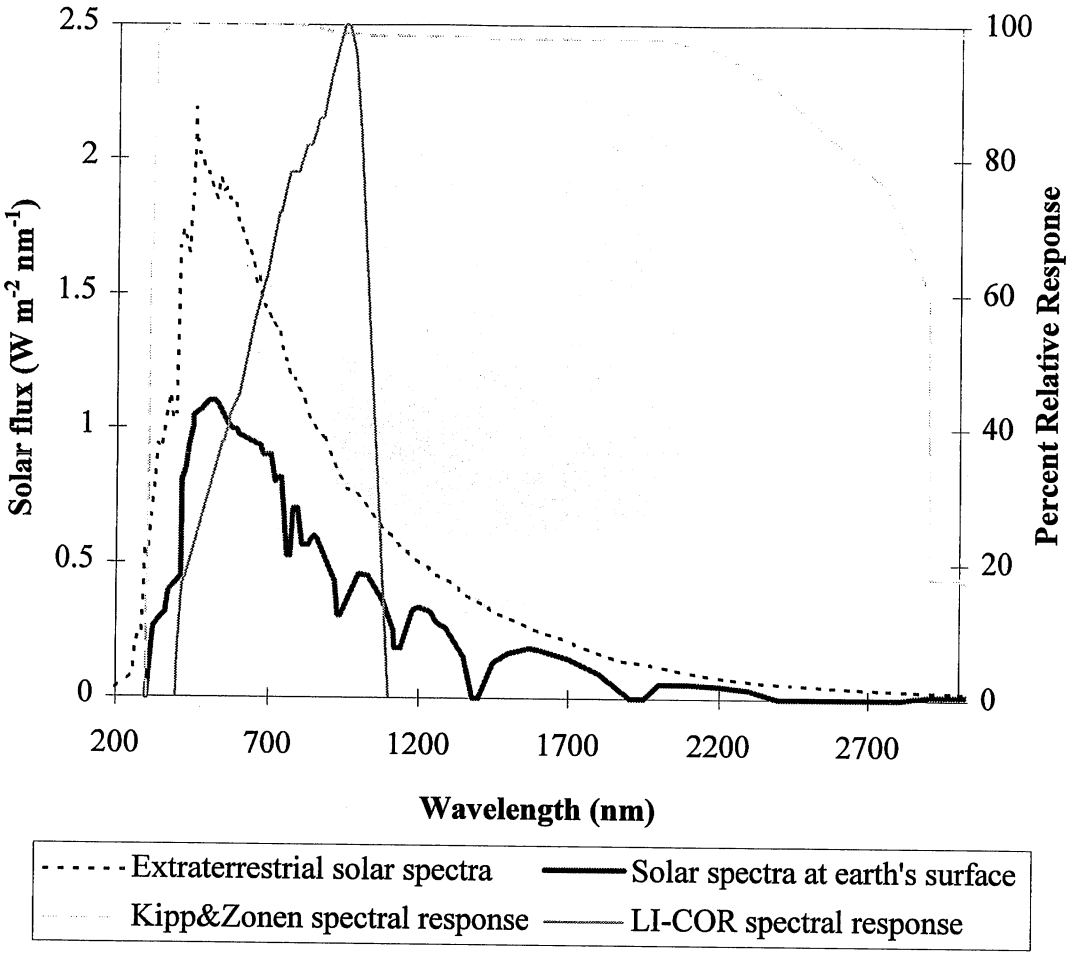

Figure 3. Extraterrestrial solar spectrum and spectral distribution of solar radiation at the earth's surface (Kasten, 1983) and the spectral response curves of the Kipp and Zonen and LI-COR pyranometers.

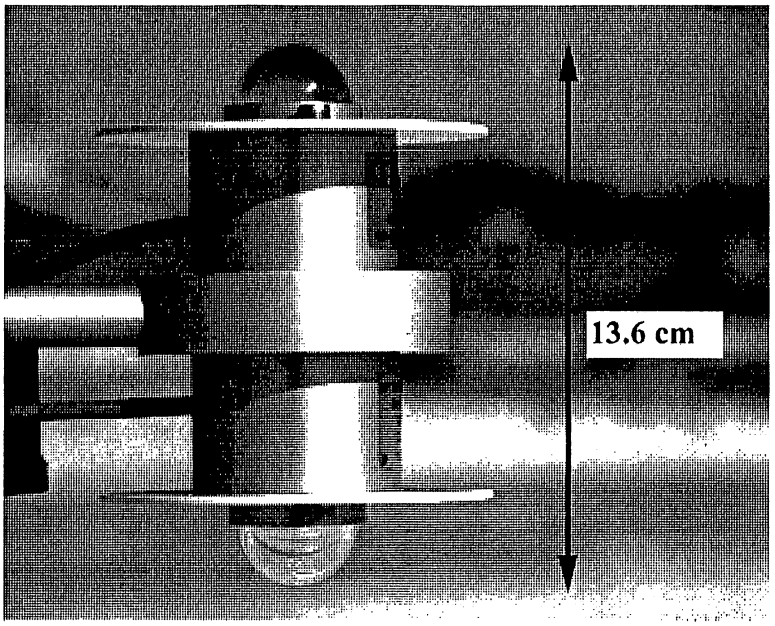

Figure 4a. Photo of Kipp and Zonen albedometer. One pyranometer is mounted to collect incident solar radiation, while the other is mounted to collect reflected solar radiation.

Figure 4a

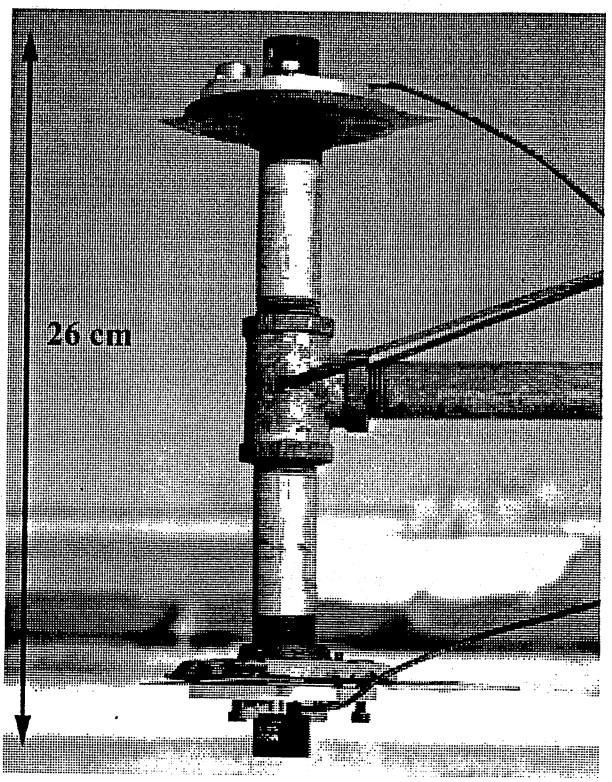

Figure 4b. Photo of LI-COR albedometer.

Figure 4.

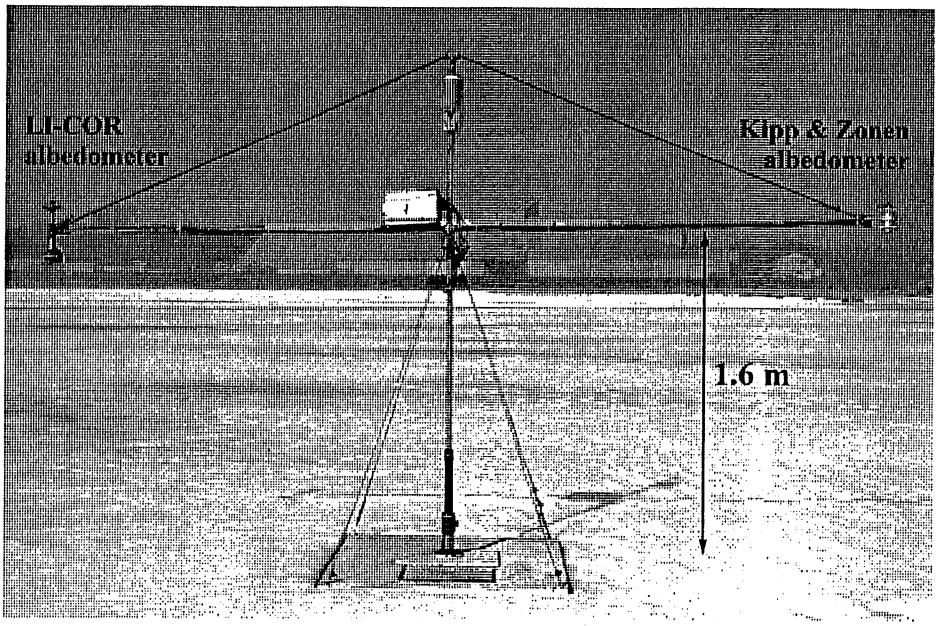

Figure 5. Photo of equipment on Ryan Lake. Each albedometer is mounted 1.6 m above the lake surface. A thermistor with protective housing is mounted on the center pole, and a data logger is mounted near the center pole.

Figure 5

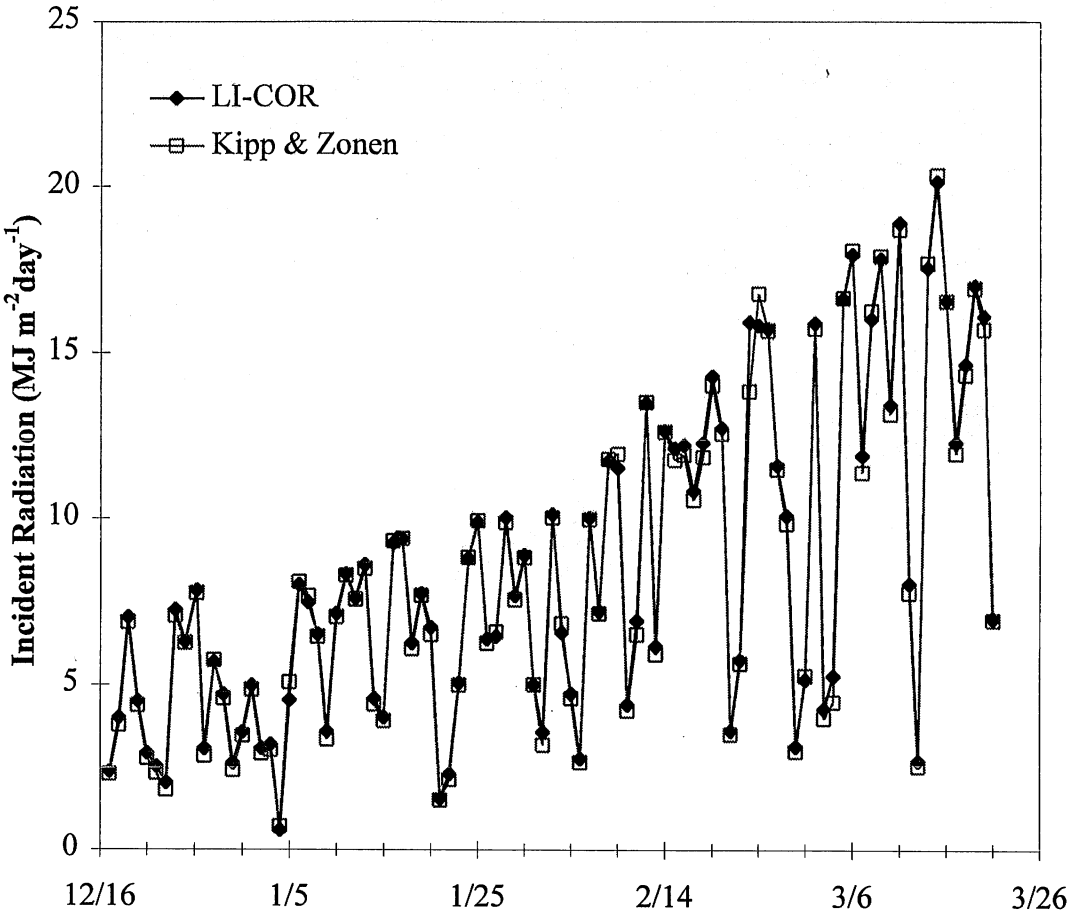

Figure 6. Total daily incident solar radiation measured by LI-COR and Kipp and Zonen pyranometers on Ryan Lake, December 17, 1996 to March 21, 1997.

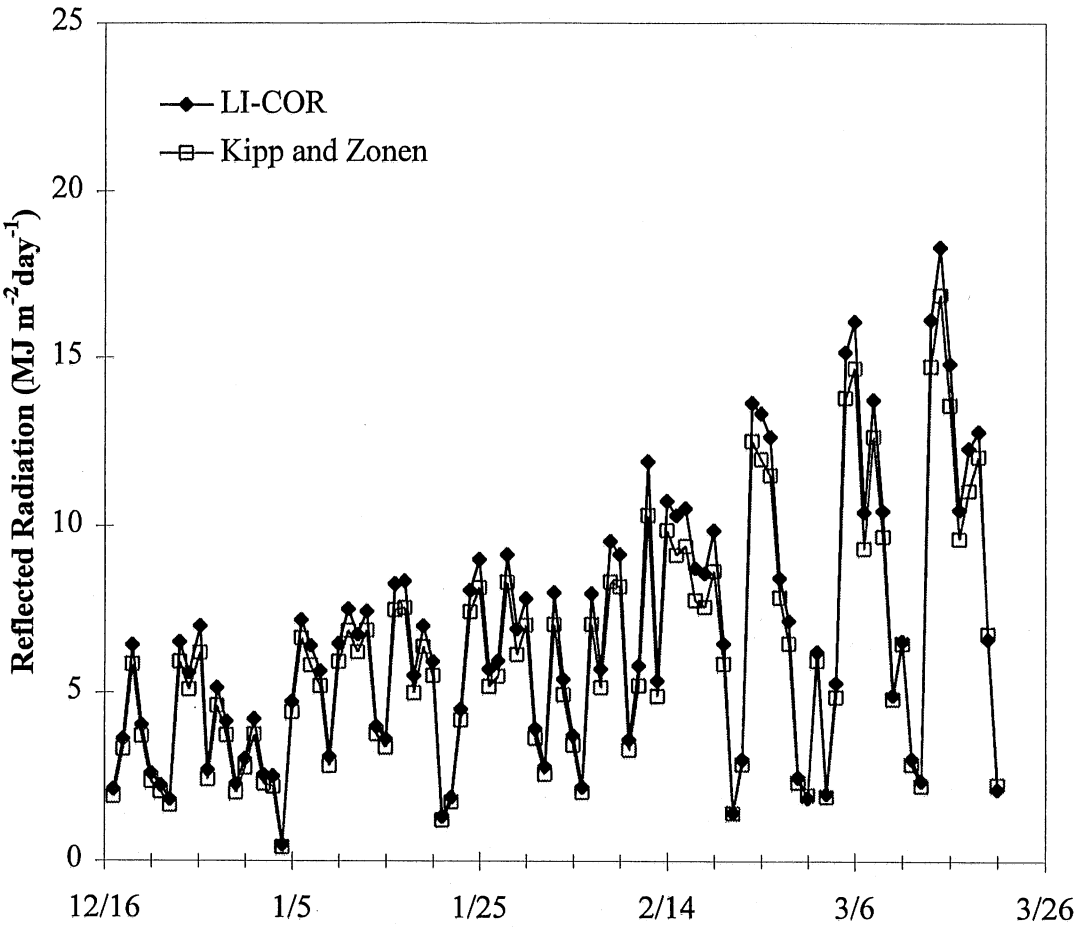

Figure 7. Total daily reflected solar radiation measured by LI-COR and Kipp and Zonen pyranometers on Ryan Lake, December 17, 1996 to March 21, 1997.

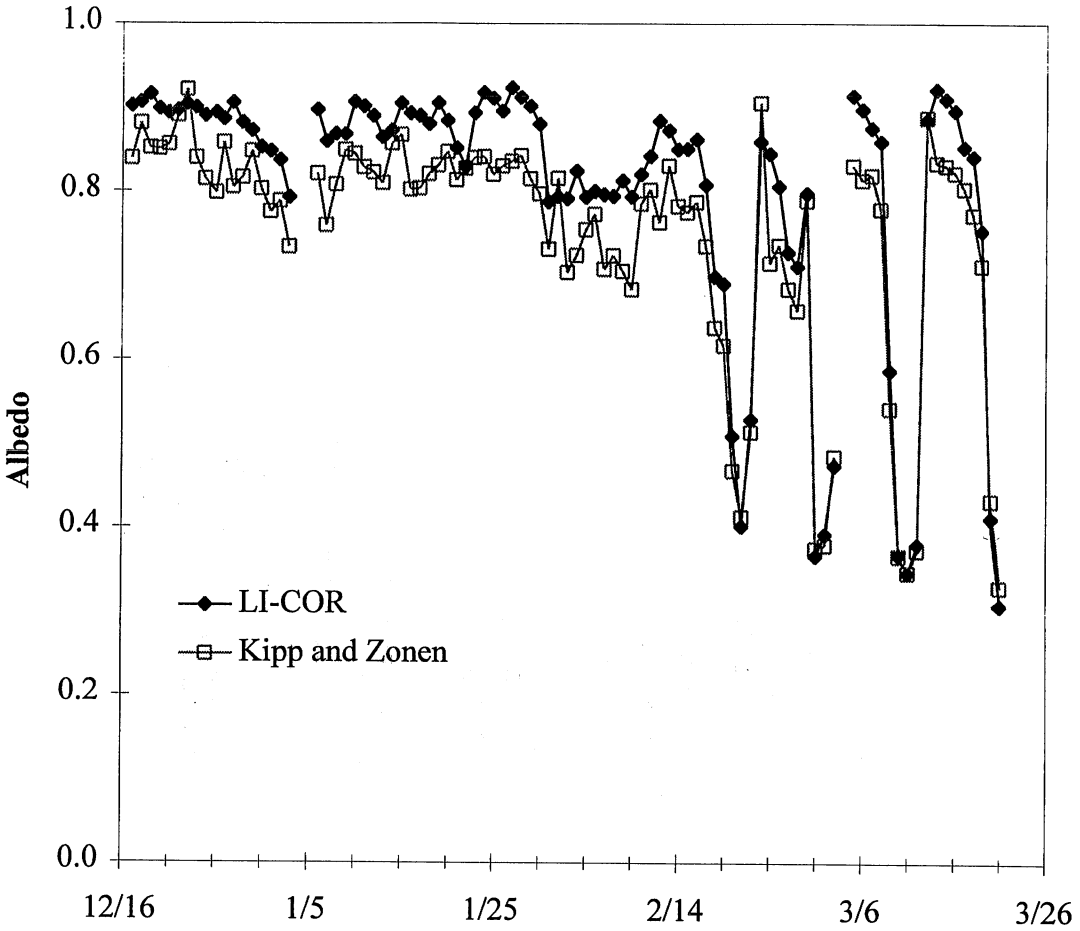

Figure 8. Average daily albedo calculated from radiation data of LI-COR and Kipp and Zonen pyranometers collected on Ryan Lake, December 17, 1996 to March 21, 1997.

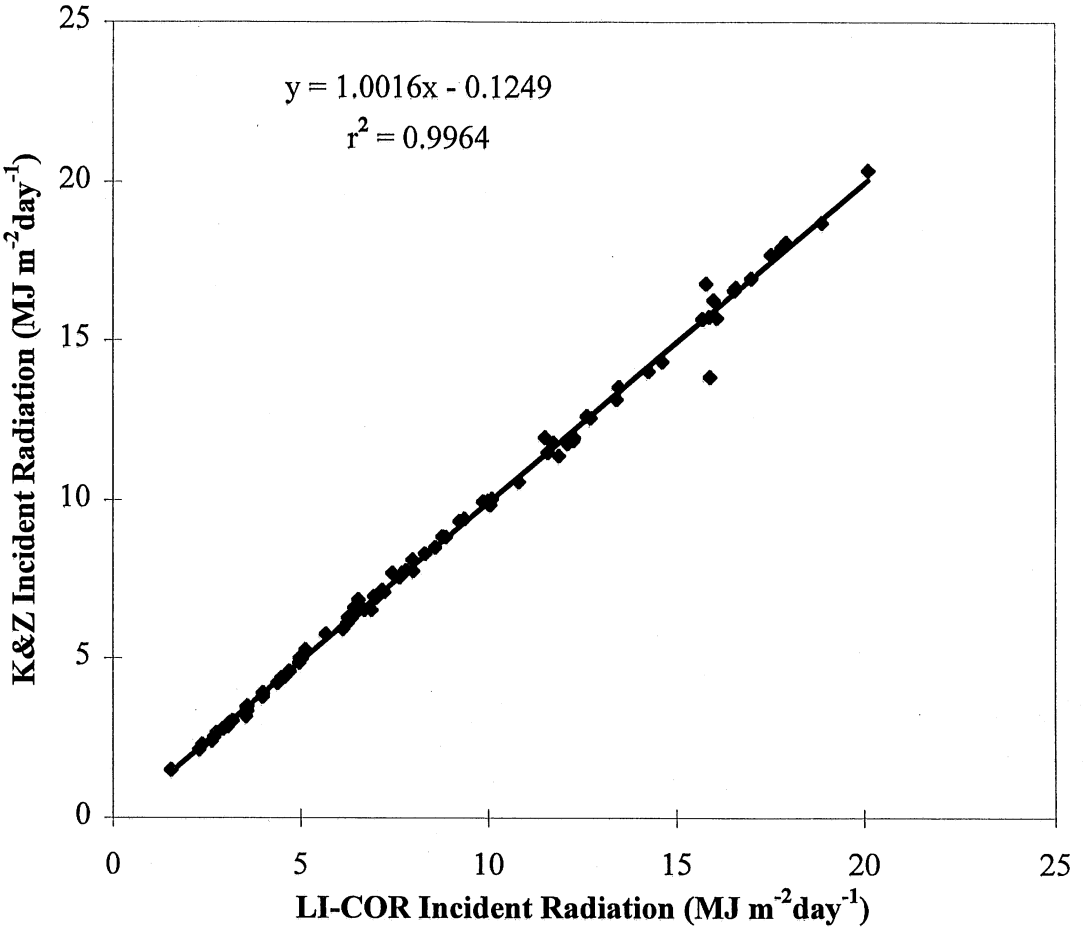

Figure 9a. Kipp and Zonen daily incident solar radiation versus LI-COR daily incident solar radiation.

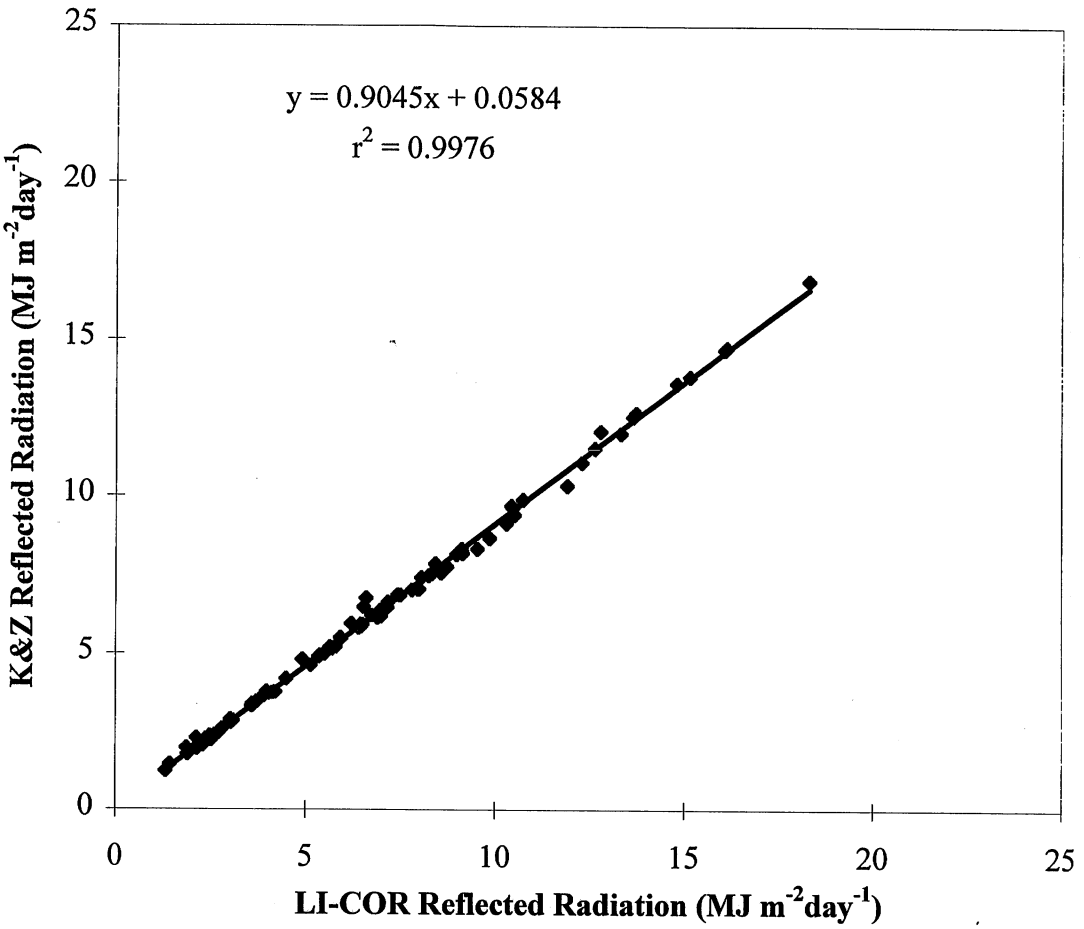

Figure 9b. Kipp and Zonen daily reflected solar radiation versus LI-COR daily reflected solar radiation.

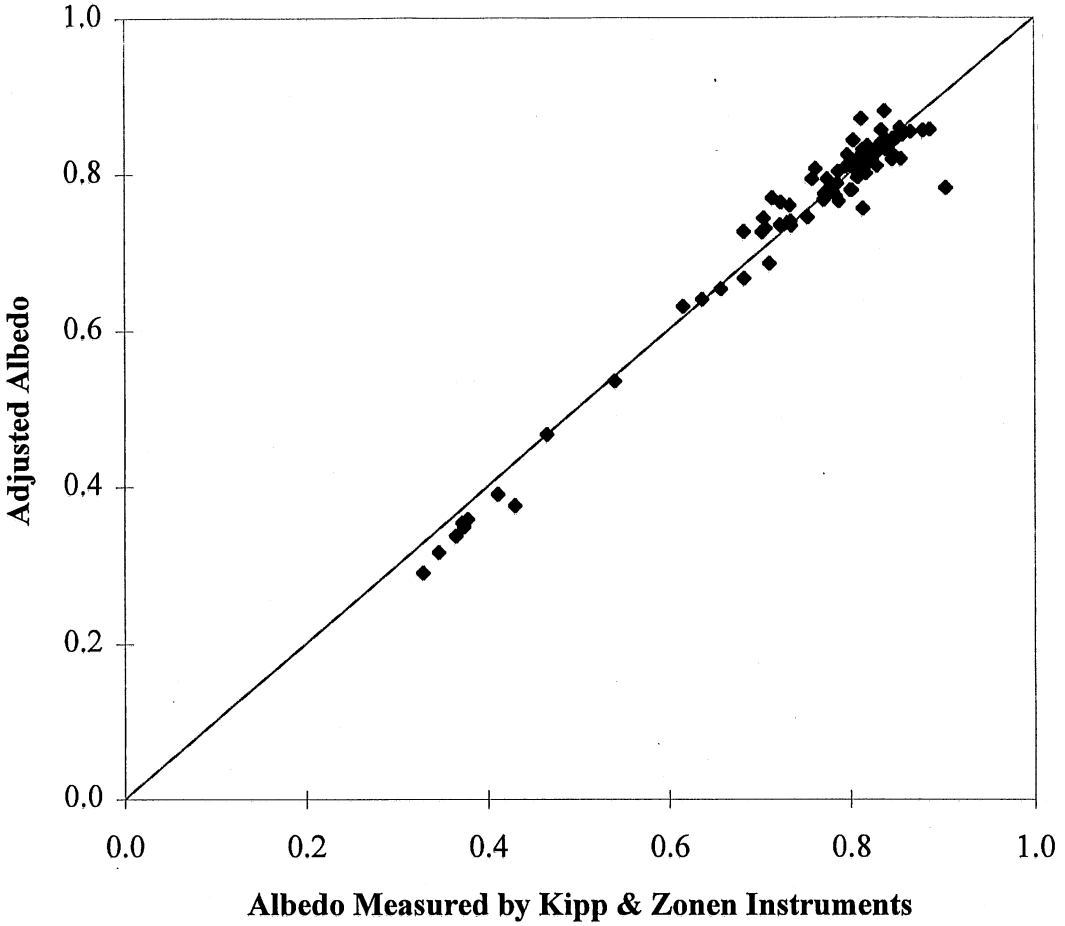

Figure 10. Adjusted daily albedo from LI-COR radiation data versus Kipp and Zonen measured albedo. The adjusted albedo was obtained from LI-COR measurements and Equation 5.